JOINT TRANSPORTATION
RESEARCH PROGRAM
INDIANA DEPARTMENT OF TRANSPORTATION
AND PURDUE UNIVERSITY

# Practical Implementation of Superabsorbent Polymers (SAP) for Internally Cured Concrete

Chibueze S. Ajuonuma, Raikhan Tokpatayeva, Akul N. Seshadri, Alberto Castillo, Jan Olek, and Kendra A. Erk

SPR-4727 • Report Number: FHWA/IN/JTRP-2025/19 • DOI: 10.5703/1288284317899

## RECOMMENDED CITATION

Ajuonuma, C. S., Tokpatayeva, R., Seshadri, A. N., Castillo, A., Olek, J., & Erk, K. A. (2025). *Practical implementation of superabsorbent polymers (SAP) for internally cured concrete* (Joint Transportation Research Program Publication No. FHWA/IN/JTRP-2025/19). West Lafayette, IN: Purdue University. https://doi.org/10.5703/1288284317899

## AUTHORS

**Chibueze S. Ajuonuma**
Purdue University
Lyles School of Civil and Construction Engineering

**Raikhan Tokpatayeva, PhD**
Purdue University
Lyles School of Civil and Construction Engineering

**Akul N. Seshadri**
Purdue University
School of Materials Engineering

**Alberto Castillo, PhD**
Purdue University
Lyles School of Civil and Construction Engineering

**Jan Olek, PhD**
Purdue University
Lyles School of Civil and Construction Engineering

**Kendra A. Erk, PhD**
Purdue University
School of Materials Engineering
School of Sustainability Engineering and Environmental Engineering
(765) 494-4118
erk@purdue.edu
*Corresponding Author*

## JOINT TRANSPORTATION RESEARCH PROGRAM

The Joint Transportation Research Program serves as a vehicle for INDOT collaboration with higher education institutions and industry in Indiana to facilitate innovation that results in continuous improvement in the planning, design, construction, operation, management and economic efficiency of the Indiana transportation infrastructure. https://engineering.purdue.edu/JTRP.

Published reports of the Joint Transportation Research Program are available at https://docs.lib.purdue.edu/jtrp/.

## NOTICE

The contents of this report reflect the views of the authors, who are responsible for the facts and the accuracy of the data presented herein. The contents do not necessarily reflect the official views and policies of the Indiana Department of Transportation or the Federal Highway Administration. The report does not constitute a standard, specification, or regulation.

# TECHNICAL REPORT DOCUMENTATION PAGE

| 1. Report No. | 2. Government Accession No. | 3. Recipient's Catalog No. |
|---|---|---|
| FHWA/IN/JTRP-2025/19 | | |

| 4. Title and Subtitle | 5. Report Date |
|---|---|
| Practical implementation of superabsorbent polymers (SAP) for internally cured concrete | July 17, 2025 |
| | **6. Performing Organization Code** |

| 7. Author(s) | 8. Performing Organization Report No. |
|---|---|
| Chibueze Ajuonuma (https://orcid.org/0009-0009-6640-4802)<br>Raikhan Tokpatayeva, PhD (https://orcid.org/0000-0003-3663-5131)<br>Akul N. Seshadri (https://orcid.org/0009-0007-9528-1587)<br>Alberto Castillo, PhD (https://orcid.org/0009-0000-0959-8684)<br>Jan Olek, PhD (https://orcid.org/0000-0003-0467-9877)<br>Kendra A. Erk, PhD (https://orcid.org/0000-0001-9238-1928) | FHWA/IN/JTRP-2025/19 |

| 9. Performing Organization Name and Address | 10. Work Unit No. |
|---|---|
| Joint Transportation Research Program<br>Hall for Discovery and Learning Research (DLR), Suite 204<br>207 S. Martin Jischke Drive<br>West Lafayette, IN 47907 | **11. Contract or Grant No.**<br>SPR-4727 |

| 12. Sponsoring Agency Name and Address | 13. Type of Report and Period Covered |
|---|---|
| Indiana Department of Transportation (SPR)<br>State Office Building<br>100 North Senate Avenue<br>Indianapolis, IN 46204 | Final Report |
| | **14. Sponsoring Agency Code** |

**15. Supplementary Notes**

Conducted in cooperation with the U.S. Department of Transportation, Federal Highway Administration.


**16. Abstract**

Laboratory investigations and results from a year-long field trial demonstrated that plain Type IL cement and slag cement concrete that was internally cured by superabsorbent polymer (SAP) has increased strength and durability compared to SAP-free mixtures, mixtures containing colloidal nanosilica, and mixtures that were externally cured with a surface-applied curing compound. SAP was successfully delivered to fresh concrete mixtures at the ready-mixed concrete plant by using dissolvable bags containing premeasured amounts of dry SAP particles. No batching adjustments were necessary to successfully utilize SAP in the concrete mixtures.


| 17. Key Words | 18. Distribution Statement |
|---|---|
| concrete curing, admixtures, organic polymers, nanosilica, microstructures, workability, compressibility, shrinkage, slag, internal curing, superabsorbent polymer, superplasticizers | No restrictions. This document is available through the National Technical Information Service, Springfield, VA 22161. |

| 19. Security Classif. (of this report) | 20. Security Classif. (of this page) | 21. No. of Pages | 22. Price |
|---|---|---|---|
| Unclassified | Unclassified | 64, including appendices | |

# EXECUTIVE SUMMARY

## Introduction

This project investigates the use of superabsorbent polymer (SAP) particles as internal curing agents in cementitious mixtures that are currently specified for such Indiana Department of Transportation (INDOT) applications as bridge decks and full-depth patching of concrete pavements. A materials-centric research approach was employed to determine how delivery method and mixture composition influences the internal curing performance of concrete mixtures containing commercial SAPs, with a focus on emerging cement types and supplementary cementitious materials.

## Methods

A series of laboratory-based experiments and field trials were designed to determine the following:

1. evaluate the internal curing performance of commercial SAP in concrete mixtures containing Type IL cement as well as mixtures containing slag and colloidal nanosilica-based admixtures;
2. practical implementation strategies to successfully deliver and disperse SAP in concrete mixtures; and
3. direct comparisons between the strength and durability of SAP-containing mixtures with externally cured concrete.

Commercially available SAP particles were utilized for all laboratory experiments and field trials. Both plain and slag cement (30% replacement) mixtures were investigated, with and without SAP and colloidal nanosilica-based solutions. The following properties (measurements) were determined: workability (slump); consistency (air content); volumetric stability (autogenous shrinkage, drying shrinkage); strength (compression, splitting tensile, and flexural tests); durability (scaling, rate of water absorption, resistivity, formation factor, chloride ion penetration); hydration kinetics, and microstructure analysis. Cement pastes were used for measurements of degree of hydration (isothermal calorimetry); cementitious mortar samples were used to investigate shrinkage, water absorption, and ultrasonic pulse velocity; while both mortar and concrete samples were used to evaluate the workability, flowability, mechanical properties, and durability performance of internally cured SAP-modified concrete.

## Findings

- Results consistently demonstrated that the addition of SAP to cementitious mixtures, with and without slag, led to improved hydration and a refined microstructure, resulting in reduced shrinkage and significant improvements in compressive and flexural strength.
- Dry SAP particles were added to concrete mixtures by two methods: direct pouring of loose particles and addition of premeasured quantities using a dissolvable plastic bag. Concrete created using the bagged SAP displayed improved mechanical properties and a refined microstructure, likely due to more uniform dispersion of SAP particles and reduced air incorporation during mixing. The bags dissolved completely, and there was no visual evidence of dry SAP particles after standard mixing procedures.
- The overall performance of SAP-cured mixtures was greater than mixtures only containing colloidal nanosilica. However, in a few cases, the ternary combination of SAP, slag, and colloidal nanosilica displayed improved strength and stiffness.

## Implementation

In collaboration with a local ready-mixed concrete company, field trials were performed to evaluate the performance of concrete internally cured with SAP and colloidal nanosilica solutions in comparison to concrete that was externally cured using a surface-applied curing compound. Slabs were cast in September 2023 and monitored for the following 12 months. SAP was added to the concrete mixtures by dissolvable bags containing 1 lb of dry SAP particles at a dosage of 1 bag per $yd^3$ of concrete (dosage of 0.15% SAP by weight of binder). All mixtures were 0.44 water-to-cement ratio (w/c) using local Type IL cement. No water reducing admixtures (superplasticizers) were used, and no additional batching adjustments were necessary to effectively utilize the SAP internal curing agents. When slag was utilized, it was as 30% replacement of cement. Colloidal nanosilica solutions were added at a dosage of 4 oz/cwt following manufacturer guidelines.

Results from the year-long field trial demonstrated that plain cement concrete internally cured by SAP displayed increased strength and durability compared to SAP-free concrete, concrete containing colloidal nanosilica, and concrete that was externally cured with a surface-applied curing compound. Additionally, concrete mixtures incorporating SAP and slag showed improved performance in comparison with the SAP-cured plain cement concrete mixtures. This indicates an interesting synergy between SAP, supplementary cementitious materials, and Type IL cement. Key findings are listed below:

- SAP-cured mixtures displayed a reduced slump and air content compared to SAP-free mixtures. However, all mixtures were within or exceeded the target slump (3–5 in.) and within the target air content (5–8%), so no additional mixture adjustments were needed.
- Mixtures containing SAP demonstrated improved early-age flexural strength performance compared to SAP-free mixtures. The addition of SAP also counteracted the early-age strength reduction caused by the use of slag.
- The addition of SAP to both plain and slag cement concrete resulted in significant increases in compressive strength both at early and later ages when compared to the SAP-free reference mixtures.
- When compared with using a surface-applied curing compound, the addition of SAP significantly improved the compressive strength of field cast and cored samples by more than 30–50% across all ages compared to SAP-free plain cement reference mixtures with and without curing compound.

- Mixtures containing both slag and SAP displayed reduced chloride penetration depths compared to reference and SAP-only mixes. The combination of SAP and slag appeared to provide a synergistic effect, together reducing permeability and enhancing resistance to chloride penetration.
- Cores extracted from plain and slag cement concrete slabs containing SAP had a refined microstructure, with visible reductions in air voids, shrinkage cracks, and unhydrated cement particles, in comparison to SAP-free reference slabs and slabs containing colloidal nanosilica.

It is important to note that all field-cast mixtures, with and without SAP, were able to be uniformly mixed and placed without the use of any extra mixing water or the addition of workability-enhancing admixtures, including water-reducing admixtures and superplasticizers. In contrast, for concrete that is internally cured with lightweight aggregate (LWA), a series of moisture-correction calculations must be performed to ensure the mixture contains enough water to fully saturate the LWA and to facilitate mixing and placement of the concrete. For concrete that is internally cured by SAP, moisture corrections are not necessary as the SAP particles are added to the mixtures in their dry, dehydrated state. When SAP particles are added to fresh concrete mixtures, they absorb a small amount (1–2%) of the available mixing water which typically reduces the workability of the mixture but can be counteracted by the use of workability-enhancing admixtures if desired. In this field trial, no additional admixtures were required to meet or exceed the specified target slump range of 3–5 in.

CONTENTS

# LIST OF TABLES

## LIST OF FIGURES

# 1. INTRODUCTION

## 1.1 Research Motivation

The benefits of internally curing concrete using water-swollen superabsorbent polymer (SAP) particles were recently demonstrated in Joint Transportation Research Program (JTRP) Project SPR-4419 led by Erk and Olek (Adams, Bose, Mann, et al., 2022). Paste, mortar, and concrete mixtures created in the laboratory environment displayed improved hydration, accelerated strength gain, greater volumetric stability and improved cracking resistance while maintaining sufficient mixture workability to be pumped and placed without sacrificing compressive or flexural strength. The study investigated the performance of two commercial SAP formulations in mixtures of varying water-to-cement ratios (0.35–0.52) created using three different Type I cement compositions as well as select specimens created using Type III and using 30% slag substitution. Dry SAP particles less than 0.3 mm in size were added in the amount of 0.2% by weight of binder, a dosage that amounts to approximately 1 lb (0.453 kg) of SAP per $yd^3$ of concrete (0.59 kg per $m^3$). Mixture workability was successfully adjusted using high-range water reducer admixture to attain the target slump without adding extra water.

However, before attempting broad adoption of SAP-cured concrete in construction projects, practical ways to utilize SAP in the field must be investigated. Unlike lab-scale mixtures, field trials require SAP to be added to concrete mixtures in a commercially practical way. For example, small volumes of dry SAP particles could be added to mixing trucks via dissolvable (water-soluble) bags. Additionally, there is also a growing supply of and demand for limestone-rich cements (e.g., Type IL) and new supplementary cementitious materials (SCMs) and mineral admixtures (e.g., slag, silica fume, colloidal nanosilica solutions). Yet it is currently unclear how these different mixture chemistries will impact the internal curing performance of SAP.

## 1.2 Project Goals and Objectives

The goal of this project was to successfully utilize SAP particles as internal curing agents in cementitious mixtures that are currently specified for such Indiana Department of Transportation (INDOT) applications as bridge decks and full-depth patching of concrete pavements. In particular, a top priority was to anticipate and remove any uncertainties that contractors may have about the application of SAP in concrete. To achieve this goal, a materials-centric research approach was employed to determine how delivery method and mixture composition influences the internal curing performance of concrete mixtures containing commercial SAPs, with a focus on emerging cement types and SCMs. This project was designed to accomplish the following key objectives:

1. Evaluate the internal curing performance of commercial SAP in concrete mixtures containing Type IL cement as well as slag and colloidal nanosilica solutions;
2. Develop and evaluate practical field implementation strategies to successfully deliver and disperse SAP in concrete mixtures; and
3. Conduct field trials to compare the strength and durability of SAP-containing mixtures with externally cured concrete.

## 1.3 Report Outline

Chapter 2 provides a review of relevant literature about the structure and properties of SAP and the use of SAP particles in concrete applications. Chapter 3 investigates a novel approach to delivering SAP in concrete using dissolvable bags. Chapter 4 evaluates the performance of plain and slag-cement mortars modified with SAP and colloidal nanosilica solutions. Chapter 5 studies the impacts of SAP on the hydration kinetics of plain and slag-cement modified cementitious pastes. In Chapter 6, the practical implementation of SAP for internally cured concrete is demonstrated through a year-long field trial with a local ready-mixed concrete provider. Chapter 7 investigates the effect of water-to-binder ratio (0.42 and 0.44) on the internal curing performance and shrinkage of SAP-modified cementitious mortar. Chapter 8 describes the microstructure of SAP-modified concrete cores that were extracted from field-cast slabs after 365 days.

# 2. LITERATURE REVIEW

## 2.1 Internal Curing and Superabsorbent Polymers (SAPs)

A key approach to improving the durability and service life of concrete infrastructure is to control the hydration of cementitious materials through internal curing. This process increases the degree of hydration (Adams, Bose, Olek, & Erk, 2022), reduces shrinkage, and decreases cracking potential (Beushausen et al., 2014; Espinoza-Hijazin & Lopez, 2011). Conventional curing mechanisms such as water curing (e.g., spraying, ponding, use of sprinklers) and steam curing are usually applied to control the relative humidity of the cementitious system. But over the years, several other strategies such as the use of lightweight aggregates (LWA), perforated cenospheres, and more, have been employed to gradually release water within the cementitious system (Henkensiefken et al., 2009; Liu et al., 2017; Van et al., 2014).

One promising internal curing strategy is the use of SAPs. SAPs are crosslinked polymer hydrogel particles which, upon contact with aqueous fluids, have the capability of absorbing and releasing large volumes of fluid in comparison to its own dry mass, forming swollen, insoluble gel particles (Erk & Bose, 2018). SAPs are commonly used for consumer hygiene products and water treatment applications. Prior research at Purdue University has shown that SAP absorption and desorption is driven by osmotic pressure gradients and is strongly sensitive to the ions that are naturally present in cementitious pore fluid (Krafcik et al., 2017; Krafcik & Erk, 2016; Zhu et al., 2015). The many benefits of internally curing concrete using SAP particles are summarized by Schröfl et al. (2022).

The incorporation of SAP particles offers an alternative to the use of prewetted LWA for internal curing purposes (Barrett et al., 2015). Unlike LWA, dry SAP particles are of uniform morphology and composition, ensuring consistent fluid absorption and desorption performance across various mixtures and environmental conditions (Kang et al., 2017). Additionally, dry SAP particles can be added directly to wet or dry mixtures at the concrete plant or in the ready-mixed truck without any required pre-hydration steps or moisture-adjustment calculations, following

the same simplified dosing strategies that are used for other chemical and mineral admixtures (Hasholt & Jensen, 2015).

When dry SAP particles are mixed into fresh cementitious mixtures, they absorb a small amount of available water and swell (i.e., increase in volume). The exact absorption amount depends on the SAP composition as well as the SAP particle size but is typically less than a few percent of the total free water. In practice, the absorption of water by the SAP particles will decrease the workability of the mixture (Adams, Bose, Olek, & Erk, 2022). To mitigate this loss of workability in practice, 5% (by mass) extra water can be added to any mixtures that contain SAP. Alternatively, a greater amount of water reducing admixture (WRA) can be added instead of extra water to meet target slump ranges, which will increase the workability of the mixture without compromising its mechanical strength (Adams, Bose, Olek, & Erk, 2022).

As the swollen SAP particles release water, they decrease in volume and leave behind a macrovoid within the cement matrix, reflecting the size of the swollen SAP particle at the initial set time of the cement. These macrovoids typically range from tens to hundreds of microns in diameter. Many times, this SAP-related macrovoid is empty, and, in those cases, the presence of these voids can increase the freeze-thaw resistance of the material (Schröfl et al., 2022). Other times, these SAP-related macrovoids can be "filled in" with hydrated product, typically a mixture of calcium hydroxide (CH) and calcium silicate hydrates (C-S-H). This void-filling ability was found to increase for SAP compositions that contain a greater amount of polyacrylamide and particles that contain a source of silica (Bose et al., 2021; Davis et al., 2020; Seshadri et al., 2025). The rate at which water is released (desorbed) from the water-swollen SAP particles depends on the SAP composition, the kinetics of the hydration reaction, and the rate at which water within neighboring capillary porosity is depleted. In general, studies using neutron radiography and nuclear magnetic resonance methods have shown that SAP begins releasing water within an hour of mixing, with the release continuing for up to 24 hr after mixing (Schröfl et al., 2022).

### 2.2 Application of SAP in Type IL Cement and Slag Cement

The internal curing performance of SAP in Type IL portland-limestone cement mixtures has yet to be investigated. These mixtures contain a greater proportion of limestone, from 5–15% (ASTM International [ASTM], 2024g). It is common to see reductions in early age strength when Type IL is used compared to Type I cement mixtures. Such reductions may be compensated for by using SAP. In prior studies, some Type I mortars containing SAP displayed significant increases in 3-day strength values compared to SAP-free mixtures (Adams, Bose, Mann, et al., 2022).

The effectiveness of SAP internal curing agents in Type I pastes and mortars (0.42 water-to-cement ratio [w/c]) with 30% slag replacement was investigated in the SPR-4419 (Adams, Bose, Mann, et al., 2022). The workability (percent flow over time) of SAP-containing slag-mortar was significantly reduced compared to SAP-free slag-mortars. However, workability is expected to increase when additional WRA is utilized in SAP-containing slag-mortars (e.g., at a dosage greater than 0.3% by weight of binder which was used in the previous study). In isothermal calorimetry tests, there was no significant change in the size and the location of the hydration peak or total heat generated in slag-paste samples with and without SAP. The addition of SAP to slag-mortar increased the 3-, 7-, and 28-day compressive strength values compared to SAP-free slag-mortars. The increase in 3-day compressive strength was of particular interest given the reduction in early age strength that is commonly observed when using slag compared to straight cement. Flexural strength was comparable in slag-mortars with and without SAP at all ages. Additionally, there have been a number of other studies that describe the use of SAP in slag-containing mixtures. Key findings include the successful use of SAP for the mitigation of self-desiccation and consequent autogenous shrinkage of alkali-activated slag pastes, as discussed by Li et al. (2020) and Vafaei et al. (2020) and blast-furnace slag cements, as discussed by Snoeck, Jensen, and De Belie (2015) and Almeida and Klemm (2018).

### 2.3 The Interactions Between SAP, Silica Fume, and Nanosilica

SAP internal curing performance in the presence of silica has been investigated, including silica fume and nanosilica. Many early investigations of SAP internal curing utilized mixtures containing 10–20% silica fume and found that SAP mitigated self-desiccation in such mixtures (Lura et al., 2011). According to Lefever et al. (2020), cement mortar mixtures containing both SAP and nanosilica displayed decreased autogenous shrinkage while maintaining the mechanical properties of the SAP-free mortar, leading the authors to conclude that, "both additives can complement each other to obtain a cementitious mix that is less prone to shrinkage cracking without strength compromise" (p. 9). Olivier et al. (2018) showed that the addition of SAP to concrete containing nanosilica reduced shrinkage while maintaining slump.

Nanosilica (NS) is a pozzolanic mineral added to cementitious mixtures to promote the formation of C-S-H. It has been shown to accelerate cement hydration and improve the strength and durability of the mixture (Balapour et al., 2018). The small particle size of NS also provides a filling effect in the cement matrix, resulting in a denser and less permeable microstructure. However, the hydrophilic nature of NS, combined with its high surface area, increases the water demand of the mixture which can lead to increased autogenous shrinkage (Zhang et al., 2023). The denser microstructure can also lead to a larger capillary stress, which may amplify drying shrinkage. These effects become more pronounced with higher dosages of NS in the mixture. For example, when NS was used to replace ordinary portland cement at 1.2% by mass, paste chemical shrinkage increased by 58% after 28 days, and concrete volumetric shrinkage increased by 67% after 7 days, compared to mixtures without NS (Wang et al., 2020).

In contrast to the studies referenced above, even a relatively small dosage of colloidal nanosilica, a stabilized suspension of NS particles in water, can have an outsized effect on the macroscale properties of cement-based materials. Scott (2024) directly

compared the internal curing performance of LWA (expanded shale) and colloidal NS solutions in plain Type I/II mortars and mortars with 20% cement replacement with Class F fly ash. The addition of colloidal NS to both plain and fly ash mortar specimens only slightly reduced the drying shrinkage after 7 days of air-curing compared to the colloidal NS-free reference mortars. Mortars containing fly ash and LWA separately exhibited the lowest values of drying shrinkage. In autogenous shrinkage experiments conducted over a period of 7 days, specimens containing LWA showed significant expansion, fly ash mortars exhibited near-zero shrinkage, and specimens with colloidal NS exhibited the greatest shrinkage, similar to the reference mortars. The use of colloidal NS also resulted in decreased compressive strength in all cases compared to the colloidal NS-free reference mortars. These findings led the authors to conclude that the beneficial attributes of fly ash, including shrinkage mitigation, were diminished in the presence of colloidal NS.

### 2.4 Use of SAP in Concrete Field Trials

De Meyst et al. (2020) investigated the use of SAP to mitigate shrinkage in high performance concrete (HPC) containing SCMs using a large-scale demonstrator of a wall cast on a slab and restrained at the wall-slab connection by internal steel mesh and reinforcement bars. The cement *Variodur 40* from the company Dyckerhoff contained 35–64% clinker, 36–65% blast furnace slag, and 0–5% minor constituents. Irregularly shaped SAP particles with an average diameter of 100 µm were added to the mixture at a dosage of 0.3% by weight of cement. The compressive strength of the SAP-containing concrete was found to be ~11% lower than the SAP-free concrete at both 7 and 28 days. SAP addition was successfully able to mitigate shrinkage of the concrete wall demonstrator, which was reduced by 22% at the bottom, 54% at the middle, and 60% at the top of the wall demonstrator compared to the SAP-free concrete. Cracks were observed on the SAP-free wall after 21 hr whereas no cracks were observed on the SAP-concrete wall after 4 months.

Tenório Filho et al. (2020) found that the method of incorporating SAP into conventional concrete mixtures influenced autogenous shrinkage. SAP particles were 360 µm (average) in diameter and utilized at a dosage of 0.25% by weight of cement. An additional 6% of water was incorporated in SAP-containing mixtures to improve workability, increasing the total water-to-cement ratio to 0.52. Reduced shrinkage was observed when SAP was added to the materials belt with other dry components at the concrete production plant compared to when SAP was added directly to the truck after the wet mixing procedure was completed. When SAP was added to the truck, it resulted in agglomeration of SAP particles (confirmed by microscopy) and subsequently reduced internal curing performance.

SAP was also investigated for use in HPC by Lange et al. (2021), a study funded by the Illinois Tollway. This research examined and documented the use of internal curing by SAP to improve the durability of Tollway bridge decks. The project included laboratory studies to characterize material behavior and properties and field testing to measure slab performance and observe behavior with full scale truck mixers. One of their key findings was that repulpable (paper) bags did not work well for the delivery of dry SAP particles into the HPC (0.37 w/c). The bags were directly added to ready-mix trucks, but even after additional mixing (e.g., 40 extra revolutions), the bags did not fully disintegrate, resulting in dry clumps of SAP particles that were still partially protected by the bag after mixing. The dosages were 1.10, 2.05 and 2.58 lb/yd$^3$. While repulpable bags are effective for the delivery of large quantities of high-density particles (e.g., 25 lb of mineral admixtures), they may be ineffective for the relatively small dosages of low-density dry SAP particles that are needed to cure concrete: approximately 1 lb of dry SAP per 1 yd$^3$ of concrete (~0.15–0.2% dry SAP by weight of binder).

## 3. NOVEL APPROACH TO SAP DELIVERY: DRY SAP IN DISSOLVABLE BAGS

### 3.1 Overview

To address Objective 2 of this JTRP project, this section investigates the feasibility of incorporating dry SAP particles as internal curing agents in concrete utilizing two delivery methods: direct addition of the particles and addition of the particles encapsulated in dissolvable bags. The use of dissolvable bags provides a practical method of storing, handling, and dosing premeasured amounts of dry SAP particles into cementitious mixtures. Concrete specimens containing SAPs were prepared using both methods, and their properties were evaluated through compressive strength tests at 3, 7, and 28 days, flexural strength tests, ultrasonic pulse velocity (UPV) measurements, and dynamic elastic and shear modulus determinations. Results indicate that the use of dissolvable bags led to improved mechanical properties and a refined microstructure compared to direct pouring. Compressive and flexural strengths showed significant improvements, especially at early ages. UPV results confirmed higher uniformity of microstructure, while dynamic elastic and shear moduli indicated improved stiffness. The findings highlight the effectiveness of the dissolvable bags as a practical and efficient delivery method for SAP that can be easily adopted for commercial concrete applications.

This section has been published:

Ajuonuma, C. S., Tokpatayeva, R., Olek, J., & Erk, K.A. (2025). A novel approach to delivering superabsorbent polymers for internal curing of concrete. *CIB Conferences*, *(1)*39. https://doi.org/10.7771/3067-4883.2118

### 3.2 Background

The practical implementation of SAP requires measuring and directly pouring dry SAP particles into concrete mixtures (Beushausen & Gillmer, 2014; Hasholt & Jensen, 2015; Kang et al. 2017). As described in Section 2.4, this can sometimes present additional challenges such as inconsistent dispersion and agglomeration (clumping) of the SAP particles (Lange et al. 2021; Tenório et al. 2020). Similar to LWA, prewetted SAP can also be used instead of dry particles

(AzariJafari et al., 2016; Kong et al., 2015; Wang et al., 2009), but the use of prewetted SAP can result in storage and handling challenges as hydrated SAP particles are more likely to clump together and not disperse evenly during mixing (Mudiyanselage & Neckers, 2008), often resulting in performance variability and increased labor demands (Barret et al., 2015; Miller et al., 2014; Schröfl et al. 2017).

Instead of repulpable bags (Lange et al., 2021), SAP particles can be delivered using bags composed of thin plastic films created from water-soluble polymers, including polyvinyl alcohol (PVA). Water-soluble plastic bags dissolve quickly in the presence of water (e.g., in a few seconds) and were expected to dissolve within minutes of being mixed into fresh concrete. This SAP delivery method can be integrated seamlessly into standard batching and mixing practices at the concrete plant or within the ready-mixed concrete truck. The premeasured dosage of dry SAP also eliminates the risk of over or under dosing. Additionally, the amounts of SAP are also small enough that clumping and gel-blocking are prevented and good dispersion throughout the mixture is ensured without the need for additional mixing (Friedrich, 2012; Mudiyanselage & Neckers, 2008).

### 3.3 Materials

The materials utilized in this study include potable water, fine aggregate (maintained at saturated surface dry [SSD] condition), coarse aggregate (in air-dry conditions), superplasticizer (Sika Viscocrete 1000), air-entrainment admixture (Sika Air 260), slag cement (grade 100), Type IL cement, and commercially available SAP particles (crosslinked polyacrylamide particles, average diameter of 116 ± 70 microns). A single batch of Type IL cement produced by Buzzi Unicem USA conforming to ASTM International's standard specification (C595) for blended hydraulic cement specifications (ASTM, 2024g) was used throughout this research project. The chemical and physical characteristics of the cement and slag cement are given in Table 3.1. The Type IL and slag mill certifications are included in the Appendix.

The coarse aggregate and fine aggregate were locally sourced and conformed to the Indiana Department of Transportation standard specifications for #8 limestone and #23 sand (INDOT, 2024b). The maximum particle size of the sand was 4.75 mm (0.187 in.); specific gravity and fineness modulus were of 2.63 and 2.79, respectively. The specific gravity of the coarse aggregate was 2.65 and its maximum size was 25 mm. Clean, potable water sourced from the research laboratory was utilized throughout this research work as detailed in ASTM standard specification (C1602) for mixing water used in production of hydraulic cement concrete (ASTM, 2022c). Modified polycarboxylate based high-range WRA with specific gravity 1.062 ±0.01 (at 20 °C [68 °F]), pH 7.50 ± 2.00, solid content (halogens) 25.00% ± 1.20%, sodium oxide ($Na_2O$) equivalent ≤ 1.50%, Chloride ion ($Cl^-$) equivalent ≤ 0.10% was used in combination with an air entraining admixture.

TABLE 3.1
**Chemical and Physical Characteristics of OPC and Slag Cement Used.**

| Chemical composition | OPC Type IL (wt%) | Slag (wt %) (Huang et al., 2024) |
|---|---|---|
| Insoluble Residue | 0.63 | - |
| Loss on Ignition | 5.32 | - |
| Sulphur trioxide, $SO_3$ | 3.35 | 1.75 |
| Silicon oxide, $SiO_2$ | 18.36 | 34.57 |
| Calcium oxide, CaO | 62.64 | 40.69 |
| Magnesium oxide, MgO | 3.00 | 10.76 |
| Aluminum oxide, $Al_2O_3$ | 4.61 | 9.65 |
| Iron oxide, $F_2O_3$ | 2.90 | 0.73 |
| $Na_2O$ Equivalent | 0.62 | 0.34 |
| **Physical properties** | | |
| Specific Gravity (g/cm$^3$) | 3.09 | 2.89 |
| Specific Surface (cm$^2$/g) | 4142 | 5630 |

Dry SAP particles in 1-lb (0.453-kg) bagged quantities were obtained from the commercial supplier (Figure 3.1a). The inner dissolvable bag was made from a water-soluble polymer. The outer bag was made from a water-proof plastic film for storage purposes. Based on prior work, a 1-lb quantity of dry SAP was found to be sufficient to internally cure 1 yd$^3$ of concrete, equating to an approximate dosage of 0.15–0.2% dry SAP by weight of binder (Adams, Bose, Mann, et al., 2022). To use, the outer


(a) (b)

**Figure 3.1** (a) Prebagged Dry SAP Particles, for Internal Curing of 1 yd$^3$ of Concrete; (b) Scaled Down Dosage of SAP (3.5″ × 2″) Used in Lab Mixes in This Study.

TABLE 3.2
**Concrete Mixture Design.**

| Mixture ID | w/b | Cement (kg/m³) | Coarse Agg (kg/m³) | Fine Agg (kg/m³) | Water (kg/m³) | Slag (kg/m³) | SAP (kg/m³) | HRWRA (mL/100 kg) | AE (mL/100 kg) |
|---|---|---|---|---|---|---|---|---|---|
| **REF** | 0.44 | 390 | 1007 | 707 | 172 | | | - | 50 |
| **CEM IL_P** | 0.44 | 390 | 1007 | 707 | 172 | | 0.78 | 400 | 50 |
| **CEM IL_B** | 0.44 | 390 | 1007 | 707 | 172 | | 0.78 | 400 | 50 |
| **S30_P** | 0.44 | 273 | 1007 | 707 | 172 | 117 | 0.78 | 400 | 50 |
| **S30_B** | 0.44 | 273 | 1007 | 707 | 172 | 117 | 0.78 | 400 | 50 |

Note: *B* is SAP delivery using Dissolvable Bags; *P* is SAP delivery by Direct Pouring.
1 kg/m³ = 1.686 lb/yd³

plastic bag is removed and the inner dissolvable bag containing the dry SAP particles can be added directly to a ready-mix truck or batch plant mixer. For the present study, the SAP dosage and dissolvable bag size was scaled down to the quantities required for the laboratory-scale concrete mixtures (Figure 3.1b and Table 3.2).

## 3.4 Methods

### *3.4.1 Concrete Sample Preparation*

The concrete mixture designs were based on the Class C concrete (658 lb/yd³ [390 kg/m³]) as per the Indiana Department of Transportation standard specifications (INDOT, 2024a). Five concrete mixture compositions are shown in Table 3.2, comprising of the reference with plain Type IL cement (REF); concrete mixes with the addition of dry SAP particles using two different delivery approaches—direct pouring, P (CEM IL_P) and the use of dissolvable bags, B (CEM IL_B); concrete mixtures containing 30% (by weight of the total binder) of grade 100 slag cement as a replacement for Type IL cement (S30) and the SAP added by direct pouring (S30_P) and dissolvable bag (S30_B).

The water-to-binder (w/b) ratio was kept at a constant value of 0.44. Constant dosage of air entraining admixture was maintained (50 mL/100 kg or 0.77 oz/cwt). High-range water reducer (HRWRA), also known as a superplasticizer, was not used for the reference mixture, but with the SAP-modified concrete mixes, a constant dosage of 400 mL/100 kg (6.15 oz/cwt) weight of binder was maintained. The slag cement was added as 30% replacement of the Type IL cement.

The fresh concrete was mixed in the pan concrete mixer following the procedure outlined in the ASTM standard practice (C192) for making and curing concrete test specimens in the laboratory (ASTM, 2025). During the first step of the mixing process, the weighted amounts of fine and coarse aggregate, along with the required dosage of air entraining admixture were placed in the pan and mixed for 30 s. This was followed by the addition of dry SAP particles (either by direct pouring or encapsulated in dissolvable bag) and the addition of ~95% of the mixing water, corrected for the moisture content of the aggregate. These ingredients were then mixed for 5 min at moderate speed until a consistent homogeneity of the mixture was achieved. Subsequently, the mix was allowed to rest for 2 min, after which the remainder of the water (~5%), part of which was premixed with the WRA, was added and mixing continued for an additional 2 min. After completing the mixing process, the fresh concrete was tested for slump and air content.

The fresh concrete mixes were cast into 4 × 8 in. (102 × 204 mm) cylinders—used for compressive strength testing—and 4 × 4 × 16 in. (102 × 102 × 408 mm) beams—for determining flexural strength, ultrasonic pulse velocity, the dynamic modulus of elasticity, and shear modulus of elasticity. The molds with freshly cast concrete were covered with plastic sheets and stored for 24 hr at room temperature in the laboratory. After demolding, the specimens were kept under the plastic sheets (air-cured) in the laboratory at a temperature of 23 °C (73.4 °F). until the prescribed testing time (3, 7, and 28 days). At each testing age, the flexural and compressive strength data were collected from three individual specimens.

### *3.4.2 Workability and Air Content*

Slump and total air content were determined on all fresh concrete mixes according to ASTM standard test method (C143) for slump of hydraulic cement concrete (ASTM, 2020b), and ASTM standard test method (C231) for air content of freshly mixed concrete ASTM, 2024a). The target slump was 3–5 in. (76.2–127 mm) while the target air content was 5–8%.

### *3.4.3 Flexural Strength and Compressive Strength*

The flexural strength of concrete beams was evaluated following ASTM standard test method (C78) for flexural strength of concrete using simple beam with third point loading after 28 days of curing (ASTM, 2022e). The compressive strength was evaluated by following the procedures of ASTM standard test method (C39) for compressive strength of cylindrical concrete specimens with machine loading rate consistently maintained at 1 kN/s or 224.8 lbf/s (ASTM, 2024b).

### *3.4.4 Ultrasonic Pulse Velocity (UPV)*

The UPV test was performed in accordance with ASTM standard test method (C597) for ultrasonic pulse velocity through concrete on 4 × 4 × 16 in. (100 × 100 × 400 mm) beams air-cured 28 days at the temperature of 23 °C using a piezoelectric transducer with a resonant frequency of 54 kHz in a direct transmission mode (ASTM, 2024b). A gel couplant was used to ensure good acoustic contact between the transducer and the concrete beam specimens.

### 3.4.5 *Dynamic and Shear Modulus of Elasticity*

The dynamic modulus and shear modulus of elasticity were performed in accordance with ASTM standard test method (E1876) for dynamic Young's modulus, and Poisson's ratio by impulse excitation of vibration for resonant frequency on 4 × 4 × 16 in. concrete beams (ASTM, 2022d). The dynamic Young's modulus was determined using the resonant frequency in flexure, while the dynamic shear modulus was found using torsional resonant vibrations.

## 3.5 Results

### 3.5.1 *Workability and Air Content*

It is worth noting that for both SAP delivery methods, no trace of the dissolvable bags, SAP clumps or dry SAP particles were seen in the fresh concrete mixtures. Table 3.3 shows the slump values and the air content for both the reference mixture and mixes with the SAPs using various delivery methods. The reference mix had slump values higher than the target values, although no high-range WRA was used. As expected, the addition of SAP decreased the concrete slump values due to the small amount of mixing water (1–2%) that is absorbed by the dry particles. Direct pouring of SAP resulted in a 36% decrease in slump when compared with the reference mix while the addition of SAP using dissolvable bags resulted in a 29% decrease in slump. For slag cement, both SAP delivery approaches showed the same slump values.

Table 3.3 also shows the measured values of fresh concrete air content. All concrete mixes showed air content within the design target. The plain concrete mixes prepared using direct pouring of dry SAP particles showed a 7.1% increase in air content in comparison to the reference mix while using dissolvable bags resulted in a 7.1% reduction in air content. This suggests that additional air is entrained in the fresh mixture as the collection of SAP particles is being poured from the bucket into the mixture. By comparison, less air would likely be entrained when a single dissolvable bag is added to the mixture. However, with the slag cement, the trend is reversed, with SAP delivered by the dissolvable bag resulting in higher air content than with direct pouring of SAP. More investigation is needed.

TABLE 3.3
**Slump and Air Content of Fresh Concrete.**

| Mix I D | Slump (in./mm) | Air Content (%) |
|---|---|---|
| REF | 7.0 / 177.8 | 7.0 |
| CEM IL_P | 4.5 / 114.3 | 7.5 |
| CEM IL_B | 5.0 / 127.0 | 6.5 |
| S30_P | 4.75 / 120.7 | 6.6 |
| S30_B | 4.75 / 120.7 | 7.5 |

Note: Target Slump = 3–5 in.; Target Air Content = 5–8%

### 3.5.2 *Flexural Strength*

The flexural strength values of the concrete beams obtained at 28 days are shown in Figure 3.2. Flexural strength values for all mixes ranged from 600–720 psi (4.14–4.96 MPa), with the reference mix showing a value of 600 psi (4.14 MPa). Most SAP-modified mixtures showed a significant increase in flexural strength in comparison to the reference mix. Concrete mixes with direct pouring of SAP particles recorded a flexural strength value of 720 psi (4.96 MPa), a 20% increase when compared to the reference mix (600 psi or 4.14 MPa). The SAP delivery approach with dissolvable bags resulted in a 12% increase (670 psi or 4.62 MPa) from the reference. This shows an 8-percentage point variation in flexural strength between the

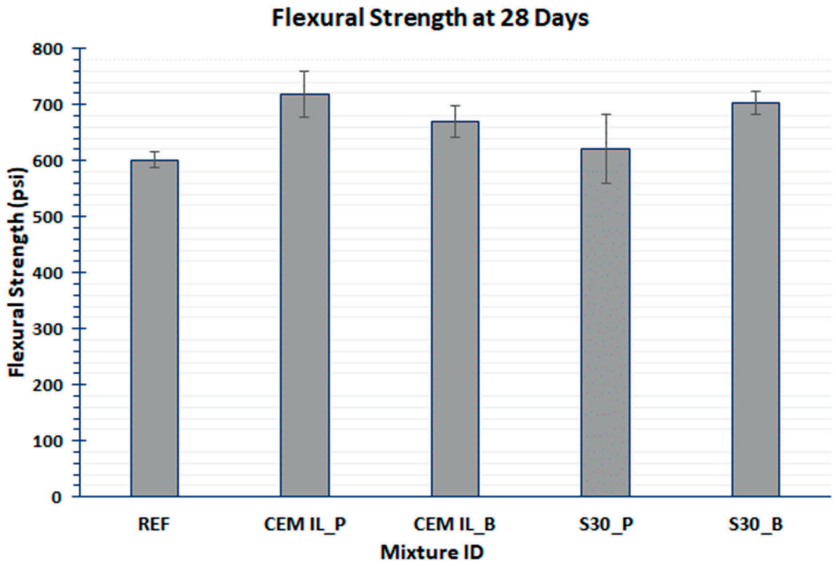


**Figure 3.2** Flexural Strength of Concrete Mixes at 28 Days. Note: 1 psi = 0.006895 MPa.

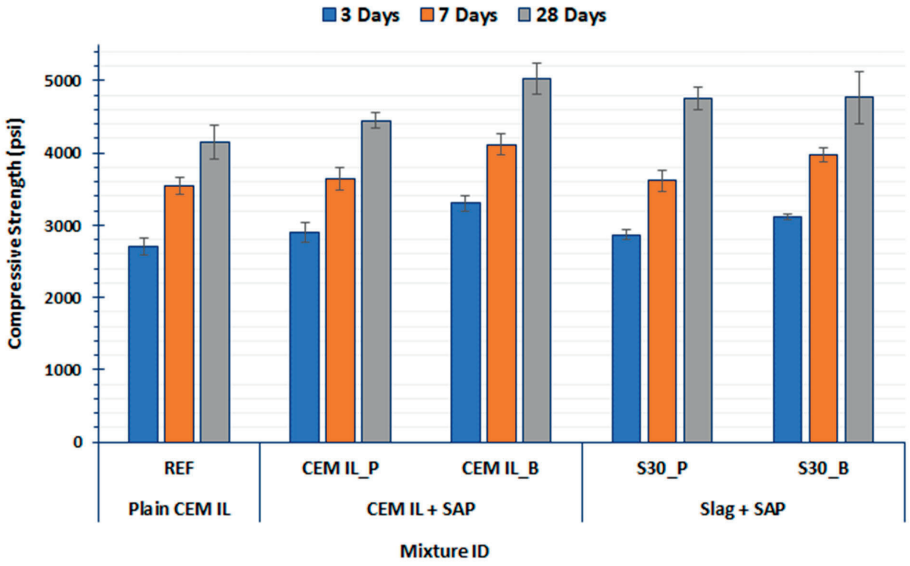


**Figure 3.3** Compressive Strength of Concrete Mixture at 3, 7, and 28 Days. Note: 1 psi = 0.006895 MPa.

different delivery approaches. But with slag cement, the SAP delivery using dissolvable bag resulted in higher flexural strength values (704 psi or 4.86 MPa) in comparison to the mix with direct pouring. Another observation is that mixes with higher air content seem to have higher flexural strength than those with lower air content.

### *3.5.3 Compressive Strength*

Figure 3.3 shows the compressive strength results for all concrete mixes at 3, 7, and 28 days. The trend of increased compressive strength with age was consistent for all testing ages and SAP delivery approaches. In general, addition of SAP improved the compressive strength compared to the SAP-free reference mixture, but slight strength reductions were observed for the slag cement mixes. For the plain concrete mixture, the direct pouring of SAP into the mixtures resulted in increased compressive strengths of 7%, 3%, and 7% at 3, 7, and 28 days, respectively, when compared with the reference mix. The concrete mixes with SAP particles added using dissolvable bags also resulted in increased compressive strengths of 22%, 16%, and 20% at 3, 7, and 28 days, respectively, when compared with the reference mix. The higher values of compressive strength obtained using the dissolvable bags in comparison to the direct pouring of SAP may be attributed to the lower air content, as lower air content in the fresh concrete increases the compressive strength. For the slag cement concrete, a slight increase in strength values was also recorded for concrete mixtures with SAP added using dissolvable bags in comparison to the mixes with direct pouring of SAP. The variation in compressive strength values between SAP delivery using dissolvable bag and direct pouring of SAP for the slag cement mixtures was 8.8%, 10.0%, and 0.3% higher for of 3, 7, and 28 days, respectively.

### *3.5.4 Ultrasonic Pulse Velocity*

UPV was conducted to assess both material quality, uniformity, and the presence of flaws which can impede the strength characteristics. The UPV test was conducted on concrete beam specimens and the results obtained for all the mixes at 3, 7, 14, and 28 days are reported in Figure 3.4. A consistent trend of increased UPV with age was observed for all the mixes indicating additional cement hydration products generated with continuous hydration. Both methods of SAP addition into concrete mixtures resulted in a marginal increase in UPV between 1–4% at 3, 7, 14, and 28 days when compared with the reference mixture. The observed UPV trends were similar to the compressive strength trends, suggesting that irrespective of the SAP delivery method, the particles do not impart negatively on the compressive strength. Comparable values were also recorded with direct SAP addition and dissolvable bags for mixtures containing slag cement.

### *3.5.5 Dynamic Modulus of Elasticity and Shear Modulus of Elasticity*

Figure 3.5a presents values for the dynamic modulus of elasticity (DME) evaluated using resonant frequency in flexure, and Figure 3.5b shows the shear modulus of elasticity (G) for concrete mixture. These moduli are indicators of the concrete stiffness and resistance to deformation. All SAP-modified mixes showed a slight increase in dynamic modulus compared to the reference mixture, indicating a marginal improvement in stiffness under dynamic loads which could be beneficial for applications subjected to repeated loading, such as pavements and bridge deck. The comparable values of the moduli for each of the SAP-modified mixtures are indicators of the effectiveness of the SAP delivery method using the dissolvable bag.

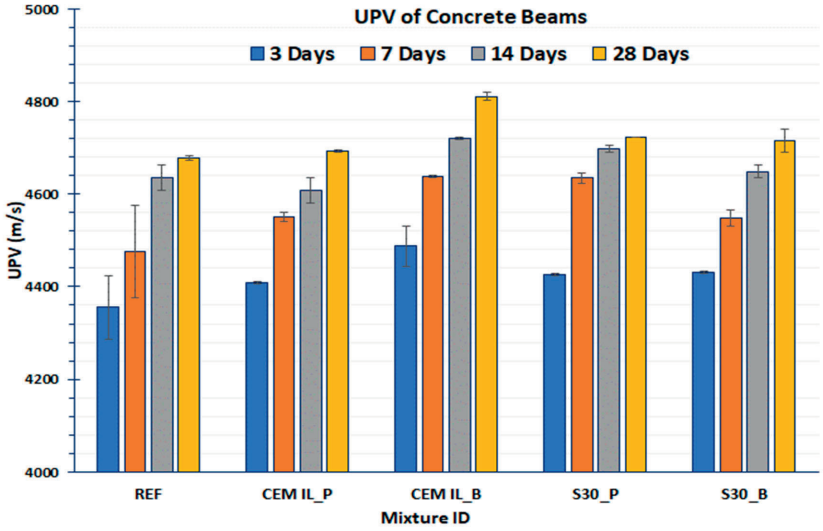


**Figure 3.4** Ultrasonic Pulse Velocity (UPV) of the Various Concrete Mixes at 3, 7, 14, and 28 Days.

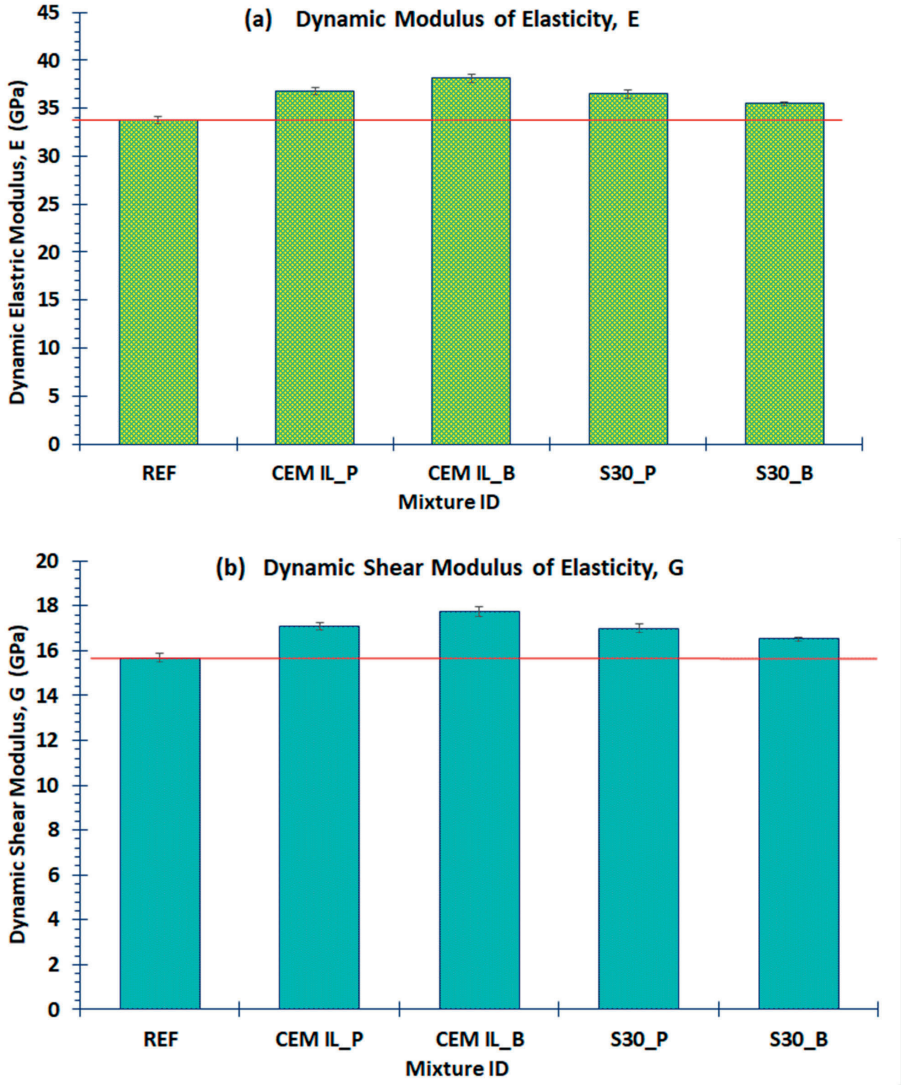


**Figure 3.5** (a) Dynamic Modulus of Elasticity, E, for Concrete Mixtures, and (b) Dynamic Shear Modulus of Elasticity, G, for Concrete Mixtures.

### 3.6 Conclusions and Implications

This study evaluated the performance of two distinct SAP delivery approaches: direct pouring and use of dissolvable bags. Findings provide valuable insights into the optimization of SAP application techniques with the following conclusions:

- Despite the SAP delivery approach used, there were reductions in slump values. For plain concrete mixtures, SAP addition by direct pouring resulted in higher air content and reduced workability, and, in contrast, SAP addition using dissolvable bags results in lower air content with slightly higher slump value. It is likely that direct pouring of dry SAP particles resulted in a greater amount of air being incorporated into the fresh mixtures, in comparison to the addition of one dissolvable bag of dry SAP.
- The dissolvable bag delivery method showed a notable improvement in compressive strength compared to direct pouring of SAP. Mixes with dissolvable bags generally outperformed those with direct pouring by approximately 10–20%, depending on the degree of air void reduction.
- UPV results showed enhanced microstructural integrity in specimens where SAP was added using dissolvable bags. The higher velocity in these specimens reflects reduced internal voids and denser microstructure. Conversely, direct pouring of SAP resulted in slightly lower UPV values.
- The enhanced elastic modulus is consistent with a stiffer material and improved microstructure observed in dissolvable bag specimens, underscoring the importance of controlled SAP integration in achieving superior elastic properties. The dynamic shear modulus also followed a similar trend, with higher values observed in dissolvable bag specimens. This suggests better resistance to shear deformations, critical for the durability and long-term performance of concrete.

While the dissolvable bag delivery system shows immense promise, further research is needed to address long-term effects, such as assessing the impact of residual bag materials, if any, on concrete microstructure and durability. Also, optimization and fine-tuning bag material properties may be necessary for faster dissolution and compatibility with different mix designs, including low-water mixtures for high performance and concrete printing applications.

## 4. PERFORMANCE OF PLAIN AND SLAG CEMENT MORTARS MODIFIED WITH SAP AND COLLOIDAL NANOSILICA SOLUTIONS

### 4.1 Overview

This section addresses Objective 1 of the JTRP project by evaluating the workability, water absorption, strength properties, and UPV of plain and slag cement mortars containing SAPs and colloidal nanosilica admixtures. It is well known that individual use of SAP and colloidal nanosilica enhances the hydration of cementitious mixtures. However, it remains unclear whether any beneficial synergy exists between SAP and colloidal nanosilica solutions, particularly in limestone-blended cement mixtures and mixtures containing SCMs. The goal of this section is to evaluate the early and later age performance of both plain Type IL cement mortars and mortars with 30% slag cement replacement, containing commercially available SAP particles and colloidal nanosilica solutions, used separately and in combination. The SAP-modified mortars exhibited enhanced performance attributed to improved hydration due to internal curing, especially when compared to mixtures without SAP. Results show that, relative to reference mixtures, mortars with SAP developed higher strength, attained higher UPV values, and demonstrated lower water absorption and drying shrinkage. These findings suggest a refinement and densification of the microstructure resulting from improved hydration. In plain and slag cement mortars, the addition of colloidal nanosilica admixtures alone was not effective in achieving optimum performance of the mortar, as it increased water absorption and drying shrinkage while reducing UPV and strength values.

This section has been published:

Ajuonuma, C. S., Tokpatayeva, R., Erk, K. A., Olek, J. (2025). Evaluation of performance of plain and slag cement mortars modified with superabsorbent polymers and nanosilica. *Transportation Research Record*. https://doi.org/10.1177/03611981251387127

### 4.2 Materials

The materials used in this study included potable water, fine aggregates, superplasticizers, air-entraining admixture, slag cement, Type IL cement, colloidal nanosilica, and SAP. The SAP particles used were polyacrylamide-based, with dry diameter of less than 300 µm (Figure 4.1a), and were incorporated at an approximate dosage of 0.2% SAP by weight of binder. Additionally, two commercially available colloidal nanosilica-based solutions were used in this study, referred to as Nanosilica 1 (NS1) and Nanosilica 2 (NS2), with the latter being a combination of NS1 and modified nanosilica. Both are proprietary materials consisting of solid nanosilica particles dispersed in a liquid medium, as illustrated in Figure 4.1b. A single batch of Type IL cement, conforming to ASTM standard specification (C595) for blended hydraulic cement specifications, was used throughout this research (ASTM, 2024g). The slag cement, Grade 100, conformed to the ASTM standard specification (C989) for slag cement use in concrete and mortars as used as a partial (30% by weight) replacement for Type IL cement (ASTM, 2024h). The chemical and physical characteristics of both Type IL cement and the slag cement were reported previously in Table 3.1. The fine aggregate used was locally sourced and met the INDOT standard specifications for #23 sand (INDOT, 2024b). The maximum particle size was 4.75 mm (0.187 in.), specific gravity and fineness modulus of 2.63 and 2.79, respectively. Clean, potable water, obtained from the research laboratory, was used throughout this study, in accordance with ASTM standard specification (C1602) for mixing water used in production of hydraulic cement concrete (ASTM, 2022c).

A modified polycarboxylate-based high-range WRA with a specific gravity at 20 °C (68 °F) of 1.062 ± 0.01, pH of 7.50 ± 2.00, solid content (halogens) of 25.00% ± 1.20%, $Na_2O$ equivalent ≤ 1.50%, $Cl^-$ equivalent ≤ 0.10% was used in combination with an air entraining admixture. The mortar mixture

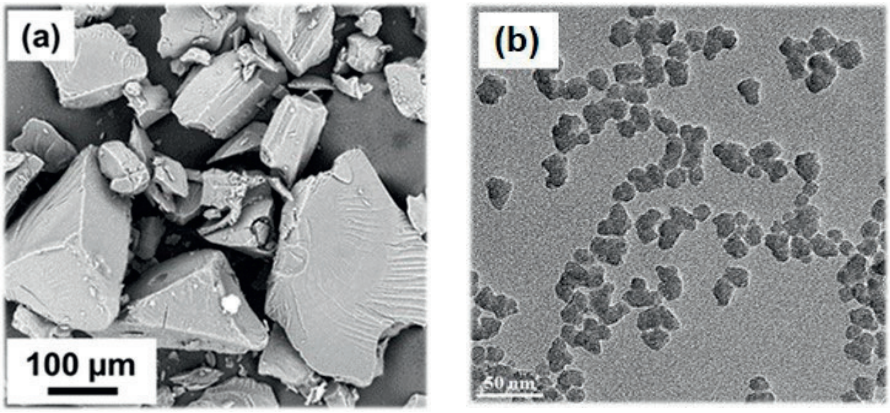


**Figure 4.1** (a) Scanning Electron Micrograph of Dry SAP Particles; (b) Transmission Electron Micrograph of Solid Silica Particles Present in the NS1 and NS2 Solutions.

designs used in this research were based on Class C concrete as per the INDOT standard specifications (INDOT, 2024a). The mortar mixture proportions were created following the guidelines outlined in ASTM standard guide (C1810) for comparing performance of concrete-making materials using mortar mixtures (ASTM, 2022a). A total of ten mixture proportions were designed, including the reference mixture (with Type IL cement as the sole binder), a mixture containing 30% (by weight of the total binder) of grade 100 slag cement as a replacement for Type IL cement, and mixtures containing various combinations of colloidal nanosilica solutions and SAP particles, as shown in Table 4.1.

No extra water was added to these mixtures to compensate for the water absorbed by the SAP particles. Although the addition of SAP did decrease the workability of the fresh mixtures, all mixtures were within the target flow range (170–230 mm) and were successfully cast. A previous study from Adams, Bose, Olek, and Erk (2022) determined that extra water is not necessary for mixtures containing SAP unless their workability is severely compromised (e.g., to the point where the mixture cannot be cast). In those few cases, WRA can be added to improve workability without negatively affecting the later-age compressive strength.

The mixes were labeled based on the materials used, as follows and used in Table 4.1:

- REF: The reference mix with Type IL cement
- REF+NS1: Mixes containing one colloidal nanosilica solution
- REF+NS2: Mixes with a combination of the two colloidal nanosilica solutions
- S30: Mixes with 30% cement replacement by slag cement
- S30+NS1: Mixes with 30% slag and one colloidal nanosilica solution
- S30+NS2: Mixes with 30% slag and a combination of the two colloidal nanosilica solutions
- REF+SAP: Mixes incorporating 0.2% superabsorbent polymer by weight of binder
- S30+SAP: Mixes with 30% slag and SAP
- S30+SAP+NS1: Mixes with 30% slag, SAP, and one colloidal nanosilica solution
- S30+SAP+NS2: Mixes with 30% slag, SAP, and a combination of the two colloidal nanosilica solutions

TABLE 4.1
**Mortar Mixture Designs.**

| Mixture ID | w/b | Cement (kg/m$^3$) | Fine Agg (kg/m$^3$) | Water (kg/m$^3$) | Slag (kg/m$^3$) | Nanosilica (mL/100 kg) | SAP (kg/m$^3$) | HRWRA (mL/100 kg) | AE (mL/100 kg) |
|---|---|---|---|---|---|---|---|---|---|
| REF | 0.44 | 364 | 939 | 160 | | | | 184 | 74 |
| REF+NS1 | 0.44 | 364 | 939 | 160 | | NS1: 261 | | 184 | 74 |
| REF+NS2 | 0.44 | 364 | 939 | 160 | | *NS2: 783 | | 184 | 74 |
| S30 | 0.44 | 255 | 939 | 160 | 109 | | | 184 | 74 |
| S30+NS1 | 0.44 | 255 | 939 | 160 | 109 | NS1: 261 | | 184 | 74 |
| S30+NS2 | 0.44 | 255 | 939 | 160 | 109 | *NS2: 783 | | 184 | 74 |
| REF+SAP | 0.44 | 364 | 939 | 160 | | | 0.73 | 553 | 74 |
| S30+SAP | 0.44 | 255 | 939 | 160 | 109 | | 0.73 | 553 | 74 |
| S30+SAP+NS1 | 0.44 | 255 | 939 | 160 | 109 | NS1: 261 | 0.73 | 553 | 74 |
| S30+SAP+NS2 | 0.44 | 255 | 939 | 160 | 109 | *NS2: 783 | 0.73 | 553 | 74 |

Note: * NS2 is a combination of two colloidal nanosilica solutions (**NS1** (261 mL/100 kg) + **modified NS1** (522 mL/100 kg).
1 kg/m$^3$ = 1.686 lb/yd$^3$

## 4.3 Methods

### *4.3.1 Mixing of Mortars and Preparation of Test Specimens*

Reference mortar mixtures were prepared from the concrete mixture proportions to quantities suitable for mortar mixtures as stipulated in ASTM standard guide (C1810) for comparing performance of concrete-making materials using mortar mixtures with a constant ratio of cementitious (cement + slag) to sand by weight of 1:2.58 (ASTM, 2022a). The w/b ratio was kept at a constant value of 0.44 and the high-range WRA dosage was varied according to mixture compositions and requirements, ranging from 0.17–0.50% of the weight of the binder. The slag cement was added as 30% replacement of the cement, and the colloidal nanosilica solutions were added in proportions of 4 oz/cwt (261 mL/100 kg) for NS1 and 12 oz/cwt (780 mL/ 100 kg) for NS2.

Mixing of mortars was performed at room temperature using the mechanical mixer conforming to the requirements of the ASTM standard practice (C305) for mechanical mixing of hydraulic cement pastes and mortar of plastic consistency (ASTM, 2020a). Each mortar mixture preparation began with dry mixing of the solid components (sand, cement, and, depending on the mixture, slag and SAP) for 30 s at low speed (140 ± 5 r/min). Subsequently, a portion of the mix water was added, and mixing continued at a medium speed for 2 min until consistent homogeneity was achieved. The remaining water, part of which was premixed with the superplasticizer, was then incorporated. This was followed by an additional 3 min of mixing at medium speed (285 ± 10 r/min). The mixer then stopped, and the mixture was let to rest for 1 min. After this, the mortar collected on the sides of the mixing pan was scraped down into the batch, and mixing resumed at medium speed for 30 s. The mixer then stopped, set to medium speed, and mixing continued for 1 min. The impact of SAP, slag cement, and colloidal nanosilica on flow and workability of different mortar mixes was evaluated using the flow table test and the mini slump cone test, as specified in ASTM standard test method (C1437) for flow of hydraulic cement mortar and ASTM standard guide (C1810) for comparing performance of concrete-making materials using mortar mixtures, respectively (ASTM, 2015, 2022a).

Following the slump and flow tests, the mortar mixtures were cast into molds of various dimensions to prepare specimens for mechanical and durability testing: 50 × 50 × 50 mm (2 × 2 × 2 in.) cubic molds for compressive strength, 40 × 40 × 160 mm (1.57 × 1.57 × 6.3 in.) beam molds for flexural strength, and 25 × 25 × 285 mm (1 × 1 × 11 in.) prismatic molds for drying shrinkage. After filling, the molds were vibrated for 1 min using a vibrating table to eliminate entrapped air bubbles. Following casting, the molds were covered with plastic sheets and left undisturbed at an ambient temperature for 24 hr. The specimens were then demolded, covered with plastic sheets, and air-cured in the laboratory at 23 °C (73.4 °F), except for the drying shrinkage samples for which the curing regime used is subsequently discussed. The curing period lasted either 3, 7, or 28 days, depending on the test. Three specimens were tested for flexural and compressive strength, while four samples were used for the drying shrinkage evaluation.

### *4.3.2 Flexural Strength and Compressive Strength*

The flexural strength of the mortars was evaluated following ASTM standard test method (C348) for flexural strength of hydraulic cement mortars after 7 and 28 days of curing (ASTM, 2021b). Similarly, the compressive strength was evaluated following the procedures outlined in ASTM standard test method (C109) for compressive strength of hydraulic cement mortars, using 50 mm (2 in.) cube specimens, with machine loading rate consistently maintained at 1 kN/s (224.8 lbf/s; ASTM, 2024c).

### *4.3.3 Water Absorption*

The percent absorption test was performed according to ASTM standard test (C642) method for density, absorption and voids in hardened concrete on 50 × 50 × 50 mm (2 × 2 × 2 in.) mortar cubes which were air-cured at 23 °C (73.4 °F) for 28 days (ASTM, 2021a). The specimens were first weighed, then placed in an oven at 105 ± 5 °C (221 ± 41 °F) for 24 hr and weighed again to obtain comparative mass, with the difference between two successive values not exceeding 0.5% of the lowest value recorded. The specimens were then immersed in water at 21 °C (70 °F) for not less than 48 hr, and the saturated surface-dried mass was determined when two successive values of mass of the surface-dried sample at intervals of 24 hr show an increase in mass of less than 0.5% of the larger value, after which the absorption is determined.

### *4.3.4 Ultrasonic Pulse Velocity*

The UPV test was conducted in accordance with ASTM standard test method (C597) for ultrasonic pulse velocity through concrete on 40 × 40 × 160 mm (1.57 × 1.57 × 6.3 in.) beams, air-cured for 28 days at a temperature of 23 °C (73.4 °F; ASTM, 2022f). A pair of piezoelectric transducers (transmitter and receiver) with a resonant frequency of 54 kHz were used in direct transmission mode, and a gel couplant was applied to ensure proper acoustic contact between the transducer and the cementitious mortar specimens.

## 4.4 Results and Discussions

### *4.4.1 Flow*

The results of the flow table test are presented in Table 4.2. The REF mixture exhibited a flow of 223 mm (8.78 in.), with reference mixtures containing colloidal nanosilica admixtures (NS1 and NS2) showing similar flow of 220 mm and 214 mm (8.66 in. and 8.42 in.), respectively. Comparable flow values were also observed in mixtures containing slag, both with and without colloidal nanosilica. As expected, the addition of SAP to the reference mixture reduced its flow value to 200 mm (8 in.), a 10% reduction. A similar reduction in flow was observed in the three slag mixtures containing either SAP alone or SAP in combination with NS1 and NS2.

TABLE 4.2
**Fresh Properties of Mortars with Varying Mixture Compositions.**

| Mixture ID | w/b | Flow (mm) | Slump (mm) |
|---|---|---|---|
| REF | 0.44 | 223 | 96 |
| REF+NS1 | 0.44 | 220 | 97 |
| REF+NS2 | 0.44 | 214 | 73 |
| S30 | 0.44 | 220 | 92 |
| S30+NS1 | 0.44 | 225 | 98 |
| S30+NS2 | 0.44 | 225 | 104 |
| REF+SAP | 0.44 | 200 | 54 |
| S30+SAP | 0.44 | 203 | 80 |
| S30+SAP+NS1 | 0.44 | 191 | 46 |
| S30+SAP+NS2 | 0.44 | 196 | 41 |

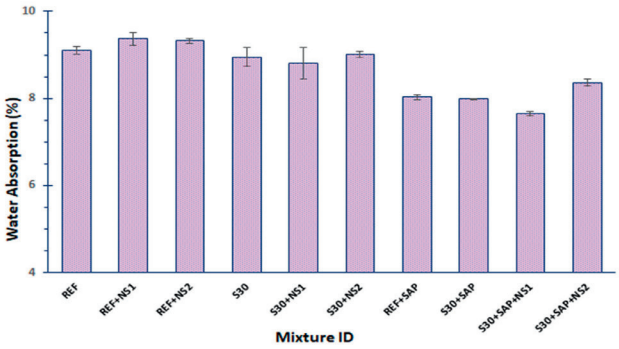


**Figure 4.2** Water Absorption for Cementitious Mortar at 28 Days.

### *4.4.2 Workability*

The workability of the cement mortars was evaluated using the mini slump cone test, with results ranging from 41–104 mm (1.61–4.09 in.) as presented in Table 4.2.

The REF mixture and REF+NS1 exhibited similar slump values of 96 mm (3.78 in.) and 97 mm (3.82 in.), respectively. However, REF+NS2 experienced 24% reduction in slump, with a value of 73 mm (2.87 in.). This reduction in slump can be attributed to higher dosage of colloidal nanosilica. The mixes with slag cement alone, as well as those with slag cement and either of the two colloidal nanosilica admixtures, exhibited slump values similar to REF. As expected, the addition of SAP particles significantly reduced the slump of the reference mixture, resulting in a 44% decrease compared to SAP-free reference, with a recorded slump of 54 mm (2.12 in.). A greater slump reduction was observed in the SAP-modified mixes containing slag cement and colloidal nanosilica, with values of 46 mm (1.81 in.) in the system with NS1 and 41 mm (1.61 in.) in a system with NS2.

Recent studies on improving the workability of SAP-containing mixtures suggest that adding extra water is the most cost-effective method for restoring flow (Hasholt & Jensen, 2015; Snoeck et al., 2014; Snoeck, Velasco, et al., 2015). A more conventional approach involves incorporating greater dosages of high-range WRA which will improve the workability of the mixture without reducing its compressive strength (Adams, Bose, Olek, & Erk, 2022; Krafcik & Erk., 2016; Mechtcherine et al., 2017; Mignon et al., 2015). Researchers have also explored a combination of these strategies in SAP-modified cementitious systems (Ma et al. 2017).

### *4.4.3 Water Absorption*

The water absorption value for REF at 9.1% sets the baseline for comparison, with other values ranging between 7.7–9.4%, as shown in Figure 4.2. Higher absorption indicates higher porosity, which may negatively impact durability. The addition of colloidal nanosilica to the plain mortar mix (REF+NS1 and REF+NS2) slightly increased the water absorption, by 2.7 and 2.3%, respectively. The S30 mixture exhibited a slightly lower water absorption (8.9%) when compared with REF. The combination of slag cement with colloidal nanosilica (S30+NS1 and S30+NS2) resulted in water absorption values similar to S30. The incorporation of SAP in REF and S30 resulted in significantly reduced absorption values, which were further reduced in the presence of NS1 but increased with NS2.

### *4.4.4 Flexural Strength*

Mortar beams were tested for flexural strength at 7 and 28 days, with strength values ranging from 3.4–5.7 MPa (493–827 psi) and 3.5–6.3 MPa (508–914 psi), respectively, as shown in Figure 4.3. The INDOT 2024 standard specifications recommends a minimum modulus of rupture value for concrete at 7 days as 3.9 MPa (570 psi; (ASTM, 2021b). The addition of both the colloidal nanosilica solutions and slag either maintained or slightly improved the flexural strength at 7 days. However, the trends were reversed at 28 days, with the decline in flexural strength observed in some of the mixes. Mixtures containing SAP displayed significant increases in both 7- and 28-days strength values compared with the REF and S30 control mixtures. Also, interestingly, comparison of the slag-cement mortar mixes without SAP (S30, S30+NS1 and S30+NS2) and those with SAP (S30+SAP, S30+SAP+NS1 and S30+SAP+NS2), shows significant increase in flexural strength. The combination of slag, SAP and colloidal nanosilica admixtures effectively improved the flexural strength, especially at later age.

### *4.4.5 Compressive Strength*

Figure 4.4 presents the compressive strength trends of plain and slag cement mortar mixtures determined at 3, 7, and 28 days. The addition of slag (S30) led to a 16% increase in 3-day strength compared to the plain cement mixture (REF). However, a moderate strength reduction was observed at later ages for S30 compared to REF. Nonetheless, it is worth mentioning that factors such as dilution effect, resulting from lesser cement content, and the curing regime used (mortar samples were covered with plastic sheet and stored in air at room temperature) might have resulted in lesser degree of hydration of cement, thereby affecting the strength properties at 7 and 28 days. Additionally, since slag is a latent hydraulic material, its reactivity is slower than

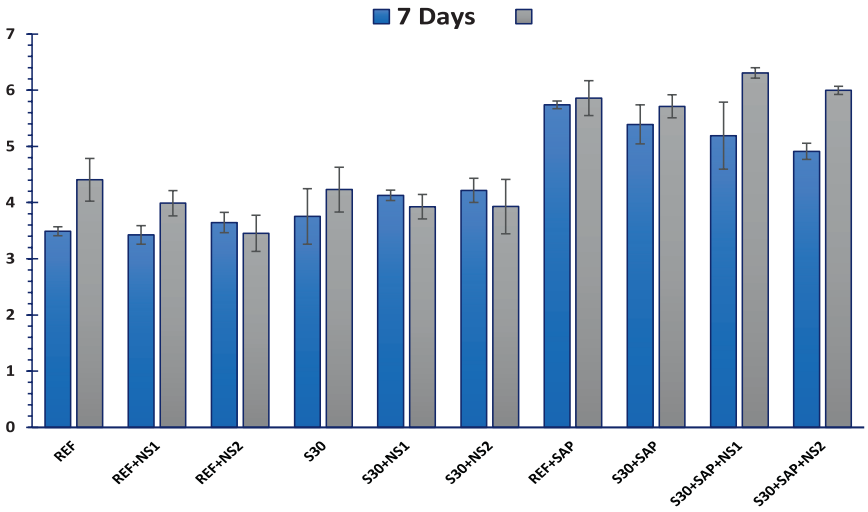


**Figure 4.3** Cement Mortar Flexural Strength for All Mixture Composition. Note: 1 MPa = 145.04 psi.

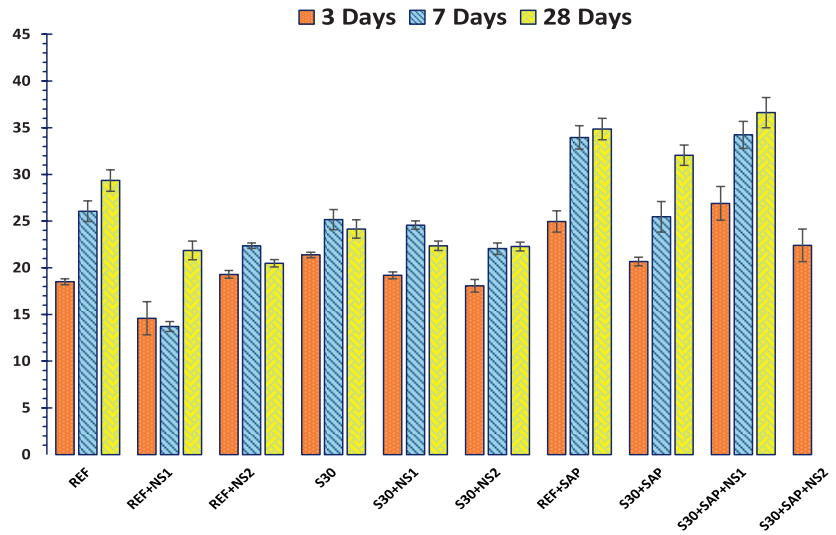


**Figure 4.4** Cement Mortar Compressive Strength for All Mixture Compositions. Note: 1 MPa = 145.04 psi.

that of portland cement, and higher strength gains are expected at later ages (i.e., 56 and 90 days).

Plain and slag cement mixtures incorporating SAP achieved strengths comparable to or higher than both reference mixtures, REF and S30, at all ages. At 3 days, the SAP-modified mixture achieved a strength of 25.0 MPa (3626 psi), representing a 35% increase compared to REF (18.5 MPa [2683 psi]). This strength enhancement continued at 7 and 28 days, with values reaching 34.0 MPa (4931 psi) and 34.9 MPa (5062 psi), corresponding to 30% and 19% increases, respectively. In contrast, the addition of NS1 and NS2 to plain and slag cement mixtures resulted in significantly reduced strength values in almost all cases, with the exception of the 3-day strength of REF+NS2 which were comparable to REF. These results highlight the positive influence of SAPs in promoting hydration and mitigating self-desiccation, leading to improved long-term strength development.

### *4.4.6 Ultrasonic Pulse Velocity*

Figure 4.5 shows the UPV results for the mortars studied. The UPV values ranged from ~3300 m/s to 3800 m/s. Generally, UPV is expected to increase with the age of the mortar as the continuous hydration of cement particles generates more hydration products, which fill the capillary pores and densify the matrix. In this study, although all mortar samples were tested at the age of 28 days, mortars modified by the addition of SAP displayed the highest UPV values, reaching 3800 m/s. This indicates refinement and densification of microstructure. Also,

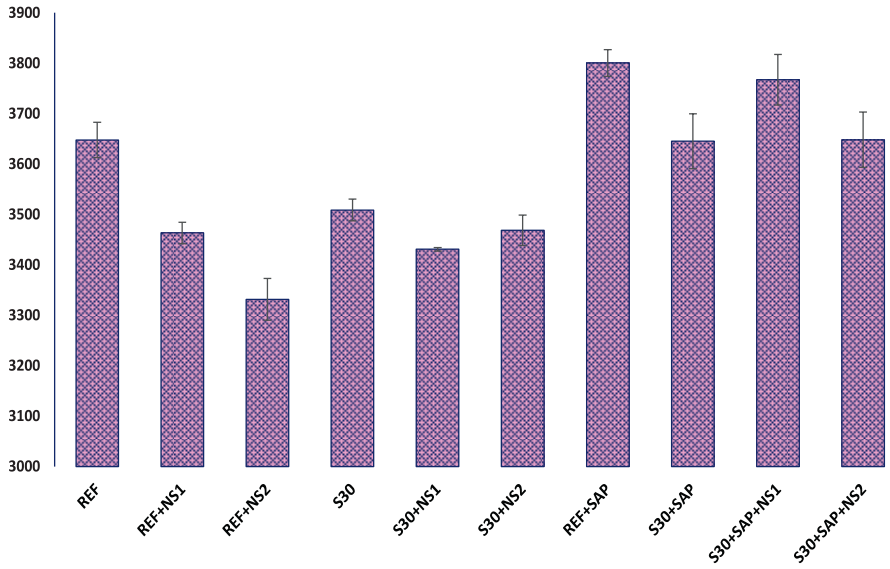


**Figure 4.5** Ultrasonic Pulse Velocity (UPV) of the Various Mixture Compositions.

the SAP-modified mortar mixes with slag and colloidal nanosilica solutions either maintained or surpassed the UPV values of the reference mortar with values of 3646 m/s, 3767 m/s, and 3648 m/s, respectively. In contrast, the addition of colloidal nanosilica solutions, NS1 and NS2, to the plain and slag cement mortars resulted in significantly reduced UPV values. Overall, the results obtained were in good agreement with water absorption and compressive strength results.

### 4.5 Conclusions and Implications

Overall, this study shows that the incorporation of SAP is sufficient to internally cure Type IL plain cement and slag cement mortars, forming a dense cement microstructure that displays greater flexural and compressive strength. From the experimental results, the following conclusions can be drawn:

- The addition of SAP to Type IL cementitious mixtures significantly improved the performance of both plain and slag-modified mortars. Data from water absorption measurements and UPV suggested that the presence of SAP increased the density of the cementitious matrix in comparison to the SAP-free reference mortars. This resulted in the observed increases in flexural and compressive strength for SAP-containing mixtures.
- The addition of colloidal nanosilica solutions to the Type IL mixtures reduced the overall performance of most plain and slag-modified mortars. There was no evidence of microstructure refinement, as the addition of colloidal nanosilica did not significantly change the water absorption values and significantly decreased the UPV values, compared with results for the nanosilica-free reference mortars. Additionally, the flexural and compressive strength of both plain and slag-modified mortars remained the same or decreased in the presence of colloidal nanosilica.
- Some additional performance increases were observed for ternary blends of slag, SAP, and colloidal nanosilica. Data trends were similar to the SAP-containing mortars but with a notable increase in 28-day flexural strength and compressive strength at all ages in the presence of a single nanosilica solution (NS1). When the nanosilica solutions were combined (NS2), the strength increases were reduced.

## 5. IMPACT OF SAP ON THE HYDRATION KINETICS OF PLAIN AND SLAG CEMENT-MODIFIED CEMENTITIOUS PASTES

### 5.1 Overview

This section addresses Objective 1 of the JTRP project by investigating the influence of SAP on the hydration kinetics of plain and slag cement-modified cementitious pastes using isothermal calorimetry. Key findings indicate that SAP significantly alters the hydration profile of both plain and slag cement pastes. In plain cement, SAP accelerates early hydration due to improved water availability, leading to enhanced initial reaction rates. For slag cement pastes, SAP sustain hydration over extended periods, promoting the pozzolanic reaction between slag and calcium hydroxide. This delayed reaction results in prolonged heat evolution and improved long-term hydration efficiency. The study highlights the potential of SAP to optimize hydration kinetics, reduce autogenous shrinkage, and improve microstructural development in both plain and slag cement systems, contributing to more durable and sustainable cementitious materials.

### 5.2 Methods

Isothermal calorimetry testing was conducted on cementitious pastes following the ASTM standard practice (C1679) for measuring hydration kinetics of hydraulic cementitious mixtures using isothermal calorimetry standard at a temperature of 23 °C (73.4 °F; ASTM, 2022b). The materials and mixtures described in this section are the same as those described in the

previous chapter, see Section 4.2. To prepare the test specimens, 50 g cementitious materials were weighed, and the required amount of water needed to achieve the target w/b ratio of 0.44 was measured out. When preparing paste specimens containing slag or SAP, these ingredients were first dry mixed by hand for 2 min to ensure uniformity before the mixing water was added. Once the water was incorporated, all ingredients were then hand mixed for an additional 2 min to obtain a homogeneous paste. Once mixed, approximately 10 g of the paste was carefully transferred into a pre-tared glass ampoule, which was then hermetically sealed using caps firmly secured with a crimping tool. Eyelets were installed on the caps to facilitate placement and removal of the ampoules from the calorimeter. Heat flow data were collected using TAM Air Isothermal Calorimeter for 14 days. This extended testing period, compared to the more typical 7 days, was adopted to evaluate the internal curing performance of SAP-modified pastes over a prolonged hydration period. Since SAPs gradually release stored water, their effect on hydration extends beyond the early stages, requiring extended monitoring to capture their continued influence beyond the initial 7 days. It should be noted that, despite the relatively small heat output beyond the 7 days, there was no observable drift in the data and therefore the data was deemed to be reliable.

## 5.3 Results

Key parameters derived from the heat flow curves and cumulative heat curves are summarized in Table 5.1. The heat flow results for all paste mixtures (Figure 5.1) contained an early peak, occurring within the first hour, corresponding to the initial wetting process and the dissolution of cementitious particles. Following this, a dominant hydration peak was observed between 1–7 hr, which was primarily associated with the hydration of alite ($C_3S$), a key compound in portland cement. The formation of calcium silicate hydrates and calcium hydroxide accelerated during this phase, contributing to hardening. The incorporation of additives such as slag, SAP, and colloidal nanosilica modified this reaction. Secondary humps were observed between 9–12 hr in the heat flow curves (Figure 5.1). These secondary humps were attributed to the formation of calcium sulfo-aluminates and carboaluminates and were less visible in mixtures containing SAP. Additionally, the Type IL cement also influenced the hydration process as the fine limestone particles act as a nucleation site, promoting the formation of the C-S-H. On the other hand, the formation of carboaluminates may compete with formation of calcium sulfo-aluminates, potentially leading to reduction in the intensity of the second peak.

The addition of SAP and slag resulted in a reduction of the height of the hydration peak by 4.9% and 6.6%, respectively. The corresponding heat flow values for these mixtures

TABLE 5.1
**Heat Flow (mW/g) and Cumulative Heat Generated (J/g) After 14 Days.**

| Mixture ID | Heat Flow at the Hydration Peak (mW/g) | Time to Peak hydration (hr) | Thermal Setting Time (hr) | Cumulative Heat Generated (J/g) |
|---|---|---|---|---|
| REF | 4.52 | 7.04 | 2.81 | 338.16 |
| REF+NS1 | 4.50 | 7.01 | 2.79 | 333.57 |
| REF+NS2 | 4.54 | 6.89 | 2.75 | 365.58 |
| S30 | 4.22 | 7.30 | 2.90 | 342.28 |
| S30+NS1 | 4.21 | 7.30 | 2.95 | 347.82 |
| S30+NS2 | 4.23 | 7.18 | 2.85 | 332.05 |
| REF+SAP | 4.30 | 7.03 | 2.82 | 336.78 |
| S30+SAP | 4.22 | 7.13 | 2.85 | 334.06 |

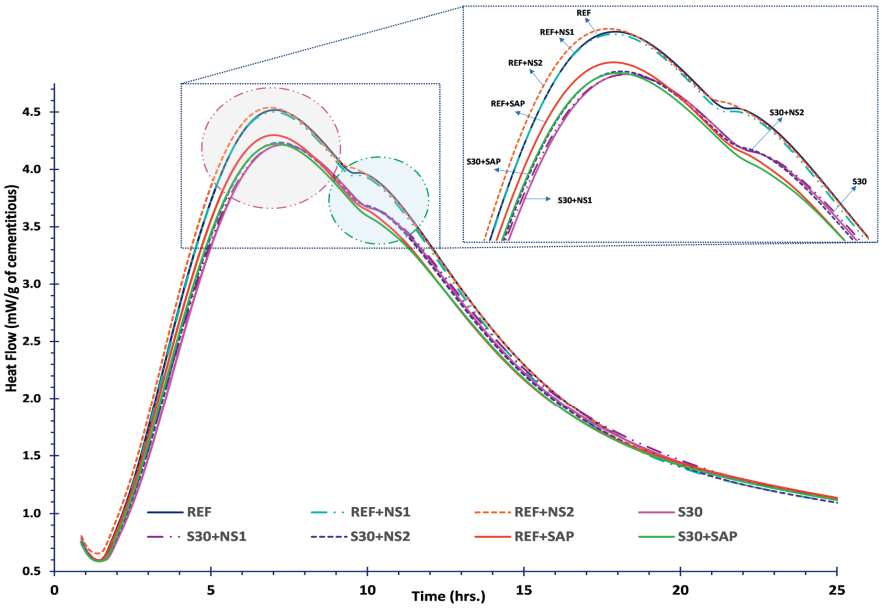


**Figure 5.1** Isothermal Calorimetry Curves Showing Heat Flow (mW/g) for Cement Pastes.

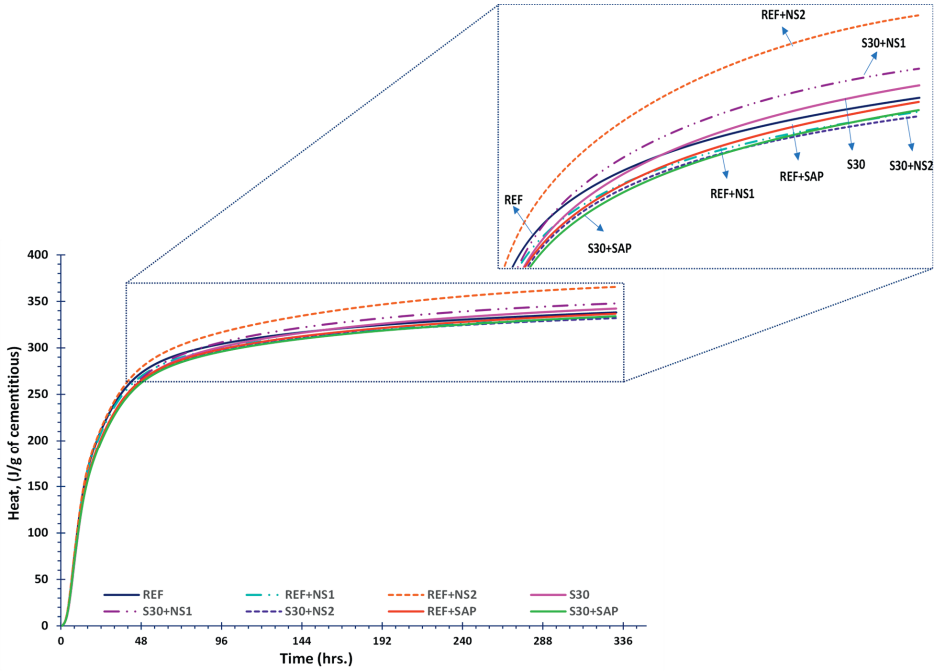


**Figure 5.2** Cumulative Heat (J/g) Generated by Hydrating Cementitious Pastes.

were 4.3 and 4.2 mW/g, respectively. Additionally, as shown in Figure 5.1, the incorporation of colloidal nanosilica into the reference mixture (REF+NS1) did not cause significant changes in the hydration kinetics. The heat flow curves for REF+NS1 closely matched those of the reference mix, with the two curves nearly superimposing each other, suggesting that nanosilica did not significantly alter the early hydration behavior.

It is worth noting that the acceleration part of the curve for REF +NS2 was somewhat steeper than the corresponding sections of the curves for the other mixtures. This indicates a faster early hydration rate for the mix with NS2. Additionally, this mixture developed a higher main peak (indicated by the purple circle in Figure 5.1), suggesting a more pronounced or accelerated hydration reaction compared to all other mixes. This could be attributed to the higher concentration of nanosilica particles in NS2 compared to NS1, as the heat flow curve for REF+NS1 was practically identical to that of REF. On the other hand, all mixes containing slag exhibited a somewhat slower acceleration rate, indicated by a shallower slope of the acceleration portion of the heat flow curve, which slightly increased the final setting time.

Another interesting observation was the disappearance of the second hump, known as sulfate depletion peak, in the mixes upon addition of the SAP (see green circle in Figure 5.1). This phenomenon can be attributed to the dominance of the hydration of the silicates over the formation of calcium-sulfate-hydrates, facilitated by continuous supply of water by SAPs over a period of 8–10 hr after mixing. As mentioned earlier, SAP particles absorb water and release it gradually over time, contributing to internal curing. This ensures steadier hydration process, which can improve durability and reduce the risk of cracking in hardened concrete.

The curves presented in Figure 5.2 show that the cumulative heat generated by the hydrating reference paste with NS2 (REF+NS2) was the highest. The cumulative heat of the hydrating reference cementitious paste incorporating SAP (REF+SAP) was about 336.8 J/g, which was slightly lower (~0.4%) than the cumulative heat of 338.2 J/g observed in the reference mixture (REF).

## 5.4 Conclusions

The heat flow results for all mixtures show an early peak within the first hour, followed by a dominant hydration peak associated with the hydration of alite between 1–7 hr. The incorporation of additives such as slag cement, colloidal nanosilica, and SAP modifies the hydration reactions. Key findings are as follows:

- For mixtures containing colloidal nanosilica, NS2 exhibited a steeper curve and higher hydration peak when compared to NS1, suggesting higher concentration of colloidal nanosilica particles in the solution.
- Slag cement pastes showed a reduced acceleration rate (shallow slope), which slightly increased the final setting time.
- The addition of SAP results in the disappearance of the secondary hump (sulfate depletion peak), suggesting the dominance of the hydration of the silicates over the formation of calcium-sulfate-hydrates, facilitated by continuous supply of water by SAP over a period of 8–10 hr after mixing.
- The inclusion of SAP and slag resulted in reductions of 4.9% and 6.6%, respectively, in the maximum heat flow in main hydration peak. The cumulative heat generated by the hydrated cementitious paste incorporating SAP was just slightly (0.4%) lower than the values obtained for the reference mixture.

## 6. PRACTICAL IMPLEMENTATION OF SAP FOR INTERNALLY CURED CONCRETE

### 6.1 Overview

This section addresses Objective 3 of the JTRP project by demonstrating the practical implementation of ready-mixed internally cured concrete using superabsorbent polymers in collaboration with a local concrete provider. Six concrete mixtures were created with Type IL cement at a constant w/b of 0.44 and including various amounts of SAP, slag, and colloidal nanosilica solutions. Comprehensive characterization was conducted to evaluate workability, air content, hydration kinetics, compressive strength, flexural strength, and durability (rate of water absorption, scaling resistance, chloride penetration depth, and resistivity). Results from the year-long evaluation demonstrated that plain cement concrete internally cured by SAP displayed increased strength and durability compared to SAP-free concrete, concrete containing colloidal nanosilica solutions, and concrete that was externally cured with a surface-applied curing compound. Additionally, concrete mixtures incorporating SAP and slag cement showed improved performance in comparison to SAP-cured plain cement and no-SAP slag-cement concrete mixtures. This indicates an interesting synergy between SAP, slag, and Type IL cement.

### 6.2 Composition of Concrete Mixtures

The concrete mixtures used in the field trial were designed based on INDOT's Class C concrete specifications (658 lb/yd$^3$ [390 kg/m$^3$] of cementitious materials) in accordance with Section 702 of the Indiana Department of Transportation standard specifications 2024 (INDOT, 2024a). A total of six different mixtures were produced, with their target compositions summarized in Table 6.1. As already mentioned, all field mixtures were designed to be batched at a constant w/b of 0.44. The plain reference mixture (REF) labeled #6 contained 658 lb/yd$^3$ (390 kg/m$^3$) of Type 1L cement whereas the reference slag cement mixture (REF+Slag) labeled #8 contained 30% weight replacement of cement by Grade 100 slag cement. The chemical and physical characteristics of Type IL cement and slag cement were reported previously in Table 3.1. Companion plain and slag cement mixtures containing SAP were also produced. These mixtures contained approximately 0.15% SAP by the weight of the binder and were labeled #10 ("REF+SAP") and #11 (REF+Slag+SAP). The final two mixtures were plain and slag cement mixtures modified by the addition of 4 oz/cwt (261 mL/100 kg) of colloidal nanosilica. These mixtures were labeled as #7 (REF+NS1) and #9 (REF+Slag+NS1). It is important to note that all field-cast mixtures, with and without SAP, were created without the use of any extra mixing water or the addition of workability-enhancing admixtures like WRA.

The materials used in the concrete mixtures included potable water, fine aggregate, coarse aggregate (maintained at saturated surface dry (SSD) condition), slag cement (Grade 100), Type IL cement, colloidal nanosilica solution (at a dosage of 4 oz/cwt [261 mL/100 kg]), commercially available SAP particles, and an air-entraining admixture (Sika® Air 260). Both the fine and coarse aggregates were locally sourced and conformed to INDOT standard specifications for #23 natural sand and #8 limestone, respectively (INDOT, 2024b). The fine aggregate had a maximum particle size of 4.75 mm, a specific gravity of 2.63, and a fineness modulus of 2.79. The specific gravity of the coarse aggregate was 2.65.

### 6.3 Batching and Mixing Procedures

All mixtures were produced in September 2023 at a commercial ready-mixed concrete plant located in Westfield, Indiana, using a fully automated batching and mixing system. Dry SAP particles were incorporated into the concrete mixtures using dissolvable bags (see Figure 6.1 and Chapter 3 for additional details) which were manually added directly into the mixer. Each bag contained 1 lb of dry SAP particles, and the dosage rate was one bag per cubic yard of concrete (equivalent to approximately 0.15% SAP by weight of binder). Before being added to the mixer, the dissolvable bags were removed from

**Figure 6.1** Dry SAP Particles in 8 × 6 in. Dissolvable Bags.

TABLE 6.1
**Target Concrete Mixture Proportions.**

| Slab # | Mixture ID | w/b | Cement (lb/yd$^3$) | Coarse Aggr. (lb/yd$^3$) | Fine Aggr. (lb/yd$^3$) | Nanosilica (fl oz/cwt) | Slag (lb/yd$^3$) | SAP (lb/yd$^3$) | AE (fl oz/cwt) |
|---|---|---|---|---|---|---|---|---|---|
| 6 | REF | 0.44 | 658 | 1630 | 1160 | | | | ~0.9 |
| 7 | REF+NS1 | 0.44 | 658 | 1630 | 1160 | 4 | | | ~0.8 |
| 8 | REF+Slag | 0.44 | 461 | 1630 | 1160 | | | | ~0.8 |
| 9 | REF+Slag+NS1 | 0.44 | 461 | 1630 | 1160 | 4 | 197 | | ~0.8 |
| 10 | REF+SAP | 0.44 | 658 | 1630 | 1160 | | 197 | 1 | ~0.8 |
| 11 | REF+Slag+SAP | 0.44 | 461 | 1630 | 1160 | | 197 | 1 | ~0.9 |

Note: 1 lb/yd$^3$ = 0.5933 kg/m$^3$, 1 fl oz/cwt = 65 mL/100 kg.

their outer waterproof plastic storage bags. As previously noted, no water-reducing admixtures were used in the SAP-containing mixtures, and no additional batching adjustments were required. The bags dissolved completely, and there was no visual evidence of dry SAP particles after standard mixing procedures.

### 6.4 Casting of the Slabs and Companion Test Specimens

Once batched, the mixes were used to cast six different slabs. The casting of slabs involved placing concrete in wooden formworks with dimensions of 8 ft × 8 ft × 10 in. (2.44 m × 2.44 m × 25.4 cm) (Figure 6.2 and Figure 6.3). As shown in Figure 6.2, polystyrene discs approximately 11 in. (280 mm) in diameter were inserted into partially shortened 5-gallon plastic buckets. These assemblies were then affixed to wooden planks and installed inside the formworks. These units served as block-outs to delineate the location of circular specimens within the slabs which were later extracted and used for the determination of scaling resistance of concrete.

In addition to the six slabs, a total of 198 cylindrical specimens 4 × 8 in. (100 × 200 mm) were cast for compression, resistivity, and rate of water absorption test, as shown in Figure 6.4. Half of these cylinders were sealed and transported to the Pankow Laboratory at Purdue University where they were demolded after 24 hr and cured in lime-saturated water until testing. The remaining cylinders were treated with a curing compound and stored in an environmental chamber at Purdue until testing. Furthermore, twelve beams measuring 6 × 6 × 18 in. (152.4 × 152.4 × 457.2 mm) were prepared for flexural strength testing, as shown in Figure 6.5, and eighteen beams 3 × 3 × 12 in. (76.2 × 76.2 × 304.8 mm) were cast for drying shrinkage measurements.

A general view of various slabs cast during the field trials is provided in Figure 6.6. Each slab, along with at least one companion cylinder from the same batch, was instrumented with a thermocouple placed at mid-depth and connected to the datalogger to monitor the temperature history of the concrete (Figure 6.7 and Figure 6.8). Concrete cores were extracted from

**Figure 6.2** Assembled Formwork for Slab Casting.


**Figure 6.3** Field Casting of 8 ft × 8 ft × 10 in. Concrete Slabs.

**Figure 6.4** Field-Cast 4 × 8 in. Concrete Cylinders.

**Figure 6.5** Field-Cast 6 × 6 × 18 in. Concrete Beams.


**Figure 6.6** Overview of the Slabs Cast in the Field.

**Figure 6.7** Thermocouples Embedded in Concrete Cylinders.

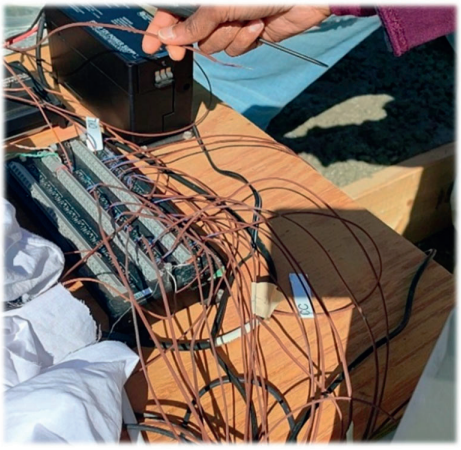

**Figure 6.8** Datalogger for Monitoring Concrete Temperature.

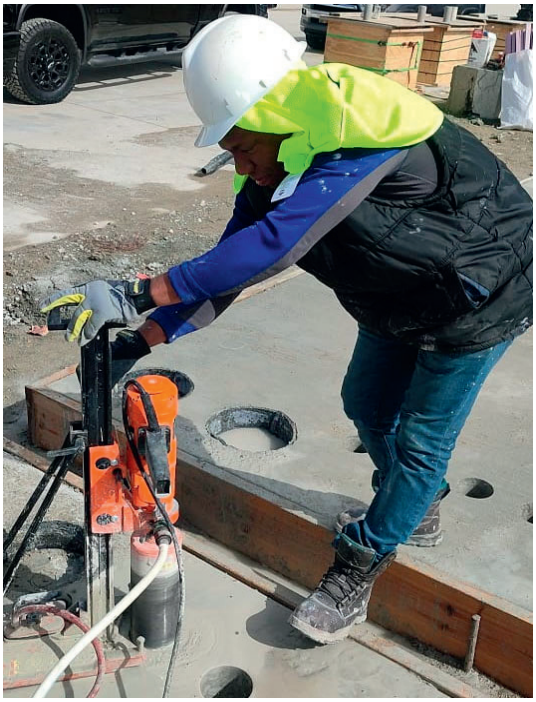

**Figure 6.9** Extracting Cores From the Slabs.

the slabs at various ages to obtain specimens needed for testing (Figure 6.9).

## 6.5 Field Curing Regimes

Immediately after casting, parts of two slabs, #6 (REF) and #8 (REF+Slag), were protected with a surface-applied, film-forming curing compound (Meadow 1600), as shown in Figure 6.10. The remaining surface areas of these slabs, as well as the entire surfaces of slabs #7, #9, #10, and #11 were air cured (i.e., left uncovered). Differences in curing for each slab are summarized in Table 6.2. Curing compound was also applied to the surfaces of some cylinders and beams, as shown in Figure 6.5. After 24 hr, those cylinders and beams were transferred to the laboratory and stored under ambient conditions until testing.

**Figure 6.10** Application of a Spray-On Curing Compound to Half of Slab #6 (REF) and #8 (REF+Slag). The Plastic Sheet on the Other Half of the Slab Was Removed After Spraying.

TABLE 6.2
**Field Curing Regimes of the Slabs.**

| Slab No. | Mixture ID | Curing Regime: No Curing Compound (NC) | Curing Regime: Curing Compound (CC) |
|---|---|---|---|
| 6 | REF | NC | CC |
| 7 | REF+NS1 | NC | - |
| 8 | REF+Slag | NC | CC |
| 9 | REF+Slag+NS1 | NC | - |
| 10 | REF+SAP | NC | - |
| 11 | REF+SAP+Slag | NC | - |

## 6.6 Testing Methods

### *6.6.1 Testing of Fresh Concrete Properties*

Total air content (Figure 6.11) and slump (Figure 6.12) of all fresh concrete mixes were measured in accordance with the ASTM standard test method (C143) for slump of hydraulic-cement concrete and ASTM standard test method (C231) for air content of freshly mixed concrete by the pressure method,

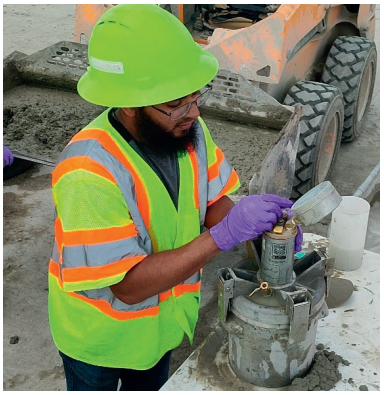

**Figure 6.11** Evaluation of Concrete Air Content.

**Figure 6.12** Evaluation of the Concrete Workability (Slump).

respectively (ASTM 2020b, ASTM, 2024a). The target slump range was 3–5 in. (76.2–127 mm) and the target air content was 5–8%. Each concrete batch was also tested for unit weight in accordance with ASTM standard test method (C138) for density (unit weight), yield, and air content (gravimetric) of concrete (ASTM, 2024d).

### *6.6.2 Flexural Strength and Compressive Strength Testing*

The flexural strength of concrete was evaluated in accordance with ASTM standard test method (C78) for flexural strength of concrete by use of simple beams with third point loading using 6 × 6 × 18 in. (152.4 × 152.4 × 457.2 mm) beams, tested 4 days after casting to align with INDOT's practice of using such test to determine earliest possible time for opening the pavement to traffic (ASTM, 2022e). For each mixture composition, the average modulus of rupture was calculated using the results obtained from two beams. Compressive strength was evaluated at 7, 28, 56, 90, and 365 days for both the field-cast concrete cylinders and cores extracted from the field-cast slabs following the procedures of ASTM standard test method (C39) for compressive strength of cylindrical concrete specimens (ASTM, 2024b). A constant loading rate of 1 kN/s (224.8 lbf/s) was maintained throughout the testing. At each testing age, cores were extracted from the field slabs, sealed in Ziploc bags, placed in plastic cylinders, and transported to the laboratory. The cores were then trimmed to standard dimensions of 4 × 8 in. (100 × 200 mm) before testing. Reported strength values represent the average of three specimens.

### *6.6.3 Splitting Tensile Strength*

The splitting tensile strength of concrete was evaluated in accordance with ASTM standard test method (C496) for splitting tensile strength of cylindrical concrete specimens using cores extracted from the slabs at 180 days (ASTM, 2017). As these cores were taken directly from the slabs, the specimens were assumed to have been cured under field conditions.

### *6.6.4 Scaling Resistance*

The scaling resistance test was performed according to ASTM standard test method (C672) for scaling resistance of concrete surfaces exposed to deicing chemicals (ASTM, 2012). Cylindrical test specimens were 10 in. (260 mm) in diameter and 4 in. (100 mm) in height and were extracted from the field slabs 28 days after casting and stored in ambient conditions (23 °C) until testing. For specimens treated with the surface-applied curing compound, a 2000 psi power washer was used to clean the surface prior to testing. Circular dikes, 2 in. (50 mm) in height, were constructed on the surface of each specimen and filled with 0.5 in. (2 cm) thick layer of 4% calcium chloride ($CaCl_2$) solution. The specimens were then subjected to 50 freeze-thaw cycles consisting of freezing at –18 °C (0 °F) for 16 hr and thawing at 4 °C (40 °F) for 8 hr. The deicing solution was replaced after every fifth cycle. The removal of the preformed test specimens from the slabs and their preparation for testing are shown in Figure 6.13.

(a) Extraction of Test Specimen From the Field.

(b) Specimens for Scaling Resistance Test.

(c) Specimens for Scaling Resistance Test.

(d) Diked Specimen Ponded With Chloride Solution.

**Figure 6.13** Specimen Preparations for Scaling Resistance Testing.

### 6.6.5 *Resistivity and Formation Factor*

The resistivity and formation factor values were determined following American Association of State Highway and Transportation Officials (AASHTO) standard method of test for electrical resistivity of a cylinder tested in a uniaxial resistance test, T402 (AASHTO, 2023), using both cast and core cylinders with nominal dimensions of 8 in. (200 mm) in length and 4 in. (100 mm) in diameter. All specimens were conditioned by immersion in a calcium hydroxide-saturated solution (artificial pore solution) as stipulated by the standard. Resistivity measurements were conducted 91 days after casting. Cylinders cast in the field remained in their plastic molds for the first 24 hr, stored adjacent to the slabs, before being transported to the laboratory. They were then demolded and immersed in the artificial pore solution until the time of testing. Cores used for resistivity testing were extracted from the slabs 85 days after casting, transported to the laboratory, and stored in the artificial pore solution for 6 days prior to testing. The test setup is shown in Figure 6.14.

Resistance values of concrete (R) were obtained as the average of six measurements: three measurements per specimen conducted on two separate specimens. These values were used to calculate the concrete resistivity (ρ) using Equation 6.1. The formation factor (F), defined as the ratio of concrete resistivity (ρ) to the resistivity of the pore solution ($\rho_0$), was calculated using Equation 6.2, shown below:

$$\rho = R \times \left(\frac{A}{L}\right) \qquad \text{Equation 6.1}$$

$$F = \frac{\rho}{\rho_0} \qquad \text{Equation 6.2}$$

Where: R = measured electrical resistance (Ω), $A$ = cross-sectional area of the specimen (m²), $L$ = length of the specimen (m), $\rho$ = the concrete resistivity (Ω·m), $\rho_0$ = pore solution resistivity (assumed 0.127 Ω·m as per AASHTO standard practice for developing performance engineered concrete pavement mixtures, R 101-22 (AASHTO, 2022).


**Figure 6.14** Test Setup for Concrete Resistance Measurements.

### 6.6.6 *Chloride Ion Penetration (Ponding Test)*

The ponding test was conducted to evaluate the depth of chloride ion penetration through concrete under prolonged exposure to chloride solutions. At 28 days after casting, dikes were constructed on the surface of the field-cast slabs and filled with 4% calcium chloride solution and maintained for extended period, simulating real-world conditions of chloride exposure. The dikes were subsequently covered with plastic sheets and wooden planks to minimize evaporation, prevent contamination, and avoid dilution of the chloride solution. After 150 days of exposure, concrete cores were extracted from the slabs to estimate the depth of chloride penetration. The entire process, from dike installation and ponding to core extraction, is illustrated in Figure 6.15. Once transported to the laboratory, the cores were split longitudinally, and a 0.1M silver nitrate ($AgNO_3$) was sprayed on the freshly exposed surfaces. The silver nitrate solution reacted with the chloride ions within the concrete, producing a visible color change that enabled profiling of the depth of chloride ingress.

## 6.7 Results

### 6.7.1 *Fresh Concrete Properties*

The fresh properties of all batched concrete were assessed in terms of slump, air content, and unit weight. The corresponding results are presented in Table 6.3 and illustrated in Figure 6.16.

Figure 6.16 illustrates the slump and air content for the various concrete mixtures. Although no WRA was used, the slump values for the plain Type IL and slag cement concretes exceeded the design target range of 3–5 in. (76.2–127 mm). In contrast, mixtures containing SAP exhibited slump values within the specified limits.

Consistently high slump values (~9 in. [228.6 mm]) were observed for REF, REF+NS1, REF+Slag, and REF+Slag+NS1 mixtures indicating high workability. The inclusion of colloidal nanosilica (NS1) and slag cement did not significantly affect fresh concrete consistency. As expected, notable reduction in slump occurred in REF+SAP and REF+Slag+SAP mixtures. This reduction in slump can be attributed to the SAP particles absorbing a small portion (1–2%) of the available mixing water. While this decreased workability, it did not noticeably affect placement and compaction of the mixtures. If needed, such a loss in workability can be readily mitigated by using water-reducing admixtures. The air content showed minimal variation

TABLE 6.3
**Fresh Properties of the Concrete Mixtures, Measured in the Field.**

| Slab Description | Slump (in. / mm) | Air Content (%) | Unit Weight (lb/ft³ / kg/m³) |
|---|---|---|---|
| REF | 8.75 / 222 | 7.80 | 171.5 / 2595.4 |
| REF+NS1 | 9.00 / 229 | 7.90 | 172.0 / 2602.2 |
| REF+Slag | 8.50 / 216 | 7.60 | 172.7 / 2612.8 |
| REF+Slag+NS1 | 9.00 / 229 | 7.80 | 172.6 / 2612.0 |
| REF+SAP | 3.75 / 95 | 5.50 | 178.1 / 2694.5 |
| REF+SAP+Slag | 4.88 / 124 | 5.80 | 177.1 / 2680.1 |

(a) Creation of Dikes on Field-Cast Slabs

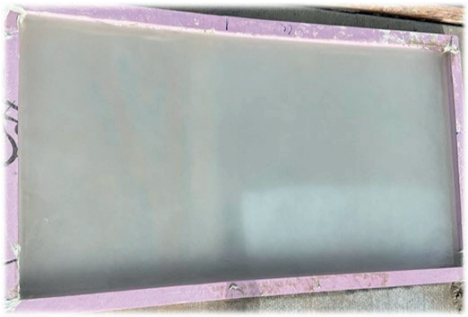

(b) Field-Cast Slab Ponded With Chloride Solution

(c) Covering Dikes to Avoid Evaporation

(d) Extraction of Concrete Cores From the Field

**Figure 6.15** Process of Ponding of Slabs and Extraction of Cores for Evaluation of Chloride Depth.

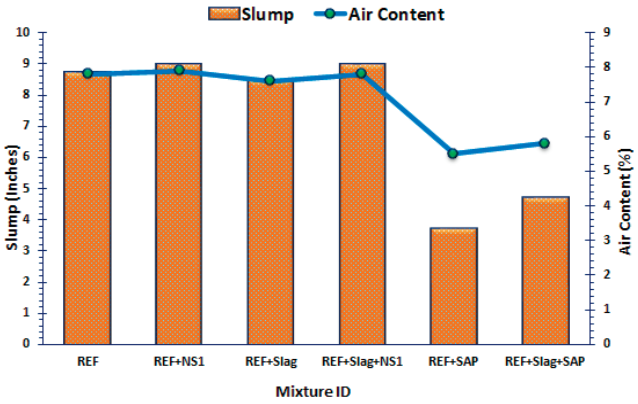


**Figure 6.16** Evaluation of the Concrete Workability (Slump) and Air Content.

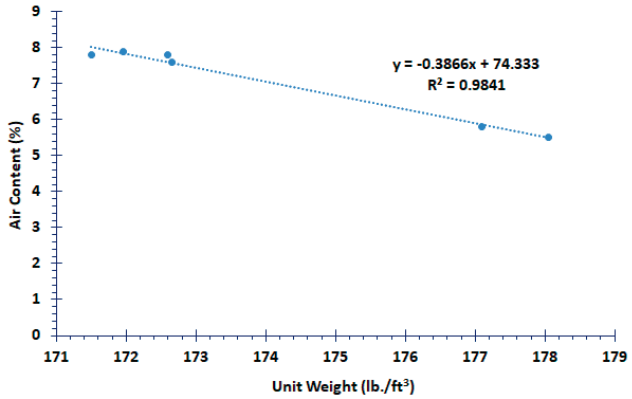


**Figure 6.17** Relationship Between Air Content and Unit Weight for Concrete Mixtures. Note: 1 lb/ft³ = 16.018 kg/m³.

among the REF, REF+NS1, REF+Slag and REF+Slag+NS1 mixtures. Although a reduction in air content was observed in REF+SAP and REF+Slag+SAP mixtures, all values remained within the design target range of 5–8%.

Figure 6.17 shows the relationship between air content (%) and unit weight (lb/ft$^3$) for the fresh concrete mixtures. The linear regression analysis reveals a clear inverse correlation between air content and unit weight, evidenced by the Equation 6.3:

$$y = -0.3866x + 74.333, \quad \boldsymbol{R^2 = 0.9841} \qquad \text{Equation 6.3}$$

Where $y$ = air content (%), and $x$ = unit weight (lb/ft$^3$). The $R^2$ value was close to 1, underscoring the robustness of the correlation, making this relationship a useful predictive tool for air content estimation based on measured density in similar mix designs. This trend indicates that as the unit weight increased, the air content decreased. This was logical since denser mixtures (higher unit weight) have reduced entrained and entrapped air. Conversely, higher air content corresponds with lower unit weight, suggesting mixtures with more voids or pores have lower density.

The reference (REF) shows moderate air content and unit weight, indicating a matrix typical of an entrained concrete. Using this as a baseline, the REF+NS1, REF+Slag, REF+Slag+NS1 mixtures exhibited comparable air content and unit weight. Slag cement enhances workability, potentially reducing entrapped air, but its fineness might slightly increase density. Both REF+SAP and REF+Slag+SAP show significantly lower air content and higher unit weight compared to the REF and REF+Slag, indicating dense well-compacted concrete.

### *6.7.2 Temperature Development*

The temperature data collected over a 10-day period from the field-cast slabs without curing compound exhibited a sinusoidal temperature variation pattern that approximately mirrored the daily fluctuation in ambient air temperature, as shown in Table 6.4, Figure 6.18, and Figure 6.19.

TABLE 6.4
**Temperature Development in Field-Cast Concrete Slabs.**

| Mixture ID | Peak Temp. (°C) | Time to Peak Temp. (hr) | Air Temp. at Peak (°C) |
|---|---|---|---|
| REF | 43.59 | 8.30 | 28.56 |
| REF+NS1 | 38.58 | 8.30 | 28.56 |
| REF+Slag | 37.86 | 10.30 | 13.35 |
| REF+Slag+NS1 | 33.14 | 9.30 | 14.42 |
| REF+SAP | 36.45 | 6.00 | 17.64 |
| REF+SAP+Slag | 35.69 | 7.00 | 14.42 |

The plain Type IL concrete mixture (REF) generated the highest heat of hydration, raising the slab core temperature to 45.6 °C (114 °F) within 8 hr of casting. The addition of colloidal nanosilica (NS1) reduced the slab core temperatures by approximately 13%, although the time to reach the peak temperature

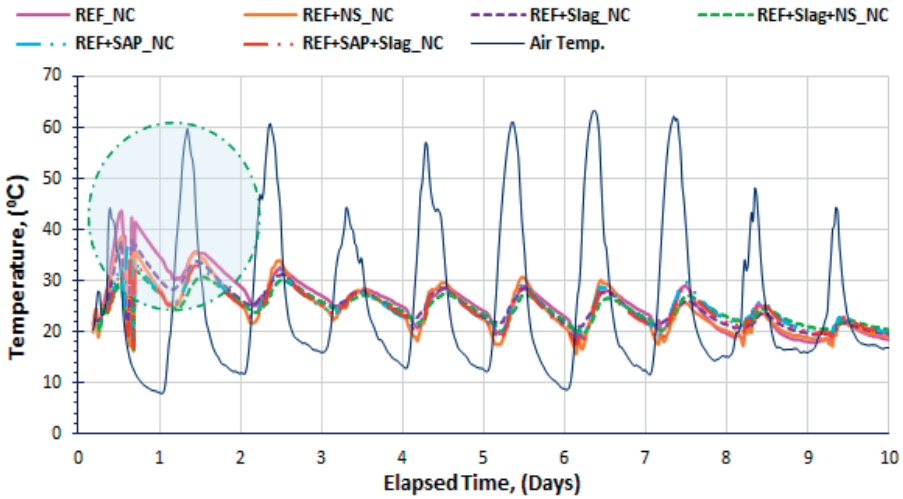


**Figure 6.18** In-Situ Temperature Profiles of Concrete Slabs and Corresponding Ambient Air Temperature Over Time.

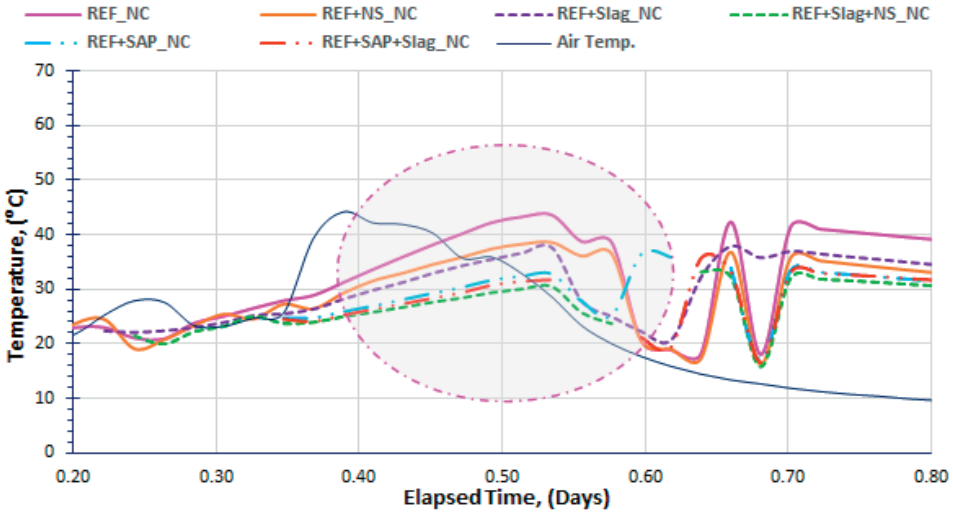


**Figure 6.19** Initial 24-Hour Temperature Profiles of Concrete Slabs and Corresponding Ambient Air Temperature Variations.

remained unchanged. Replacing 30% of Type IL cement with slag cement also lowered the slab core temperature by 13%, due to dilution effect but extended the time to peak temperature by 2 hr. This is due to the decreased cement, which reduces the proportion of tricalcium silicate ($C_3S$) available for hydration. Furthermore, the inclusion of SAP decreased the slab core temperature by 16% and shortened the time required to peak temperature by 2 hr.

### *6.7.3 Flexural Strength Results*

The flexural strength of the various mixes was evaluated at 4 days to assess their suitability for early opening of roads to traffic. The modulus of rupture results is reported in Table 6.5 and illustrated in Figure 6.20. Both the reference mixture (REF) and the mixture containing colloidal nanosilica (REF+NS1) exhibited high early-age strength, exceeding 500 psi (3.45 MPa). Mixtures containing SAP (REF+SAP and REF+Slag+SAP) demonstrated improved early-age flexural strength compared to their SAP-free counterparts. This improvement suggests that SAP helps retain internal moisture, promoting hydration and mitigating some of the early strength reduction associated with replacing Type IL cement with slag cement. Notably, the SAP-containing specimens reached flexural strengths at 4 days comparable to the INDOT standard's minimum modulus of rupture 7 days (~570 psi [3.93 MPa], indicated by dashed line in Figure 6.20).

Slag concrete mixtures (REF+Slag and REF+Slag+NS1) exhibited significantly lower values of 4-day flexural strength values, consistent with the well-known effects of slag's latent hydraulic properties slowing early strength development. This suggests that slag-based mixtures may not be suitable for structures requiring early opening to traffic without the use of additional accelerating measures. Notably, the mixture containing both slag cement and colloidal nanosilica (REF+Slag+NS1) developed the lowest flexural strength.

TABLE 6.5
**Flexural Strength of Field-Cast Slabs at 4 Days.**

| Slab No. | Mixture ID | w/cm | Flexural Strength at 4 Days (psi) | Flexural Strength at 4 Days (MPa) |
|---|---|---|---|---|
| 6 | REF | 0.44 | 515.13 | 3.55 |
| 7 | REF+NS1 | 0.44 | 524.96 | 3.62 |
| 8 | REF+Slag | 0.44 | 454.21 | 3.13 |
| 9 | REF+Slag+NS1 | 0.44 | 411.79 | 2.84 |
| 10 | REF+SAP | 0.44 | 550.63 | 3.79 |
| 11 | REF+SAP+Slag | 0.44 | 530.33 | 3.65 |

### *6.7.4 Compressive Strength*

Figure 6.21 presents the average compressive strength test results for field-cast cylinders at various curing ages. The results show the generally expended strength development trends, with all mixtures exhibiting increased compressive strength over time, indicating ongoing hydration. In the plain cement concrete, the addition of colloidal nanosilica (REF+NS1) resulted in higher compressive strength at all ages compared to the REF mixture. This improvement was likely due to accelerated hydration and microstructural densification promoted by the nanosilica.

The replacement of cement with 30% slag cement (REF+Slag) significantly improved the strength, especially at later ages (56, 90, and 365 days), with increases of 14%, 23%, 25%, 30%, and 48% at 7, 28, 56, 90, and 365 days, respectively. These gains are the result of the latent hydraulic activity of slag cement, which contributes significantly to later-age strength by reacting in the

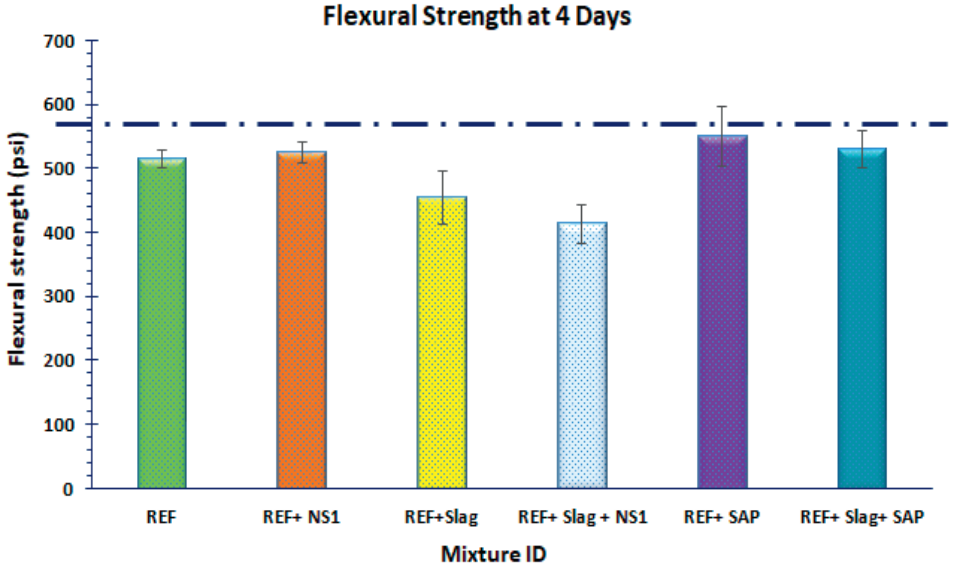


**Figure 6.20** 4-Day Flexural Strength (Modulus of Rupture) of Concrete Used in Field-Cast Slabs; Dashed Line at 570 psi Represents the INDOT Minimum Requirement. Note: 1 psi = 0.006895 MPa.

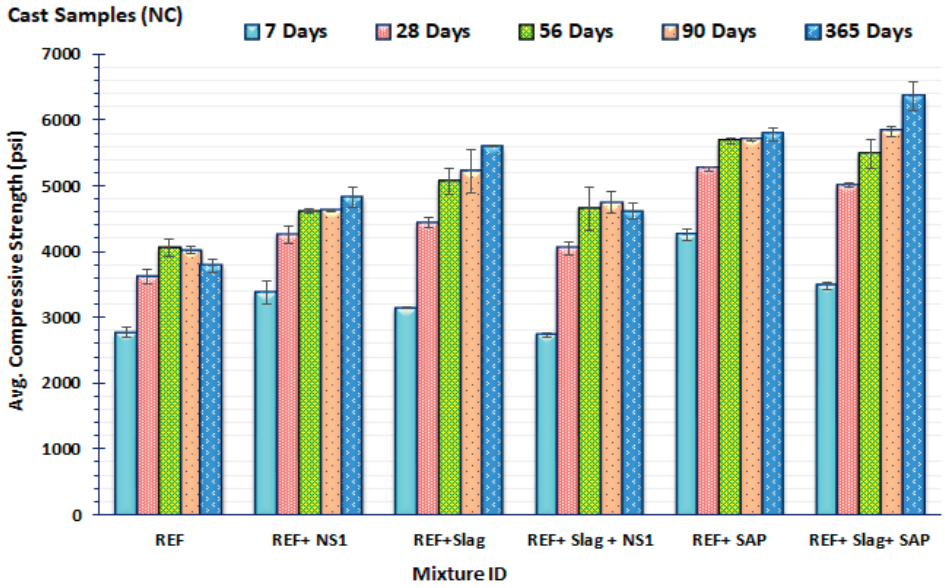


**Figure 6.21** Compressive Strength of Field-Cast Samples (No Curing Compound) at Various Ages. Note: 1 psi = 0.006895 MPa.

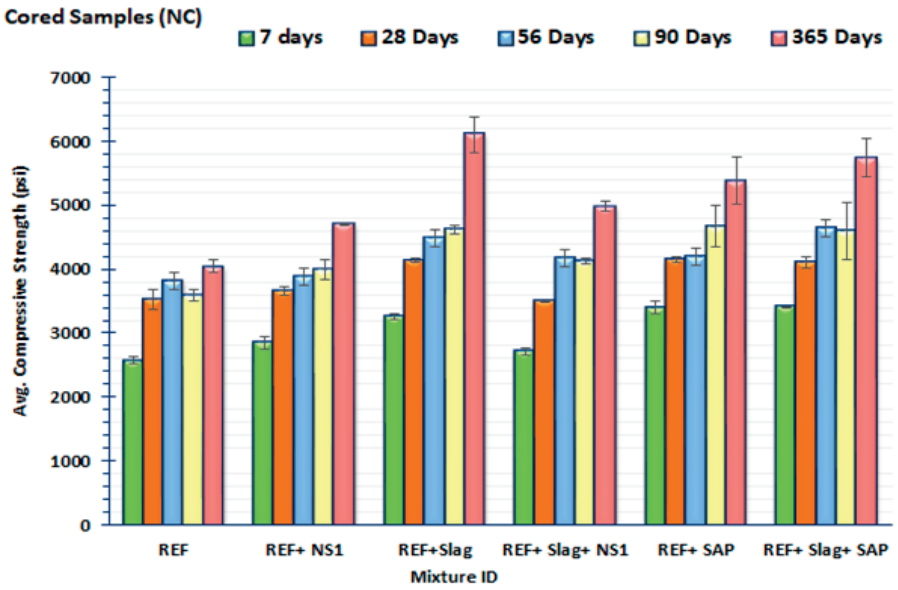


**Figure 6.22** Compressive Strength of Concrete Cores Extracted From Field-Cast Slabs (No Curing Compound), Measured at Various Ages. Note: 1 psi = 0.006895 MPa.

high-pH environment created by hydration of portland cement and forming additional C-S-H. However, the combination of slag cement and colloidal nanosilica (REF+Slag+NS1) resulted in somewhat lower compressive strength compared to the REF + Slag mixture.

The addition of SAP to plain cement concrete (REF+SAP) resulted in significant increases in compressive strength at both early and later ages, with increases of 54%, 45%, 40%, 42%, and 53% at 7, 28, 56, 90, and 365 days, respectively, compared to the SAP-free REF mixture. For mixtures with 30% slag cement, the inclusion of SAP (REF+Slag+SAP) also resulted in the increase of the compressive strength compared to REF+Slag, particularly beyond 28 days. This improvement highlights potentially synergistic interactions between the latent hydraulic activity of slag and the internal curing effect of SAP.

Similar trends were observed across all mixtures for the compressive strength of concrete cores extracted from the slabs (Figure 6.22). Addition of SAP increased the strength of plain concrete cores compared to the REF cores. But no strength gains were evident in the mixtures containing both slag and SAP compared to the REF+Slag cores. The lack of additional strength in this case is likely due to the ambient field-curing conditions, which included intermittent moisture replenishment from rain events.

### *6.7.5 Effect of Curing Regime on the Compressive Strength of the Concrete*

Figure 6.23 shows the compressive strength results for field-cast cylinders exposed to two different curing regimes: one with externally applied curing compound (CC) and one without it (NC). It is important to note that only the plain cement mixture (REF) was exposed to both of these curing regimes. The other two types of mixtures (i.e., REF+NS1 and REF+SAP) were cured without the use of an external curing compound.

As shown in Figure 6.23, the application of the curing compound improved the strength of the REF mixture by 14%, 7%, 2%, 12%, and 31% at 7, 28, 56, 90, and 365 days, respectively. The addition of colloidal nanosilica (REF+NS) resulted in moderate strength improvements at all ages compared to both REF mixtures, with and without the curing compound. In contrast, the addition of SAP (REF+SAP) resulted in a significant increase in compressive strength across all ages relative to the REF mixtures. The percentage values shown in Figure 6.23 indicate the strength increases from REF_NC to REF+SAP_NC.

Figure 6.24 presents the compressive strength results for core samples extracted from slabs cast using the same concrete mixtures as the cylinders shown in Figure 6.23. Overall, the strength trends observed in the cores closely follow those of the corresponding cylinders with slight differences in absolute values.

The influence of the previously mentioned two curing regimes was also evaluated for slag cement-based mixtures using both field-cast cylinders and cores extracted from companion slabs. As shown in Figure 6.25 (field-cast cylinders), the application of the curing compound improved the strength of the

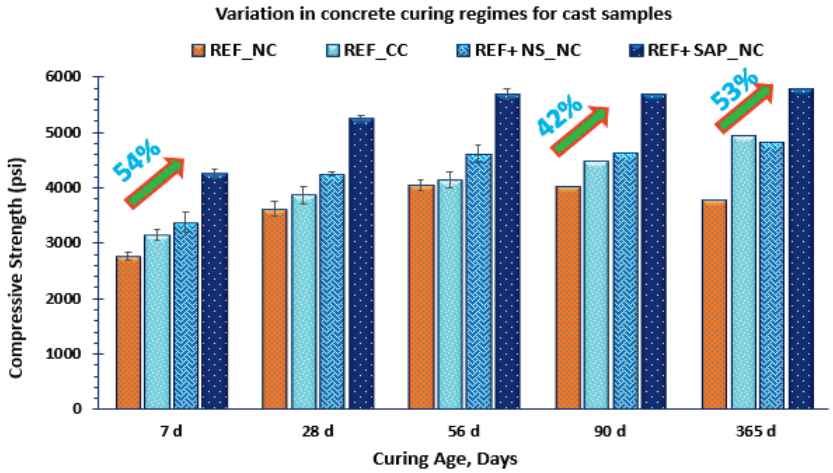


**Figure 6.23** Variation in Compressive Strength of Cast Cylinders Over Time Under Curing Conditions With and Without Curing Compound. Note: 1 psi = 0.006895 MPa.

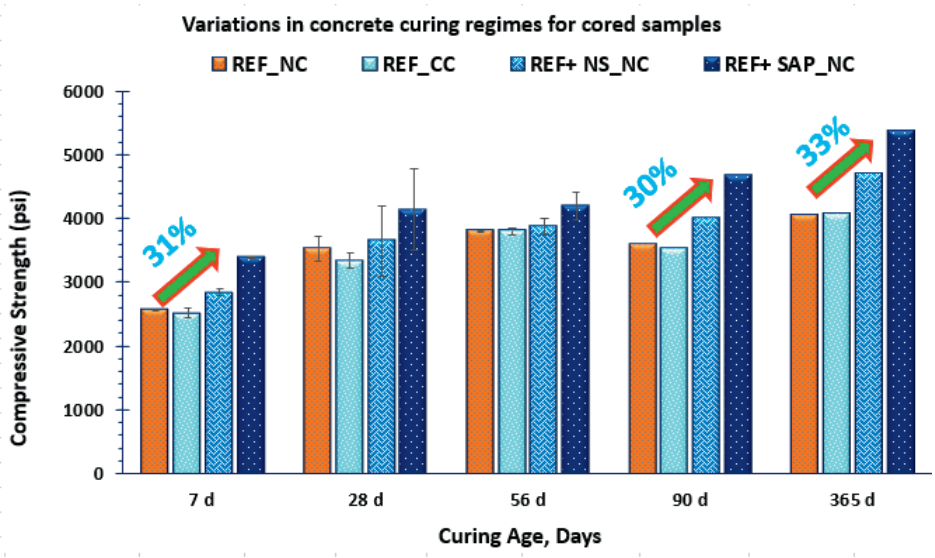


**Figure 6.24** Variation in compressive strength of Cores Extracted From Slabs Over Time Under Curing Conditions With and Without Curing Compound. Note: 1 psi = 0.006895 MPa.

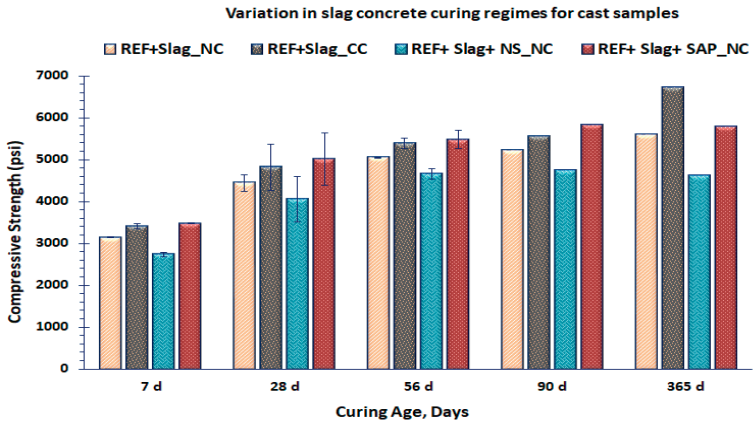


**Figure 6.25** Variation in Compressive Strength Over Time for Slag-Based Cast Cylinders Cured With and Without External Curing Compound. Note: 1 psi = 0.006895 MPa.

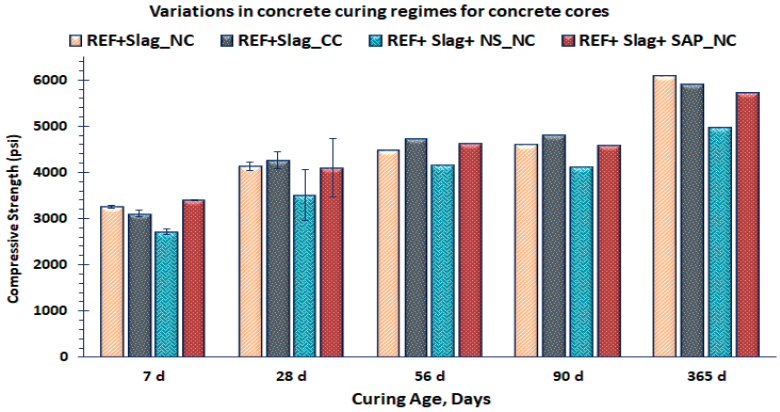


**Figure 6.26** Variation in Compressive Strength Over Time for Slag-Based Cores Cured With and Without External Curing Compound. Note: 1 psi = 0.006895 MPa.

REF+Slag mixture, which was expected given the lab (i.e., air drying) curing environment. In contrast, the addition of colloidal nanosilica reduced the strength values at all curing ages. The slag-based mixture containing SAP without curing compound (REF+Slag+SAP_NC) exhibited compressive strengths comparable to the corresponding slag cement mixture without SAP (REF+Slag_NC). Similar trends were observed in the compressive strength of field-extracted cores (Figure 6.26), though the absolute strength values varied.

### *6.7.6 Splitting Tensile Strength*

Figure 6.27 presents the splitting tensile strength of cores extracted from the field-cast slabs 180 days after casting. The addition of colloidal nanosilica appears to have reduced the tensile strength both when used alone and in combination with slag. In contrast, the incorporation of SAP, whether in plain cement or slag-based mixtures, maintained tensile strength values at levels comparable to those of the corresponding reference mixtures.

### *6.7.7 Scaling Resistance*

Concrete scaling resistance experiments are designed to evaluate the durability of concrete surfaces (ability to resist surface scaling) when exposed to freezing and thawing cycles, especially in the presence of deicing chemicals such as sodium chloride (NaCl) and calcium chloride. The surface scaling visual rating scale (Table 6.6) recommended in the ASTM standard

TABLE 6.6
**Surface Rating Scale Used for Visual Assessment of Scaling Severity (ASTM C672 [ASTM, 2012]).**

| Rating | Condition of Surface |
|---|---|
| 0 | No scaling |
| 1 | Very slight scaling (3mm (⅛ in.) depth, max, no coarse aggregate visible) |
| 2 | Slight to moderate scaling |
| 3 | Moderate scaling (some coarse aggregate visible) |
| 4 | Moderate to severe scaling |
| 5 | Severe scaling (coarse aggregate visible over entire surface) |

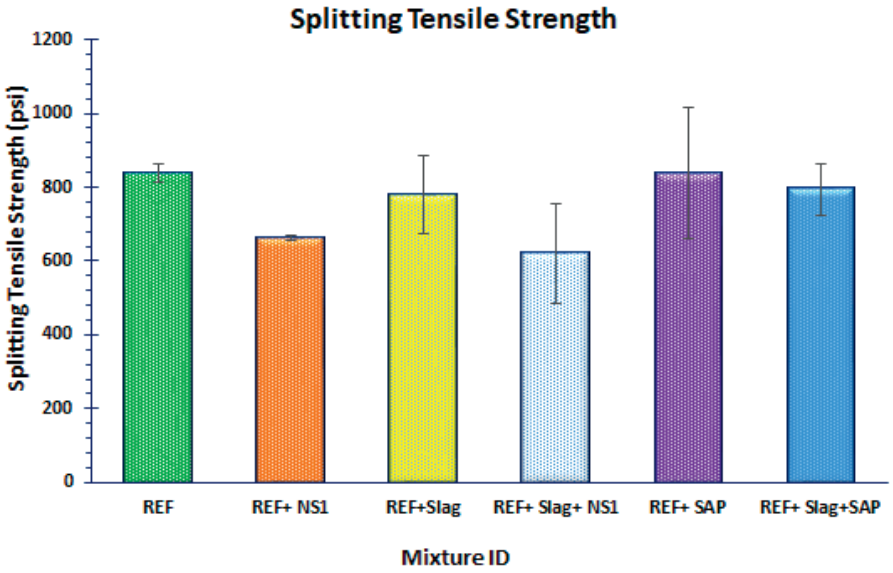


**Figure 6.27** Tensile Strength of the Various Mixture Compositions. Note: 1 psi = 0.006895 MPa.

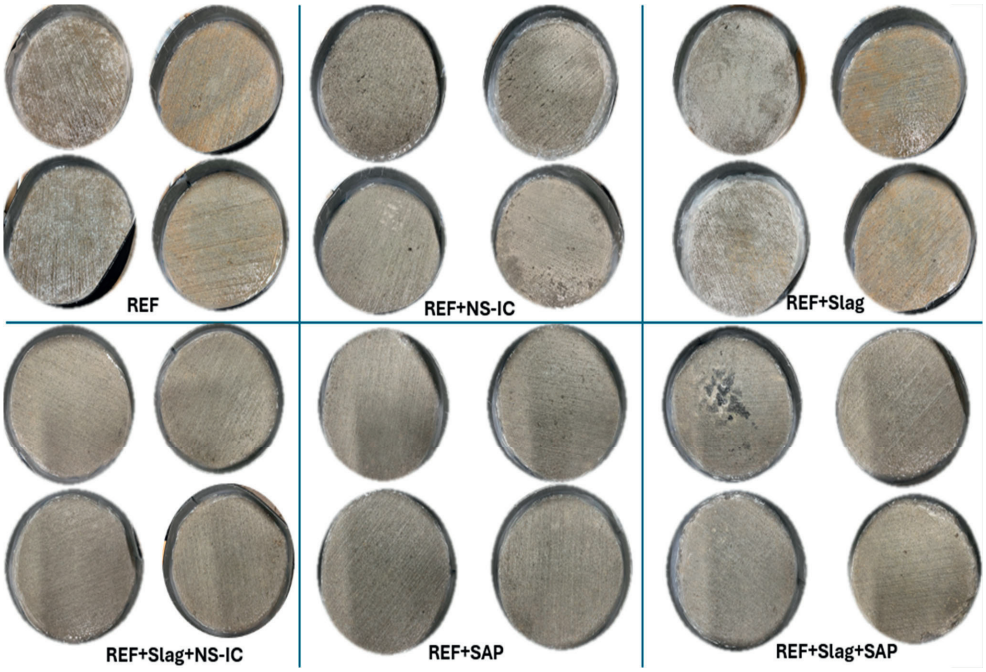


**Figure 6.28** Surfaces of Scaling Specimens After 50 Cycles of Freezing and Thawing.

test method (C672) for scaling resistance of concrete surfaces exposed to deicing chemicals standard was used to evaluate the extent of scaling (ASTM, 2012). Typically, in addition to visual rating, mass loss due to exposure to freezing and thawing cycles can be used to quantify the concrete resistance to scaling. However, none of the tested specimens showed any signs of scaling. Consequently, no mass losses were recorded, and the visual rating of all surfaces was zero (Figure 6.28). That means there were no visible signs of scaling, such as peeling, flaking, or surface roughness, indicating good scaling resistance of all the concrete mixtures used in this field trial.

### *6.7.8 Resistivity and Formation Factor*

To assess the influence of concrete microstructure on durability, especially with respect to the ingress of water and other deleterious ions, one can measure electrical resistivity of the material. As concrete is a porous material with network of

microscopic, interconnected pores, the electrical resistivity evaluates the materials' resistance to flow of electric charges. Several factors, such as the resistivity of the pore solution, volume of the pores, and their interconnectivity, all affect the resistivity of the concrete. Typically, concrete samples with higher pore density and greater volume of interconnected pores will display lower resistivity. Also, concrete with pore solutions containing higher ion concentration will show lower resistivity. The measured resistivity values for both field-cast cylinders and concrete cores are shown in Figure 6.29. These values were used to calculate the concrete formation factor (FF) using Equation 6.2 from Section 6.6.5. The resulting FF values for the cast cylinders are shown in Figure 6.30 while those for the concrete cores are presented in Figure 6.31.

The darker-shade bars shown in Figure 6.29 represent the resistivities of cast cylinders whereas the lighter (striped) bars depict the resistivity of the cores extracted from the field-cast slabs (the green and red dotted lines indicate the baseline of the references, respectively). Both sets of specimens exhibited similar trends across mixtures; however, the resistivity values of the concrete cores were consistently lower. Figure 6.30 and Figure 6.31 present combined plots of FF and resistivity values for the mixtures. Since concrete resistivity is directly related to ionic conductivity, higher resistivity indicates lower porosity and

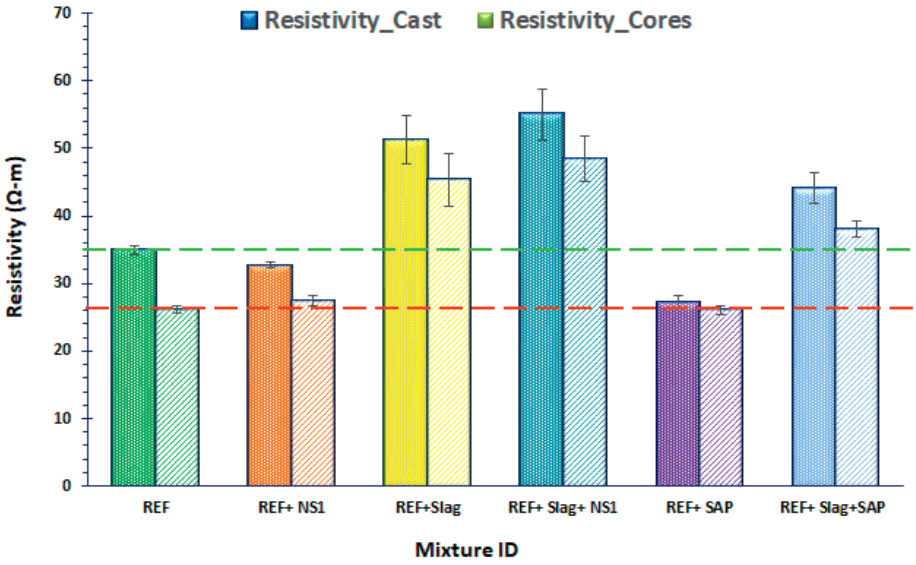


**Figure 6.29** The 91 Days Concrete Resistivity Values of Cast Cylinders and Cores for Various Mixture Compositions.

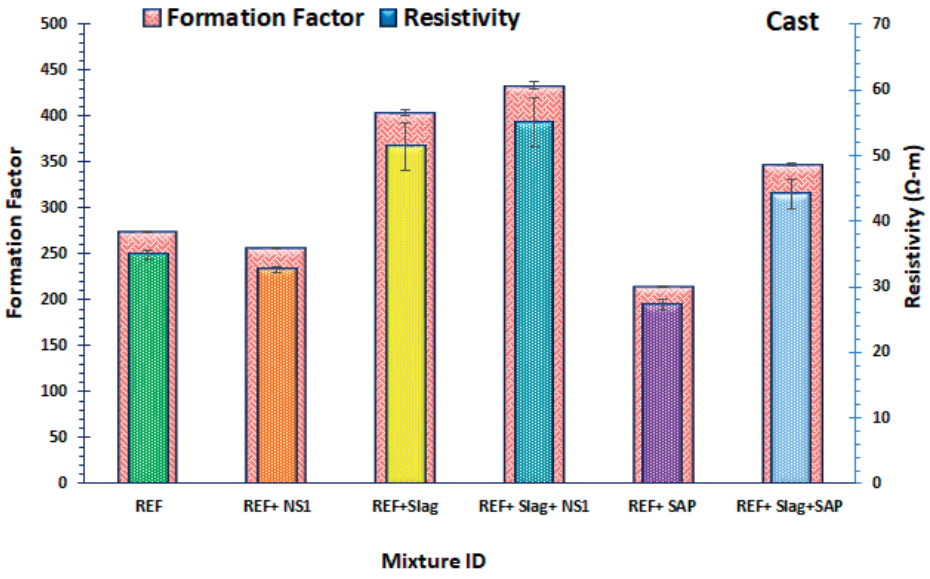


**Figure 6.30** Concrete Resistivity and Formation Factor of Field-Cast Cylinders From Various Mixtures.

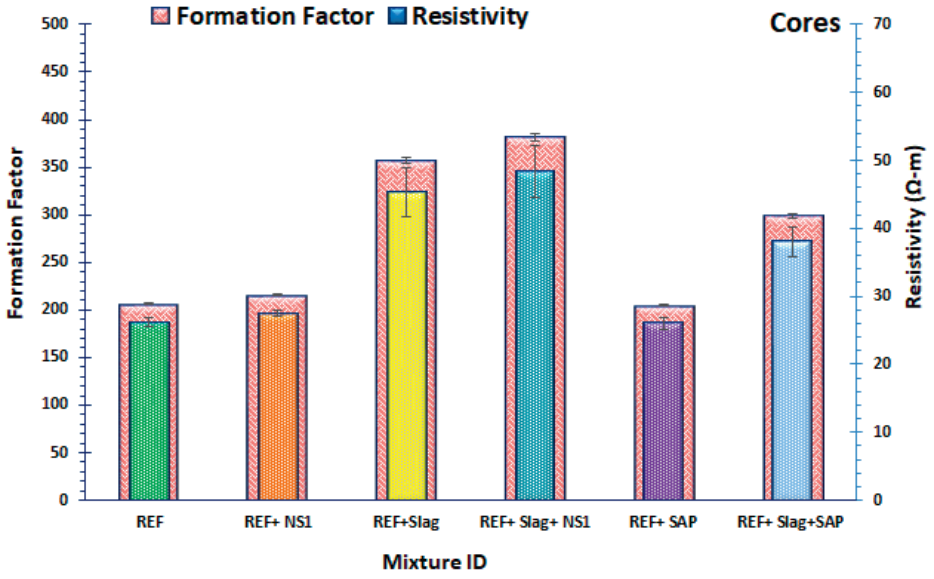


**Figure 6.31** Concrete Resistivity and Formation Factor of Cores for Various Mixture Compositions.

improved resistance to ion transport. While resistivity indicates the concrete's resistance to ion transport, the FF (defined as the ratio of saturated concrete resistivity to pore solution resistivity) reflects pore connectivity. Together, these parameters provide valuable insights into the concrete's pore structure and overall durability performance.

The reference mixture (REF), serving as the baseline for comparison, shows moderate FF and resistivity values. The REF+NS1 shows slightly reduced FF and resistivity relative to REF, suggesting that the high surface area of colloidal nanosilica might introduce finer porosity without necessarily enhancing resistance to ionic transport.

As expected, REF+Slag mixture exhibits a significant increase in both FF and resistivity, indicating an improved pore structure and reduced ionic conductivity. This enhancement is attributed to the latent hydraulic reaction of slag which refines the pore network. The REF+Slag+NS1 mixture achieves the highest values for both parameters. This synergistic effect may result from colloidal nanosilica providing nucleation sites for hydration products, while the slag further refines the pore structure. These synergistic effects reduce pore connectivity and should lead to higher durability.

REF+SAP mixture shows the lowest FF and resistivity values among all tested concrete mixtures, despite SAP's well-documented ability to mitigate shrinkage. This reduction is likely due to the presence of macrovoids introduced by SAP, which may become filled with conductive artificial pore solution, thereby lowering resistance to ionic transport.

In contrast, the REF+SAP+Slag mixture shows higher resistivity and FF values than the REF+SAP alone mixture. It appears that addition of slag, which, as mentioned earlier refines pore structure by generating additional hydration products, counteract the effects of macrovoids introduced by SAP, demonstrating a complementary effect of these two components of the mixture.

### *6.7.9 Chloride Ion Penetration Test (Ponding Test)*

Figure 6.32 shows the appearance of the split core surfaces after spraying with a 0.1M silver nitrate solution. The solution reacts with chloride ions present in the concrete, producing a distinct color contrast. Areas containing chloride ions appear white or light gray due to the formation of silver chloride (AgCl), while chloride-free zones remain brownish or gray due to the presence of silver oxide or unreacted silver nitrate. This color boundary enables clear visual estimation of chloride penetration depth.

To quantify the depth of chloride ingress, ten measurements were taken at evenly spaced intervals along each split surface using a digital caliper. These measurements were recorded from the exposed surface inward, up to the point where no further discoloration was observed. Figure 6.33 presents the average chloride penetration depths for each concrete mixture based on these 10-point measurements, providing a comparative assessment of their resistance to chloride ingress under field exposure conditions.

The results indicate that the addition of colloidal nanosilica slightly increased the depth of chloride penetration compared to the plain cement reference mixture. In contrast, the inclusion of slag led to a significant reduction in chloride penetration depth. This enhancement is primarily due to the formation of additional C-S-H, which refines the pore structure and enhances durability. When colloidal nanosilica was combined with slag, no notable change in chloride penetration depth was observed compared to the slag-only mixture. The incorporation of SAP resulted in a chloride penetration depth similar to that of the plain reference mixture. However, the mixture containing both slag and SAP demonstrated a reduced chloride penetration depth relative to both the reference and SAP-only mixtures. This suggests a synergistic effect, wherein SAP contributes to internal curing

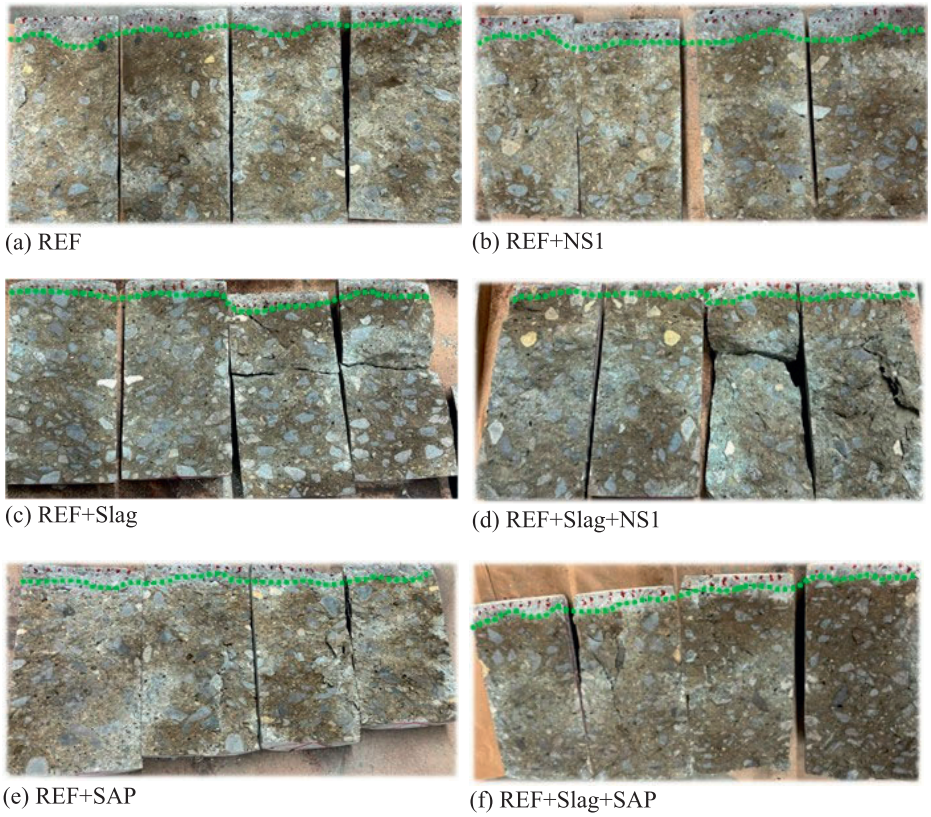


**Figure 6.32** Chloride Ingress Depths in Concrete Cores Extracted for Field-Ponded Slabs Determined by Silver Nitrate Spray Technique.

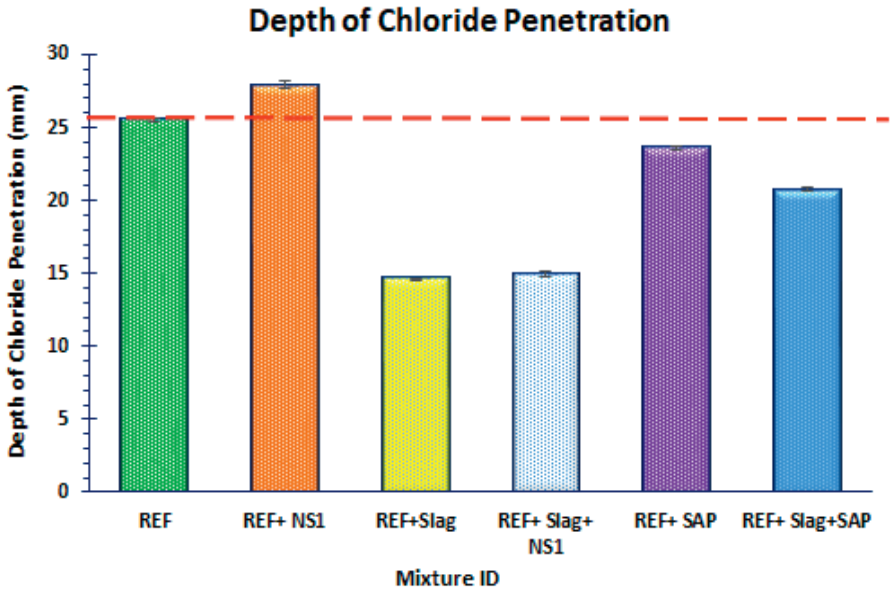


**Figure 6.33** Measured Depth of Chloride Penetration for Various Concrete Mixtures.

and slag densifies the matrix, thus reducing permeability and improving resistance to chloride ingress.

The observed trends in the depth of chloride penetration for these concrete mixtures highlight the significant influence of individual additives and their combinations on concrete durability. While slag consistently improved resistance to chloride ingress, colloidal nanosilica alone was not effective. SAP appeared to either maintain or slightly improve chloride penetration resistance relative to the reference mixture. Notably, the combination of slag and SAP reduced chloride ingress compared

to SAP-only mixture. This indicates a synergistic effect where internal curing facilitated by SAP and matrix densification from slag together reduce chloride permeability.

### 6.8 Conclusions and Future Work

Results from the year-long field trial demonstrated that both plain cement and slag cement concretes internally cured with SAP displayed increased strength and durability compared to SAP-free concrete, concrete containing colloidal nanosilica, and concrete that was externally cured with a surface-applied curing compound. Some of the key findings from this study are listed below:

- The use of dissolvable bags proved to be an effective method for SAP delivery in a ready-mixed concrete plant, ensuring uniform dispersion and consistent mixture workability.
- SAP-cured mixtures displayed reduced slump and air content compared to SAP-free mixtures. However, all mixtures met or exceeded the target slump range (3–5 in.) and remained within the target air content range (5–8%), eliminating the need for any mixture adjustments.
- Mixtures containing SAP showed improved early-age flexural strength performance compared to SAP-free mixtures. Additionally, the addition of SAP effectively mitigated the early-age strength reduction typically associated with slag cement.
- The addition of SAP to both plain and slag cement concretes resulted in significant increases in compressive strength at both early and later ages when compared to the corresponding SAP-free reference mixtures.
- Compared to the use of a surface-applied curing compound, the addition of SAP significantly improved the compressive strength of both field-cast and cored samples, yielding increases of 30–50% across all ages relative to SAP-free plain cement reference mixtures, with and without curing compound.
- Mixtures containing both slag and SAP displayed reduced chloride penetration depths compared to reference and SAP-only mixes. The combination of SAP and slag appeared to provide a synergistic effect, with SAP promoting internal curing and slag refining the pore structure.

Overall, concrete mixtures incorporating SAP and slag at 30% replacement consistently showed improved performance in comparison with the SAP-cured plain cement concrete mixtures. This indicates an interesting synergy between SAP, SCMs, and Type IL cement which warrants future investigations. Additionally, a comprehensive technoeconomic (cost-benefit) analysis should be performed on the use of SAP by the concrete ready-mixed industry to internally cure concrete, compared to other internal curing strategies like the use of presaturated lightweight aggregate or external curing strategies like ponding with water.

## 7. EFFECT OF WATER-TO-BINDER RATIO (0.42 AND 0.44) ON THE INTERNAL CURING AND SHRINKAGE (DRYING AND AUTOGENOUS) OF SAP-MODIFIED CEMENTITIOUS MORTAR

### 7.1 Overview

This section investigates the influence of water-to-binder ratio on the internal curing and shrinkage behavior of cementitious mortars modified with SAP. The performance of the mortar mixtures at a w/b ratio of 0.42 and 0.44 was assessed by examining their fresh properties (including flow, mini-slump and air content), strength characteristics (compressive and flexural strength), ultrasonic pulse velocity, and drying shrinkage. Additionally, setting time and autogenous shrinkage were evaluated at a w/b ratio of 0.44 for the field trial mixture compositions.

### 7.2 Materials

The materials utilized for the mortar mixtures were conventional components commonly employed in the production of cementitious mortars. These include Type IL cement, slag cement, fine aggregates, potable mixing water, SAP, colloidal nanosilica, and other admixtures to modify specific performance characteristics. The properties of these materials are provided in detail in Section 4.2 of this report. The mortar mix designs for w/b ratio of 0.42 and 0.44 are presented below in Table 7.1 and Table 7.2 and were obtained following the guidelines outlined in ASTM standard guide (C1810) for comparing performance of concrete-making materials using mortar mixtures (ASTM, 2022a). The values of the mortar mixture proportions shown in

TABLE 7.1
**Mortar Mixture Designs – w/b 0.42.**

| Mixture ID | w/b | Cement (kg/m³) | Fine Agg (kg/m³) | Water (kg/m³) | Slag (kg/m³) | Nanosilica (mL/100 kg) | SAP (kg/m³) | HRWRA (mL/100 kg) | AE (mL/100 kg) |
|---|---|---|---|---|---|---|---|---|---|
| REF | 0.42 | 390 | 706 | 172 | | | | 0 | 80 |
| REF+NS1 | 0.42 | 390 | 706 | 172 | | NS1: 261 | | 0 | 80 |
| REF+NS2 | 0.42 | 390 | 706 | 172 | | *NS2: 783 | | 0 | 80 |
| S30 | 0.42 | 273 | 706 | 172 | 117 | | | 0 | 80 |
| S30+NS1 | 0.42 | 273 | 706 | 172 | 117 | NS1: 261 | | 0 | 80 |
| S30+NS2 | 0.42 | 273 | 706 | 172 | 117 | *NS2: 783 | | 0 | 80 |
| REF+SAP | 0.42 | 390 | 706 | 172 | | | 0.78 | 200 | 80 |
| S30+SAP | 0.42 | 273 | 706 | 172 | 117 | | 0.78 | 200 | 80 |
| S30+SAP+NS1 | 0.42 | 273 | 706 | 172 | 117 | NS1: 261 | 0.78 | 200 | 80 |
| S30+SAP+NS2 | 0.42 | 273 | 706 | 172 | 117 | *NS2: 783 | 0.78 | 200 | 80 |

Note: * **NS2** is a combination of two colloidal nanosilica admixtures, **NS1** (261 mL/100 kg) + **modified NS1** (522 mL/100 kg).
1 kg/m³ = 1.686 lb/yd³

TABLE 7.2
**Mortar Mixture Designs – w/b 0.44.**

| Mixture ID | w/b | Cement (kg/m³) | Fine Agg (kg/m³) | Water (kg/m³) | Slag (kg/m³) | Nanosilica (mL/100 kg) | SAP (kg/m³) | HRWRA (mL/100 kg) | AE (mL/100 kg) |
|---|---|---|---|---|---|---|---|---|---|
| REF | 0.44 | 390 | 718 | 164 | | | | 0 | 80 |
| REF+NS1 | 0.44 | 390 | 718 | 164 | | NS1: 261 | | 0 | 80 |
| REF+NS2 | 0.44 | 390 | 718 | 164 | | *NS2: 783 | | 0 | 80 |
| S30 | 0.44 | 273 | 718 | 164 | 117 | | | 0 | 80 |
| S30+NS1 | 0.44 | 273 | 718 | 164 | 117 | NS1: 261 | | 0 | 80 |
| S30+NS2 | 0.44 | 273 | 718 | 164 | 117 | *NS2: 783 | | 0 | 80 |
| REF+SAP | 0.44 | 390 | 718 | 164 | | | 0.78 | 200 | 80 |
| S30+SAP | 0.44 | 273 | 718 | 164 | 117 | | 0.78 | 200 | 80 |
| S30+SAP+NS1 | 0.44 | 273 | 718 | 164 | 117 | NS1: 261 | 0.78 | 200 | 80 |
| S30+SAP+NS2 | 0.44 | 273 | 718 | 164 | 117 | *NS2: 783 | 0.78 | 200 | 80 |

Note: * **NS2** is a combination of two colloidal nanosilica admixtures, **NS1** (261 mL/100 kg) + **modified NS1** (522 mL/100 kg).
1 kg/m³ = 1.686 lb/yd³

TABLE 7.3
**Tests Procedures, Standards and Specimen Specifications for Evaluation.**

| Test Name | Procedure | Specimen Specification |
|---|---|---|
| Flow and Workability (Slump) | ASTM C1437-15; C1810-22 | Fresh cementitious paste |
| Compressive Strength | ASTM C109-20 | 50 × 50 × 50 mm mortar cubes |
| Flexural Strength | ASTM C348-21 | 40 × 40 × 160 mm mortar beams |
| Drying Shrinkage | ASTM C157-17 | 25 × 25 × 285 mm mortar prisms |
| Ultrasonic Pulse Velocity | ASTM C597-22 | 40 × 40 × 160 mm mortar beams |
| Time of Setting | ASTM C403-23 | 150 × 150 mm mortar cylinder |
| Autogenous Shrinkage | ASTM C1698-19 | 420 × 29 mm corrugated tubes |

Table 7.2 are slightly different from those presented in Table 4.1, even with the same w/b ratio of 0.44; this was due to an earlier oversight in the calculation.

## 7.3 Methods

Mixture specimens were prepared and cast in accordance with the procedures described in Section 4.3. The fresh properties, strength characteristics, and UPV were assessed. To further understand the dimensional stability and early-age behavior of the mixtures, additional tests were conducted to measure drying shrinkage, setting time, and autogenous shrinkage. The specific methods for these shrinkage assessments are outlined in the sections below. Table 7.3 lists the tests, procedures and specimen specifications.

### *7.3.1 Drying Shrinkage*

Drying shrinkage measurements were performed on 25 × 25 × 285 mm (1 × 1 × 11 in.) mortar prisms following the ASTM standard test method for length change of hardened hydraulic-cement mortar and concrete on mortar mixtures with w/b ratio of 0.42 and 0.44 (ASTM, 2024e). The cast mortar test specimens were moist cured in molds for 48 hr ± 30 min, then demolded (this extended time was to avoid damage while removing specimens) and placed in lime-saturated water maintained at 23 ± 0.5 °C (73.4 ± 0.5 °F) for a minimum of 15 min. After removal from the water, the specimens were wiped with a damp cloth and immediately placed in the comparator to obtain the initial length reading. Subsequently, the specimens were stored in a drying room maintained at a relative humidity of 50 ± 4% and temperature 23 ± 2 °C (73.4 ± 0.5 °F). Comparator readings were taken after 4, 7, 14, and 28 days of curing. The calculated values of drying shrinkage are based on the average of four measurements.

### *7.3.2 Setting Time*

The initial and final setting times of the mortar mixtures were determined in accordance with ASTM standard test method (C403) for time of setting of concrete mixtures by penetration resistance (ASTM, 2023). Fresh mortar was prepared and placed into a 150 × 150 mm cylindrical mold and level. A penetrometer with needle assemblies having the bearing areas 645, 323, 161, 65, 32, 16 mm² (1, ½, ¼, ⅒, 1/20, 1/40 *in*²) and weight was used to measure penetration resistance. Penetration measurements were started at intervals after mixing. The depth of penetration under a standard force was recorded. The initial setting time was defined as the elapsed time corresponding to a penetration resistance of 500 psi (3.5 MPa). The final setting time was identified when penetration resistance reached 4000 psi (27.6 MPa).

### *7.3.3 Autogenous Shrinkage*

Autogenous shrinkage measurement was performed on mortar mixtures with w/b ratio of 0.44, following ASTM standard test method (C1698) for autogenous strain of cement paste and

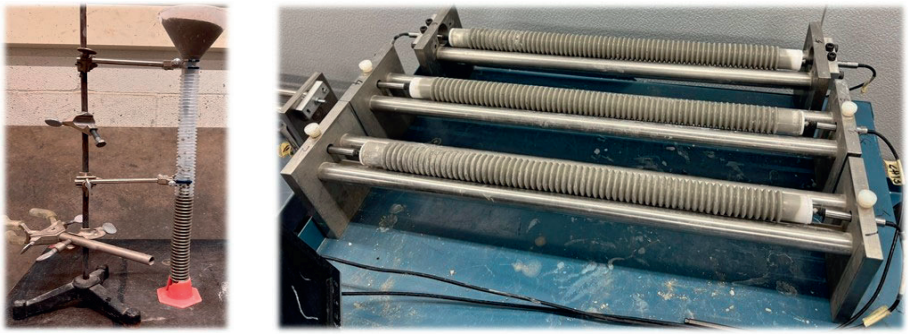

(a) (b)

**Figure 7.1** (a) Corrugated Tube Mounted on Vibrating Table and (b) LVDT Sensors Measuring Autogenous Strain.

mortar (ASTM, 2019). Fresh mortar was cast in corrugated tubes that were mounted on a support base on a vibrating table (Figure 7.1a) and sealed to prevent moisture exchange. Length changes were monitored immediately after casting using linear variable differential transformers (LVDT) attached to a computer (Figure 7.1b) which were kept in a thermostatically controlled room maintained at 23 ± 0.5 °C (73.4 ± 0.5 °F) and a relative humidity of 50 ± 4%. Deformation readings were recorded continuously for the first 3 days to capture early-age shrinkage. Initial measurement was started at the time of final setting determined using ASTM standard test method (C403) for time of setting of concrete mixtures by penetration resistance (ASTM, 2023). The average of three replicate specimens was used to evaluate the autogenous strain which was calculated using Equations 7.1 and 7.2.

$$\varepsilon_{autogenous} \frac{L(t) - L(t_{fs})}{L\,(t_{fs})} * 10^6 = \frac{R(t) - R(t_{fs})}{L\,(t_{fs})} * 10^6\ \mu m/m \qquad \text{Equation 7.1}$$

$$L(t) = L_{ref} + R(t) - 2 * L_{plug} \qquad \text{Equation 7.2}$$

Where:

$t_{fs}$ = *time of final setting,when the first length measurement is performed, min*

$L_{ref}$ = *length of reference bar,mm*

$R(t)$ = *reading of the length gauge with specimen in the dilotometer, mm*

$L_{plug}$ = *average length of end plugs,mm*

The setting time and autogenous shrinkage experiments were conducted with w/b 0.44 on six mortar mixture compositions which represents the concrete cast during the field trials. These include the reference mix with plain Type IL cement (REF), mix containing colloidal nanosilica (REF+NS1), mix with 30% slag-cement replacement (S30), mix with 30% slag-cement and colloidal nanosilica (S30+NS1), mix with 0.2% SAP (REF+SAP), for result confirmation, this mix was repeated (REF+SAP_2), and mix with 30% slag-cement and SAP (S30+SAP).

## 7.4 Results

### *7.4.1 Workability (Slump) and Air Content*

The workability (slump) of the mortar mixtures is shown in Figure 7.2. As expected, the mortar mixtures with higher w/b ratio (0.44) had higher slump values. Additionally, the trends for slump changes are similar for most of the mixtures, irrespective of the w/b ratio. In general, the addition of SAP reduced the workability, and compared to SAP-free mixtures the effect of the variation in w/b ratio was higher in the SAP-modified mixtures which showed a larger slump increase when w/b was changed from 0.42 to 0.44. Addition of colloidal nanosilica caused a slight reduction in slump at each w/b ratio. Similarly, the addition of slag cement also caused slight reduction of slump.

Figure 7.3 shows the effect of varying w/b ratio on the air content of different mortar mixtures. For mixtures with a w/b ratio of 0.44, air content ranged from approximately 7% to 11%, while those with a w/b ratio of 0.42 exhibited a wider range, from 5% to 14%. Overall, at the higher w/b ratio, SAP-free mixtures tended to show lower air content, whereas mixtures containing SAP exhibited higher air content. In contrast, at the lower w/b ratio, the trend reversed: SAP-free mixtures showed higher air content, while SAP-containing mixtures had lower air content.

In conventional cementitious systems, a higher w/b ratio increases paste volume and improves mix fluidity, which facilitates the entrainment and stabilization of air bubbles during mixing. In contrast, a lower w/b ratio typically produces a stiffer mix, making it more difficult for air to be entrapped and retained, thereby reducing air content. However, the mixtures in this study did not exhibit this expected trend. This deviation is likely attributable to adjustments made to the fine aggregate content during batching to maintain consistent total batch volumes across mixtures with different w/b ratios.

The air content of the reference mixtures (REF), approximately 8.4% for w/b 0.44 and ~9.6% for w/b 0.42, was used as baseline for comparison purposes, as indicated by green and blue dotted lines in Figure 7.3. For the mixes with w/b 0.42, the incorporation of colloidal nanosilica (NS1 and NS2) into the REF mixtures significantly increased the air content compared

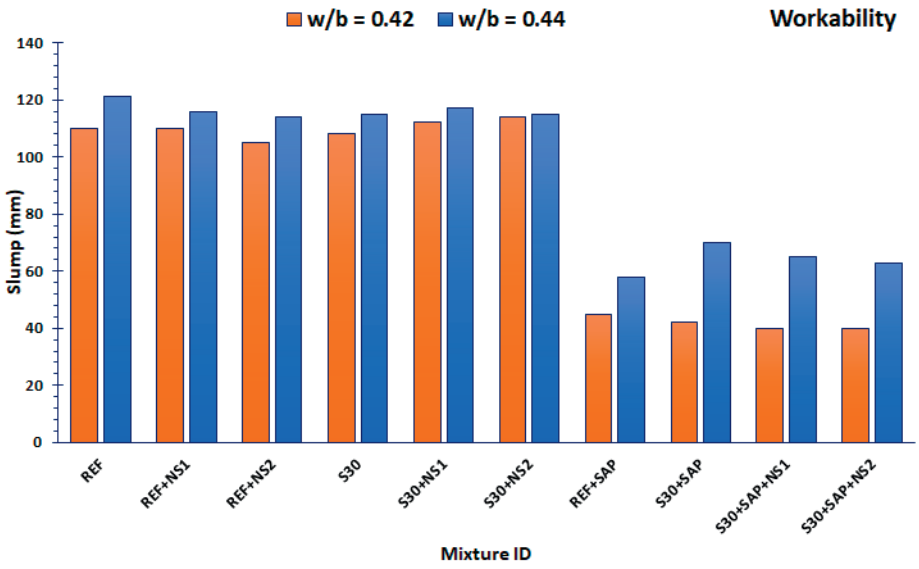


**Figure 7.2** Slump of Mortar Mixture Compositions With Varying w/b Ratio (0.42 and 0.44). Note: 1 mm = 0.0394 in.

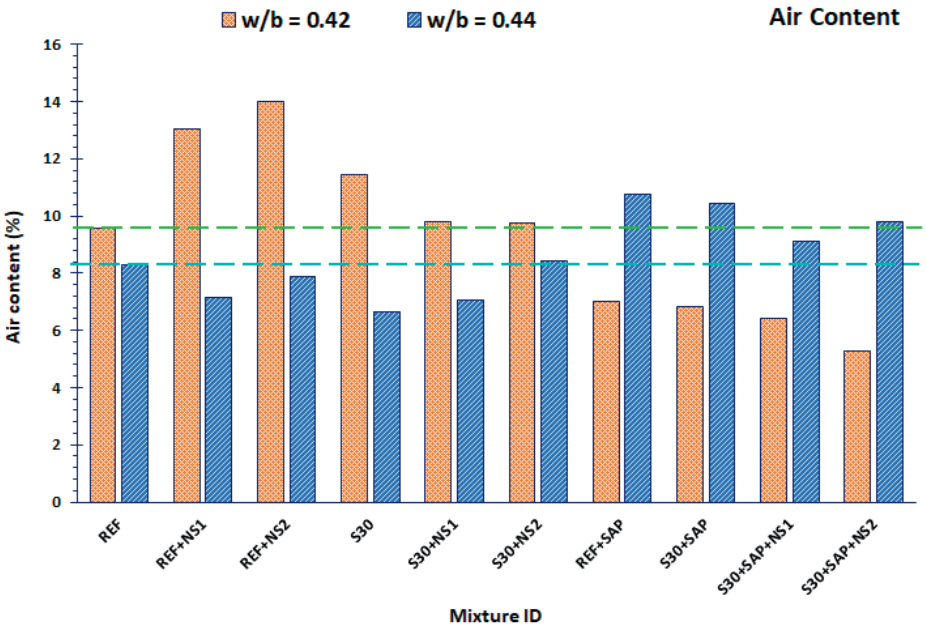


**Figure 7.3** Air Content of Mortar Mixture Compositions With Varying w/b Ratio (0.42 and 0.44), Dashed Lines Represent the Respective Reference Baseline.

to REF. This suggests that the presence of ultrafine particles may have promoted air entrainment by enhancing bubble formation and stabilization. Similarly, mixtures containing slag cement (S30) exhibited elevated air content compared to REF, likely due to fine particles of the slag contributing to increased air retention. Interestingly, when SAPs were combined with colloidal nanosilica (mixes S30+SAP+NS1 and S30+SAP+NS2), the air content was reduced relative to SAP-only mixes.

### *7.4.2 Compressive Strength*

Figure 7.4 and Figure 7.5 show the compressive strength of the various mixture composition with w/b 0.42 and 0.44 at 3, 7, and 28 days. The w/b 0.42 mixes show similar trends with consistently increasing compressive strength with age, moderate early and later age strength. At 3 days, REF and REF+NS1 mortar mixtures performed similarly (~3330 psi), while REF+NS2 mix is slightly lower. The mixes with 30% slag replacement

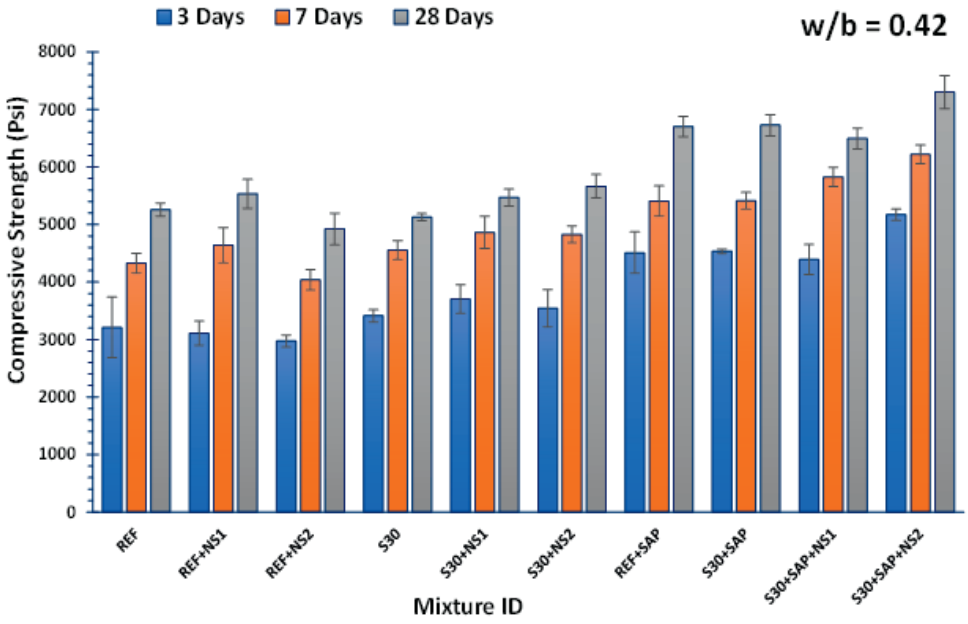


**Figure 7.4** Compressive Strength of Mixture Compositions With w/b Ratio 0.42. Note: 1 psi = 0.006895 MPa.

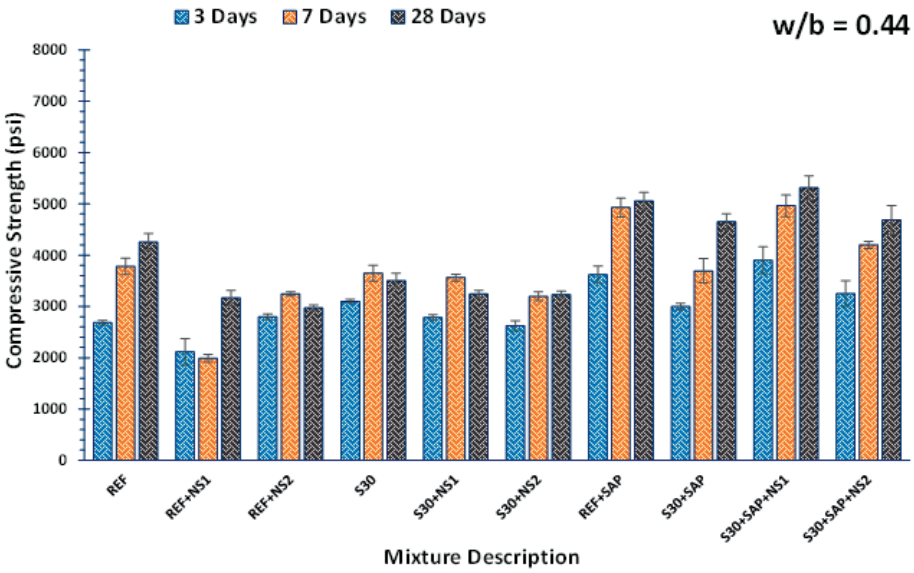


**Figure 7.5** Compressive Strength of Mixture Compositions With w/b Ratio 0.44. Note: 1 psi = 0.006895 MPa.

(S30 and S30+NS1/NS2) show moderate early strength (~3400–3600 psi). The SAP-modified mixes show higher early strength (4500–5200 psi). At 7 days, all mixes show significant increases in compressive strength. The REF+NS1/NS2 mixes show modest improvement in strength when compared to the REF, although REF+NS2 is slightly lower. The S30 mixes showed higher strength values compared to the REF, with S20+NS1/NS2 similar or slightly higher than both S30 and REF mixes.

All SAP-modified mixtures displayed increased early and 28-day strength values, compared to the SAP-free mixtures, for both w/b. The w/b 0.42 mixtures containing SAP, slag, and colloidal nanosilica had some of the highest compressive strength values, consistent with the reduced air content values reported in Figure 7.3, compared to SAP-free mixtures. Furthermore, across all mortar mixtures, the w/b 0.44 mixes had lower compressive strengths compared to the w/b 0.42 mixes due to increase water content and resulting higher capillary porosity. At higher w/b ratio, REF+NS1 and REF+NS2 mixes had reduced strengths at all ages unless used in combination with SAP and slag.

### 7.4.3 *Flexural Strength*

Figure 7.6 shows the flexural strength at 28 days for w/b 0.42 and 0.44 for the various mortar mixture compositions, the green and red dotted lines indicate the respective reference baseline for comparison purposes. The general trend shows consistently higher flexural strength values for mixes with lower w/b 0.42 across all mixtures. As expected, higher w/b ratio leads reduced strength due to increased porosity and weaker paste-aggregate bonding. The range of flexural strength were ~4.4–7.0 MPa (638–1015 psi) for w/b 0.42, and ~3.5–6.3 MPa (508–914 psi) for w/b 0.44.

Compared to the REF mixture, REF+NS1 and REF+NS2 mixes showed a decrease in flexural strength both for w/b 0.42 and 0.44, and it becomes significant at higher w/b 0.44, particularly REF+NS2. Slag cement mixtures show an increase in flexural strength compared to REF at lower w/b ratio, but addition of NS1 or NS2 results in lower strength at w/b 0.44. SAP significantly enhances flexural strength with REF+SAP and S30+SAP showing notable strength gains, particularly for w/b 0.42. Slag cement containing SAP+NS1/NS2 showed higher strength values compared to S30, indicating synergistic effect between slag, SAP and colloidal nanosilica at both w/b ratio.

### 7.4.4 *Ultrasonic Pulse Velocity*

Figure 7.7 shows the UPV of the w/b 0.42 and 0.44 mixtures. Mixes with w/b 0.42 generally have higher UPVs than those with w/b 0.44, indicating reduced permeability and better

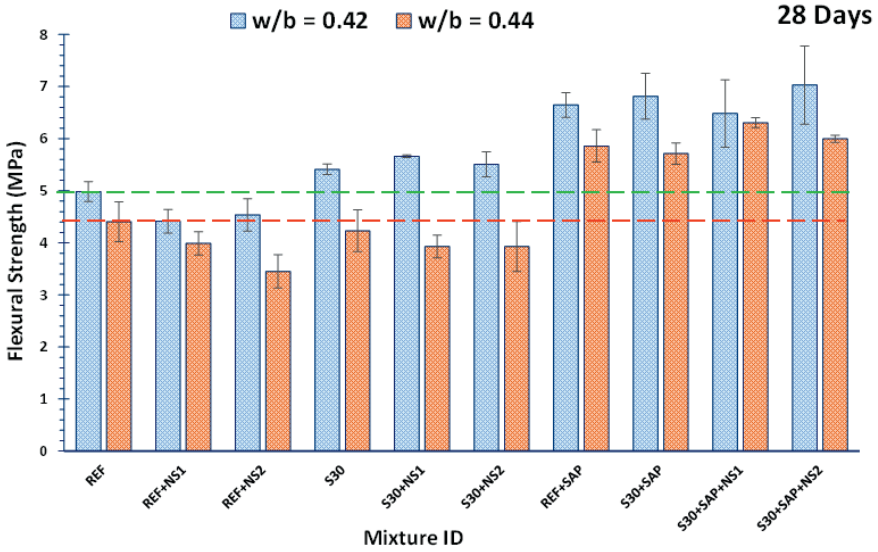


**Figure 7.6** Flexural Strength of Mixture Compositions with Varying w/b Ratio (0.42 and 0.44), Dashed Lines Represent the Respective Reference Baseline. Note: 1 MPa = 145.04 psi.

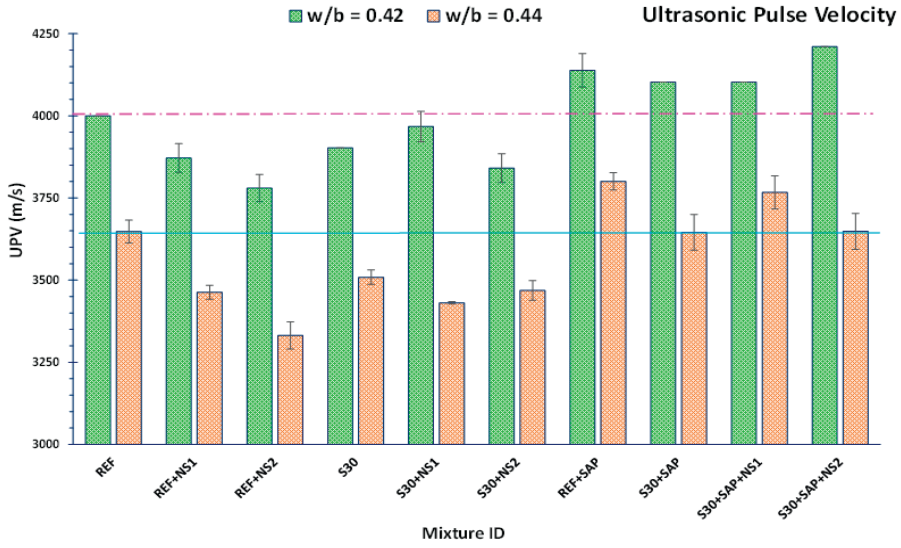


**Figure 7.7** Ultrasonic Pulse Velocity of Mixture Compositions with Varying w/b Ratio (0.42 and 0.44), Dashed Lines Represent the Respective Reference Baseline.

durability. Mixes with only colloidal nanosilica (REF+NS1/NS2, S30+NS1/NS2) have lower UPV, especially at w/b 0.44. This indicates possible dispersion challenges or ineffective pozzolanic reactions at higher water content, resulting in a less continuous matrix and increased permeability. SAP mixes show consistently high UPV values, indicating that SAPs enhance microstructural integrity. This aligns with high compressive and flexural strengths. REF+SAP and S30+SAP showed a notable UPV increase, particularly for w/b 0.42, compared to the SAP-free REF and S30 mixtures. Combination of SAP+S30+NS1/NS2 mixtures showed high UPV values, again indicating a synergistic effect between slag, SAP and nanosilica.

### *7.4.5 Drying Shrinkage*

Figure 7.8 and Figure 7.9 depict the drying shrinkage behavior of w/b 0.42 and 0.44 mixtures over a 25-day period. The higher w/b ratio mixtures generally resulted in higher shrinkage than w/b 0.42 mixtures due to more free water and the resulting capillary porosity. In general, all mixtures exhibited a rapid increase in drying shrinkage during the initial 5 days. This is typical as most drying shrinkage occurs in the initial stages when the moisture content in the mortar is high, and evaporation rates are substantial. Most mixtures show similar behavior during this initial period, indicating that the early-age shrinkage

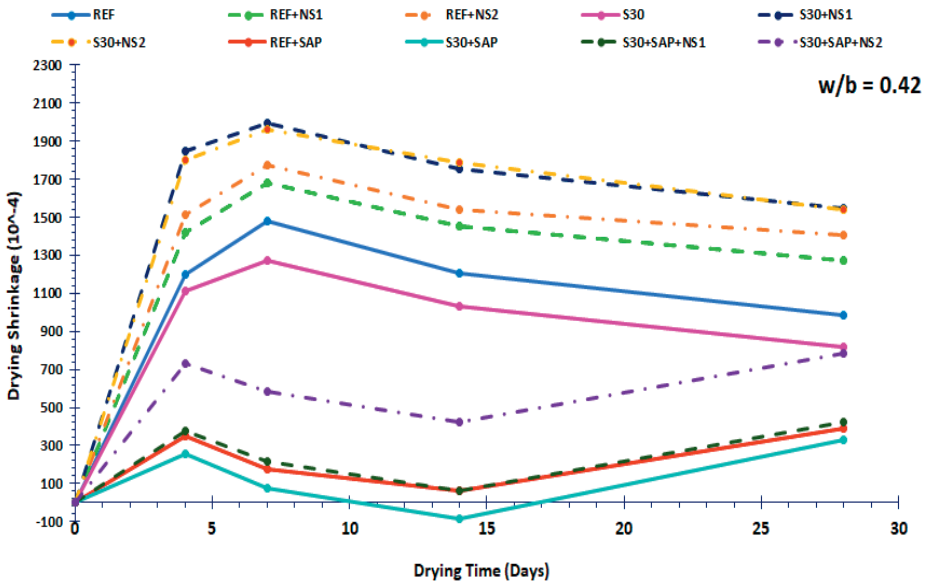


**Figure 7.8** Drying Shrinkage of Mortars Containing Different Admixtures, w/b 0.42.

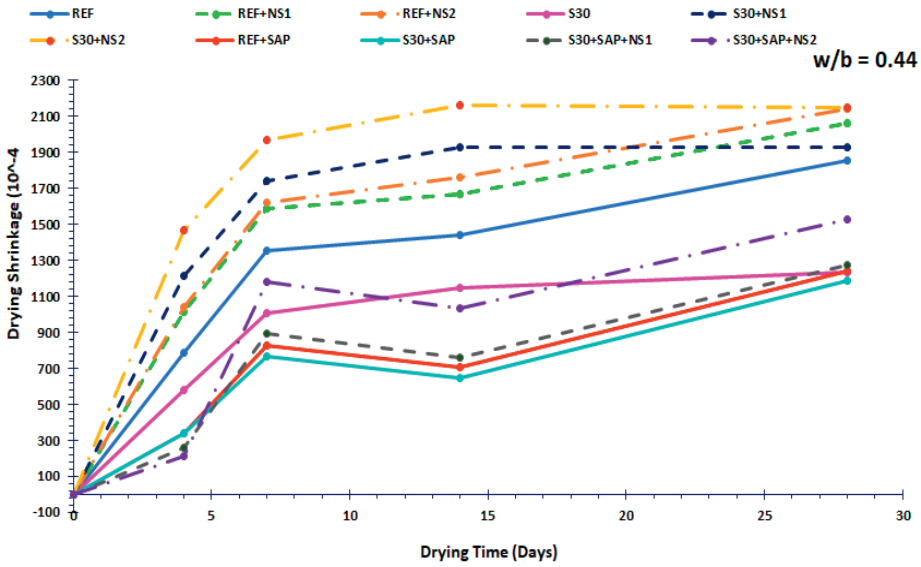


**Figure 7.9** Drying Shrinkage of Mortars Containing Different Admixtures, w/b 0.44.

was primarily driven by the water content and initial mix properties rather than the specific additives.

The relative drying shrinkage trends with additives were similar for both w/b 0.42 and 0.44 mixtures. REF and S30 mixtures show typical drying shrinkage patterns, with an initial rapid increase followed by stabilization to a value of shrinkage that was moderate compared to other mixtures. The S30 mixture exhibited a lower shrinkage compared to the REF mixture due to the dilution effect. The presence of colloidal nanosilica increased shrinkage, possibly due to its fine particle size and high reactivity, which could lead to more pronounced drying effects. The combination of slag with colloidal nanosilica significantly increased the drying shrinkage.

Mixtures containing SAP showed significantly reduced shrinkage compared to SAP-free mixtures. The initial shrinkage was much lower, stabilizing after ~15 days. SAP's ability to absorb and slowly release water helps in maintaining internal moisture and mitigates the effect of rapid water loss, thus reducing the overall shrinkage. S30+SAP mixtures display the lowest shrinkages among all mixtures. Furthermore, S30+SAP+NS1/NS2 mixtures have significantly reduced shrinkage compared to their SAP-free counterparts. The combined effect of SAP and slag seems to create an optimal moisture balance, reducing the adverse effects of nanosilica on shrinkage.

### *7.4.6 Setting Time*

The evolution of the penetration resistance (MPa) of mortar samples over time measured using a needle penetration resistance test is illustrated in Figure 7.10. The initial and final setting times are the threshold with penetration resistance of 3.5 MPa (500 psi) and 27.6 MPa (4000 psi), respectively. For all mixtures, the initial setting occurs within 270–320 min. The mixture without SAP exhibits a faster setting, with REF+NS1 achieving the fastest initial setting, followed by the S30+NS1 and S30 mixtures. This indicates that the combined effect of slag and colloidal nanosilica promotes early hydration. The addition of colloidal nanosilica enhances early hydration by providing nucleation sites for C-S-H, leading to earlier stiffening and higher penetration resistance at earlier times. S30 mix reacts more slowly but with supplementary materials like NS1 or SAP, its performance improves due to synergetic effects. The SAP-modified mixtures absorb water initially, then releases it during self-desiccation, leading to sustained hydration and accelerated setting. Most mixtures crossed the final setting threshold between 350–420 min. REF+NS1, S30, and S30+NS1 reached their final setting earlier while mixes with SAP (S30+SAP and REF+SAP) came later.

### *7.4.7 Autogenous Shrinkage*

Figure 7.11 shows the early-age deformation behavior obtained for the different w/b 0.44 mortar mixes after 72 hr. During the initial hours of hydration, all mixtures exhibited a rapid initial shrinkage phase typical for early hydration period. This coincides with the period of capillary water depletion and self-desiccation due to hydration. The peak negative strain (greatest strain) was observed around 20–25 hr. Although the SAP-modified mixtures appear to exhibit higher shrinkage compared to the SAP-free mixtures, this behavior is believed to be a test artifact related to the uptake of bleed water in the SAP-free mixtures. The results from the SAP-free mixtures were also likely influenced by bleeding. SAP-modified mixtures (REF+SAP, REF+SAP_2, and S30+SAP) displayed rapid stabilization after 30 hr, reflecting the onset of water release from the SAP particles into the pore structure. This behavior strongly indicates that the SAP effectively fulfills its internal curing function by providing additional water during the critical period of autogenous strain development.

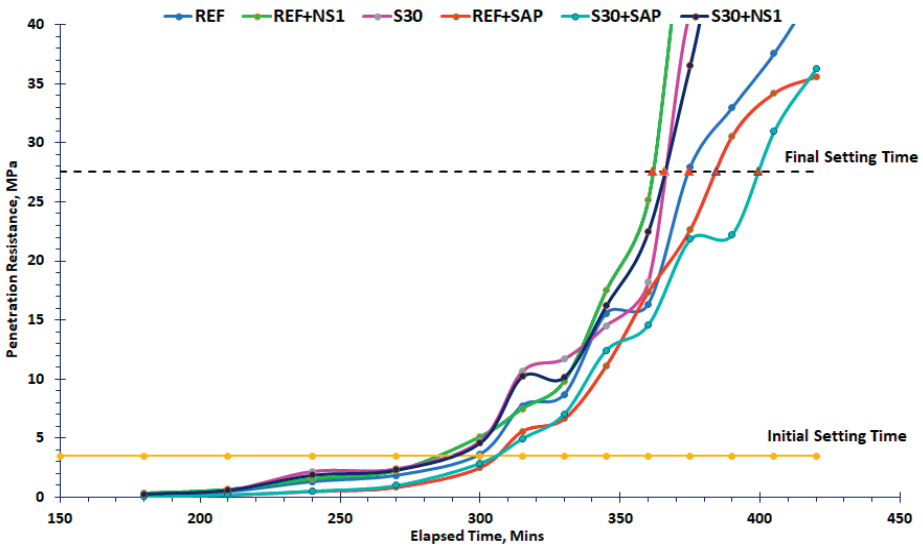


**Figure 7.10** Setting Times of Mortars Obtained by Penetration Resistance. Note: 1 MPa = 145.04 psi.

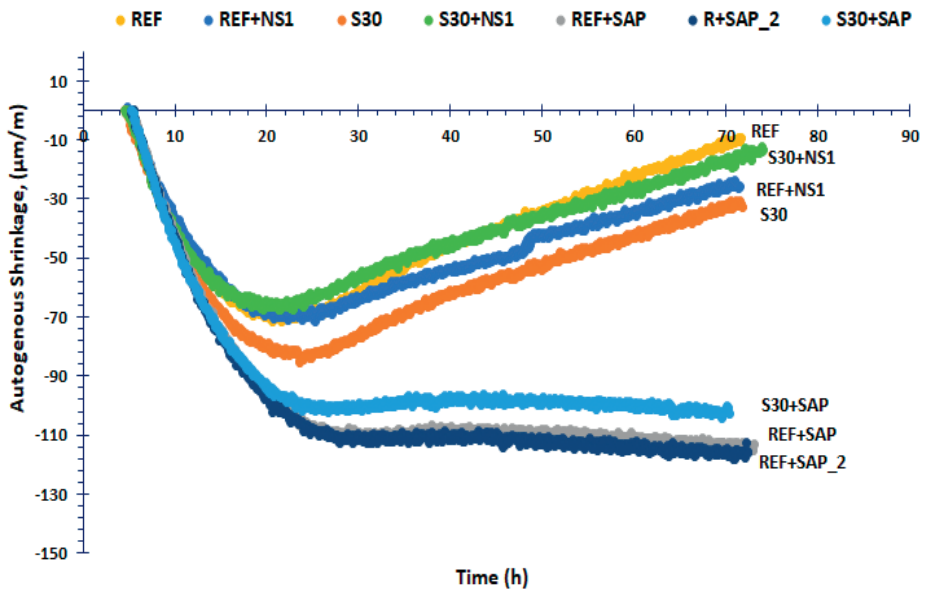


**Figure 7.11** Autogenous Shrinkage of Mortars Containing Different Admixtures, w/b 0.44.

### 7.5 Conclusions and Implications

The compressive and flexural strengths of plain and slag cement mortars at both w/b ratios were improved with the addition of SAP. Increases were largest for the lower w/b ratio mixtures (0.42) which had the lowest air content values. In contrast, the addition of colloidal nanosilica decreased strength values compared to the reference mixtures, except when combined with slag and SAP. UPV results were consistent with strength trends. Additionally, for both w/b ratios, drying shrinkage of plain and slag cement mortars was lowest for mixtures containing SAP and highest for mixtures containing colloidal nanosilica. Autogenous shrinkage experiments should be repeated in the future, as significant bleeding was observed for the SAP-free w/b 0.44 mixtures, which likely influenced the results.

## 8. MICROSTRUCTURE STUDY

### 8.1 Overview

This section describes some additional characterization that was performed on cores extracted from the field trial slabs (Chapter 6) to directly observe how the presence of SAP and colloidal nanosilica affected the plain cement and slag cement concrete microstructure. Results from both optical microscopy and scanning electron microscopy are presented below.

### 8.2 Methods

Concrete cores were extracted from field-cast slabs (described in Chapter 6) after 365 days. Cores were cut into three equal sections using a water-cooled concrete saw. The middle section of the center core was then selected and removed for characterization. This area was selected to best represent the bulk properties of the concrete cores and to avoid surface effects (e.g., surface damage from coring, carbonation, etc.). Specimen were oven dried at 50–60 °C (122–140 °F) for at least 48 hr under vacuum or desiccator conditions to avoid microstructural alteration due to moisture evaporation or hydration continuation. The procedures used for preparation of specimens for both optical and scanning electron microscopy (SEM) characterization are detailed in Figure 8.1.

For optical microscopy, specimens measuring 150 × 150 × 20 mm (3 × 3 × 0.8 in) were cut and polished. Polishing was performed using silicon carbide abrasives in successive grit sizes of 75, 35, 17.5, 12.5 µm (corresponding to No. 220, 320, 600, 800, and 1000, respectively). The surfaces were lapped sequentially with finer abrasives until a reflective finish suitable for optical observation was achieved, characterized by the clear reflection of a distant light source when viewed at an oblique angle.

An Olympus BX53M optical microscope was used to capture approximately 15 images per specimen at magnifications ranging from 25x to 400x. Lower magnifications were used for analyzing air voids and cracks, while higher magnifications facilitated evaluation of the interfacial transition zone (ITZ). The hardened air void system, including void content and distribution, was quantified following ASTM standard test method (C457) for microscopical determination of parameters of the air-void system in hardened concrete Procedure C—Contrast Enhanced Method (ASTM, 2024f). Representative images for each specimen, shown in Figure 8.2, were selected to illustrate commonly observed features.

For scanning electron microscopy, cubes of 20 mm (0.8 in.) per side were cut and mounted with epoxy using the Spurr Ultra Low Viscosity Embedding Kit. The epoxy-impregnated specimens were subsequently sectioned using a diamond-coated saw

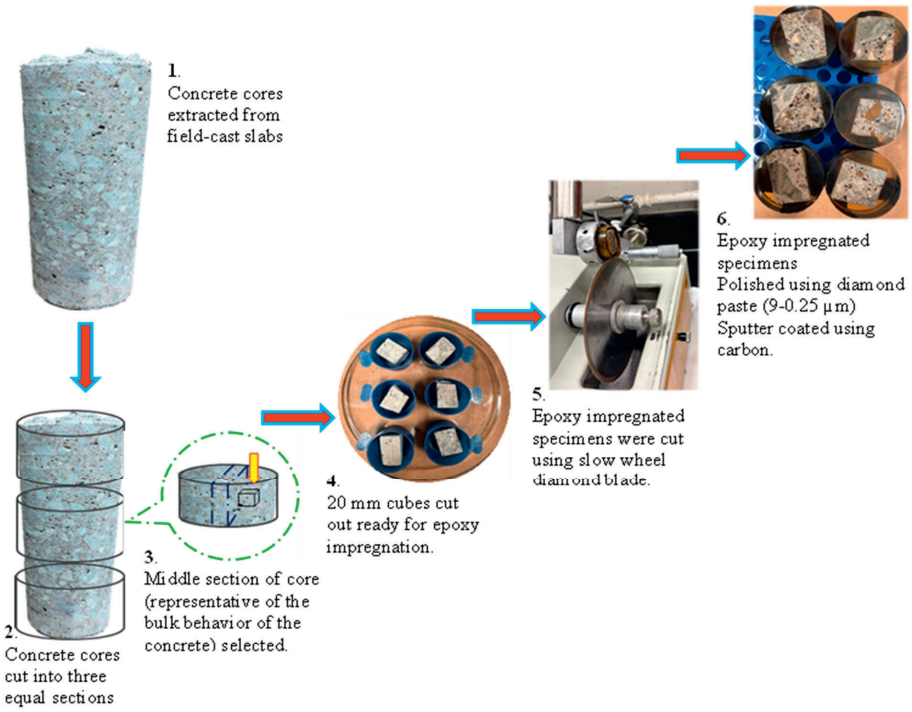


**Figure 8.1** Sample Preparation Procedures for Scanning Electron Microscopy.

(a) Slab 6: REF (b) Slab 7: REF+NS1 (c) Slab 8: S30

(d) Slab 9: S30+NS1 (e) Slab 10: REF+SAP (f) Slab 11: S30+SAP

**Figure 8.2** Optical Microscopy Images of Air Voids in Microstructure of Concretes from Various Slabs (Scale Bars Are 400 Micron).

blade and polished using progressively finer diamond-embedded lapping wheels (45 µm to 15 µm), followed by diamond polishing pastes ranging from 9 µm to 0.25 µm. Between each polishing step, specimens were cleaned with acetone to remove surface debris.

Polished specimens were sputter-coated with carbon and affixed to SEM stubs using carbon tape. Imaging was conducted using an FEI Quanta 650 SEM equipped with a backscattered electron (BSE) detector. Approximately 20 images were captured per specimen at magnifications ranging from 150x to 800x. The SEM was operated at an accelerating voltage of 30.00 kV, with a spot size of 4 nm and a working distance of 10 mm.

## 8.3 Results

Significant differences were observed in the microstructure of slag-free concretes: the reference mixture without any additives (slab #6, REF), the mixture containing colloidal nanosilica

(slab #7, REF+NS1), and the mixture incorporating SAP (slab #10, REF+SAP).

In the REF concrete, shown in Figure 8.2a, Figure 8.3a, and Figure 8.4a, air voids were uniformly distributed throughout the matrix. Shrinkage cracks were observed, along with some unhydrated cement particles, visible as white grains in Figure 8.4a. In the REF+NS1 concrete (Figure 8.2b, Figure 8.3b, and Figure 8.4b) a higher concentration of air voids with a non-uniform size distribution, typically less than 200 microns in size, was evident. Shrinkage cracks were also observed, along with a greater amount of unhydrated cement particles (Figure 8.4b), compared to the reference concrete.

The microstructure of the REF+SAP concrete, shown in Figure 8.2e, Figure 8.3e, and Figure 8.4e, contained noticeably fewer air voids, shrinkage cracks, and unhydrated cement grains, than the other two mixtures. A relatively small number of SAP-related macrovoids were also observed (Figure 8.3e and Figure 8.4e). These macrovoids, typically angular in shape and ranging from 400–600 microns in size, were sometimes partially filled with hydration products. These voids were formed as the SAP particles release adsorbed water into the surrounding cementitious matrix and simultaneously shrink in volume.

The microstructure of slag-cement concretes: including the mixture with slag only (slab #8, S30), the mixture with slag and

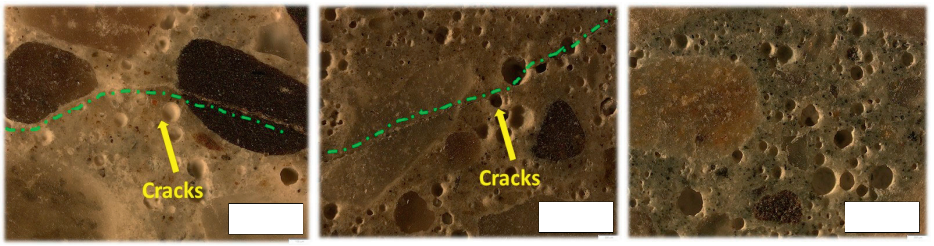


(a) Slab 6: REF (b) Slab 7: REF+NS1 (c) Slab 8: S30

(d) Slab 9: S30+NS1 (e) Slab 10: REF+SAP (f) Slab 11: S30+SAP

**Figure 8.3** Optical Microscope Images of Cracks and SAP-Related Microvoids in the Microstructure of Concrete from Various Slabs (Scale Bars are 400 Microns).

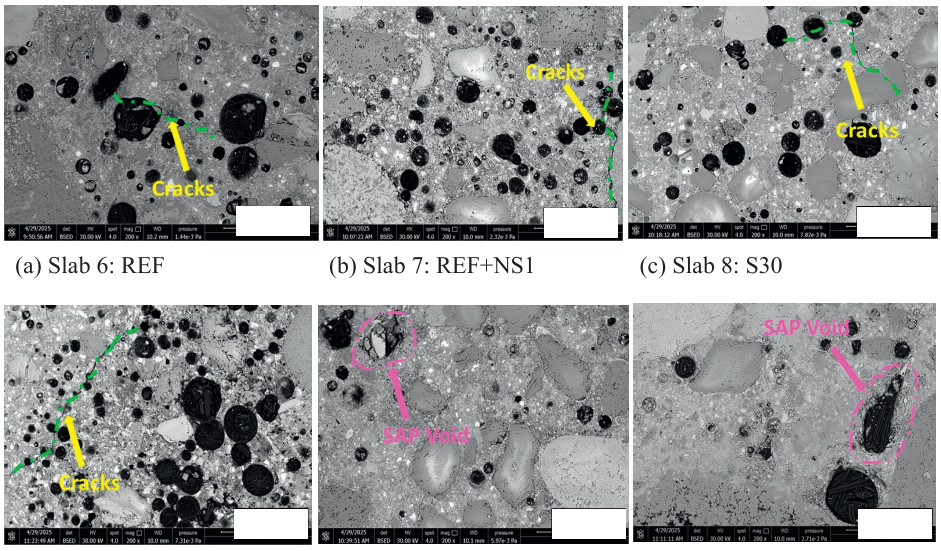


(a) Slab 6: REF (b) Slab 7: REF+NS1 (c) Slab 8: S30

(d) Slab 9: S30+NS1 (e) Slab 10: REF+SAP (f) Slab 11: S30+SAP

**Figure 8.4** Backscattered Electron Microscope Images of the Microstructure of Concrete From Various Slabs (Scale Bars Are 500 Microns).

colloidal nanosilica (slab #9, S30+NS1), and mixture with slag and SAP (slab #11, S30+SAP), displayed similar characteristics to those observed the corresponding slag-free mixtures.

In the S30 mixture, shown in Figure 8.2c, Figure 8.3c, and Figure 8.4c, air voids were uniformly distributed throughout the cement matrix. Shrinkage cracks were observed, along with some unhydrated cement and slag particles, visible as white and whitish-gray grains in Figure 8.4c. In the S30+NS1 mixture, shown in Figure 8.2d, Figure 8.3d, and Figure 8.4d, the microstructure appears more porous, with air voids estimated to be less than 100 micron in size. Shrinkage cracks were observed again, along with a larger quantity of unhydrated cement particles compared to the reference mixture, as seen in Figure 8.4d. Additionally, porous interfacial transition zones (ITZ) were also observed in higher magnification images. The matrix of the concrete cored from S30+SAP slab, shown in Figure 8.2f, Figure 8.3f, and Figure 8.4f, appeared to be denser, and contained fewer shrinkage cracks and unhydrated cement particles compared to the other slag-based mixtures.

### 8.4 Conclusions

Cores extracted from plain and slag cement concrete slabs containing SAP exhibited microstructure characterized by reduced amount of air voids, fewer shrinkage cracks, and a lower concentration of unhydrated cement particles compared to SAP-free reference slabs and those containing colloidal nanosilica. The refined microstructure observed in the SAP-cured mixtures compared to the SAP-free mixtures and mixtures containing colloidal nanosilica is consistent with the overall increase in performance of the SAP-cured concrete mixtures, including increased flexural and compressive strength.

## REFERENCES


Adams, C. J., Bose, B., Mann, E., Erk, K. A., Behnood, A., Castillo, A., Rodriguez, F. B., Wang, Y., & Olek, J. (2022). *Superabsorbent polymers for internally cured concrete* (Joint Transportation Research Program No. FHWA/IN/JTRP-2022/04). Purdue University. https://doi.org/10.5703/1288284317366

Adams, C. J., Bose, B., Olek, J., & Erk, K. A. (2022). Evaluation of mix design strategies to optimize flow and strength of mortar internally cured with superabsorbent polymers. *Construction and Building Materials*, *324*, 126664. https://doi.org/10.1016/j.conbuildmat.2022.126664

Almeida, F. C., & Klemm, A. J. (2018). Efficiency of internal curing by superabsorbent polymers (SAP) in PC-GGBS mortars. *Cement and Concrete Composites*, *88*, 41–51. https://doi.org/10.1016/j.cemconcomp.2018.01.002.

American Association of State Highway and Transportation Officials. (2022). *Standard practice for developing performance engineered concrete pavement mixtures* (AASHTO-R101-22).

American Association of State Highway and Transportation Officials. (2023). *Standard method of test for electrical resistivity of a cylinder tested in a uniaxial resistance test* (AASHTO T402-23).

ASTM International. (2012). *Standard test method for scaling resistance of concrete surfaces exposed to deicing chemicals* (ASTM C672-12).

ASTM International. (2015). *Standard test method for flow of hydraulic cement mortar* (ASTM C1437-15). https://doi.org/10.1520/C1437-15

ASTM International. (2017). *Standard test method for splitting tensile strength of cylindrical concrete specimens* (ASTM C496-17). https://doi.org/10.1520/C0496_C0496M-17

ASTM International. (2019). *Standard test method for autogenous strain of cement paste and mortar* (ASTM C1698-19). https://doi.org/10.1520/C1698-19

ASTM International. (2020a). *Standard practice for mechanical mixing of hydraulic cement pastes and mortars of plastic consistency* (ASTM C305-20). https://doi.org/10.1520/C0305-20

ASTM International. (2020b). *Standard test method for slump of hydraulic cement concrete* (ASTM C143-20). https://doi.org/10.1520/C0143_C0143M-20

ASTM International. (2021a). *Standard test method for density, absorption, and voids in hardened concrete* (ASTM C642-21). https://doi.org/10.1520/C0642-21

ASTM International. (2021b). *Standard test method for flexural strength of hydraulic-cement mortars* (ASTM C348-21). https://doi.org/10.1520/C0348-21

ASTM International. (2022a). *Standard guide for comparing performance of concrete-making materials using mortar mixtures* (ASTM C1810/C1810M-22). https://doi.org/10.1520/C1810_C1810M-22

ASTM International. (2022b). *Standard practice for measuring hydration kinetics of hydraulic cementitious mixtures using isothermal calorimetry* (ASTM C1679-22). https://doi.org/10.1520/C1679-22

ASTM International. (2022c). *Standard specification for mixing water used in the production of hydraulic cement concrete* (ASTM C1602-22). https://doi.org/10.1520/C1602_C1602M-22

ASTM International. (2022d). *Standard test method for Dynamic Young's Modulus, and Poisson's Ratio by impulse excitation of vibration* (ASTM E1876-22). https://doi.org/10.1520/E1876-22

ASTM International. (2022e). *Standard test method for flexural strength of concrete by the use of simple beam with third point loading* (ASTM C78-22). https://doi.org/10.1520/C0078_C0078M-22

ASTM International. (2022f). *Standard test method for ultrasonic pulse velocity through concrete* (ASTM C597-22). https://doi.org/10.1520/C0597-22

ASTM International. (2023). *Standard test method for time of setting of concrete mixtures by penetration resistance* (ASTM C403-23). https://doi.org/10.1520/C0403_C0403M-23

ASTM International. (2024a). *Standard test method for air content of freshly mixed concrete by pressure method* (ASTM C231-24). https://doi.org/10.1520/C0231_C0231M-24

ASTM International. (2024b). *Standard test method for compressive strength of cylindrical concrete specimens* (ASTM C39-24). https://doi.org/10.1520/C0039_C0039M-24

ASTM International. (2024c). *Standard test method for compressive strength of hydraulic-cement mortars (using 50 mm (2 in.) cube specimens)* (ASTM C109-24). https://doi.org/10.1520/C0109_C0109M-24

ASTM International. (2024d). *Standard test method for density (unit weight), yield, and air content (gravimetric) of concrete* (ASTM C138-24). https://doi.org/10.1520/C0138_C0138M-24

ASTM International. (2024e). *Standard test method for length change of hardened hydraulic-cement mortar and concrete* (ASTM C157-24). https://doi.org/10.1520/C0157_C0157M-24

ASTM International. (2024f). *Standard test method for microscopical determination of parameters of the air-void system in hardened concrete* (ASTM C457-24). https://doi.org/10.1520/C0457_C0457M-24

ASTM International. (2024g). *Standard specification for blended hydraulic cement* (ASTM C595/C595M-24). https://doi.org/10.1520/C0595_C0595M-24

ASTM International. (2024h). *Standard specification for slag cement use in concrete and mortars* (ASTM C989/C989M-24). https://doi.org/10.1520/C0989_C0989M-24

ASTM International. (2025). *Standard practice for making and curing concrete test specimens in the laboratory* (ASTM C192/C192M-25). https://doi.org/10.1520/C0192_C0192M-245

AzariJafari, H., Kazemian, A., Rahimi, M., & Yahia, A. (2016). Effects of pre-soaked super absorbent polymers on fresh and hardened properties of self-consolidating lightweight concrete. *Construction and Building Materials*, *113*, 215–220. https://doi.org/10.1016/j.conbuildmat.2016.03.010

Barrett, T. J., Miller, A. E., & Weiss, W. J. (2015). *Documentation of the INDOT experience and construction of the bridge decks containing internal curing in 2013* (Joint Transportation Research Program Publication No. FHWA/IN/JTRP-2015/10). Purdue University. https://doi.org/10.5703/1288284315532

Balapour, M., Joshaghani, A., & Althoey, F. (2018). Nano-SiO2 contribution to mechanical, durability, fresh and microstructural characteristics of concrete: A review. *Construction and Building Materials*, *181*, 27–41. https://doi.org/10.1016/j.conbuildmat.2018.05.266

Beushausen, H., & Gillmer, M. (2014). The use of superabsorbent polymers to reduce cracking of bonded mortar overlays. *Cement and Concrete Composites*, *52*, 1–8. https://doi.org/10.1016/j.cemconcomp.2014.03.009

Beushausen, H., Gillmer, M., & Alexander, M. (2014). The influence of superabsorbent polymers on strength and durability properties of blended cement mortars. *Cement and Concrete Composites*, *52*, 73–80. https://doi.org/10.1016/j.cemconcomp.2014.03.008

Bose, B., Davis, C. R., & Erk, K. A. (2021). Microstructural refinement of cement paste internally cured by polyacrylamide composite hydrogel particles containing silica fume and nanosilica. *Cement and Concrete Research*, *143*, 106400. https://doi.org/10.1016/j.cemconres.2021.106400

Davis, C. R., Bose, B., Alcaraz, A., Martinez, C. J., & Erk, K. A. (2020). Altering the crosslinking density of polyacrylamide hydrogels to increase swelling capacity and promote calcium hydroxide growth in cement voids. In W. P. Boshoff, R. Combrinck, V. Mechtcherine, & M. Wyrzykowski (Eds.), *3rd International Conference on the Application of Superabsorbent Polymers (SAP) and Other New Admixtures Towards Smart Concrete* (pp. 20–28). Springer, Cham. https://doi.org/10.1007/978-3-030-33342-3_3

De Meyst, L., Kheir, J., Tenório Filho, J. R., Van Tittelboom, K., & De Belie, N. (2020). The use of superabsorbent polymers in high performance concrete to mitigate autogenous shrinkage in a large-scale demonstrator. *Sustainability*, *12*(11), 4741. https://doi.org/10.3390/su12114741

Erk, K. A., & Bose, B. (2018). Using polymer science to improve concrete: Superabsorbent polymer hydrogels in highly alkaline environments. In F. Horkay, J. F. Douglas, & E. Del Gado (Eds.), *Gels and other soft amorphous solids* (pp. 333–356). American Chemical Society. https://doi.org/10.1021/bk-2018-1296.ch017

Espinoza-Hijazin, G., & Lopez, M. (2011). Extending internal curing to concrete mixtures with W/C higher than 0.42. *Construction and Building Materials*, *25*(3), 1236–1242. https://doi.org/10.1016/j.conbuildmat.2010.09.031

Friedrich, S. (2012). Superabsorbent polymers (SAP). In V. Mechtcherine & H. W. Reinhardt (Eds.), *Application of superabsorbent polymers (SAP) in concrete construction* (pp. 13–19). Springer Dordrecht. https://doi.org/10.1007/978-94-007-2733-5_3

Hasholt, M. T., & Jensen, O. M. (2015). Chloride migration in concrete with superabsorbent polymers. *Cement and Concrete Composites*, *55*, 290–297. https://doi.org/10.1016/j.cemconcomp.2014.09.023

Henkensiefken, R., Castro, J., Bentz, D., Nantung, T., & Weiss, J. (2009). Water absorption in internally cured mortar made with water-filled lightweight aggregate. *Cement and Concrete Research*, *39*(10), 883–892. https://doi.org/10.1016/j.cemconres.2009.06.009

Huang, D., Velay-Lizancos, M., & Olek, J. (2024). Scaling risk index of concretes containing Nano-TiO2 and supplementary cementitious materials. *Transportation Research Record*, *2678*(3), 148–161. https://doi.org/10.1177/03611981231178806

Indiana Department of Transportation. (2024a). *Division 700: Structures*. https://www.in.gov/dot/div/contracts/standards/book/sep23/700-2024.pdf. Accessed June 2024

Indiana Department of Transportation. (2024b). *Standard specifications: Section 900*. https://www.in.gov/dot/div/contracts/standards/book/sep23/900-2024.pdf

Kang, S. H., Hong, S. G., & Moon, J. (2017). Absorption kinetics of superabsorbent polymers (SAP) in various cement-based solutions. *Cement and Concrete Research, 97*, 73–83. https://doi.org/10.1016/j.cemconres.2017.03.009

Kong, X. M., Zhang, Z. L., & Lu, Z. C. (2015). Effect of pre-soaked superabsorbent polymer on shrinkage of high-strength concrete. *Materials and Structures*, *48*(9), 2741–2758. https://doi.org/10.1617/s11527-014-0351-2

Krafcik, M. J., & Erk, K. A. (2016). Characterization of superabsorbent poly (sodium-acrylate acrylamide) hydrogels and influence of chemical structure on internally cured mortar. *Materials and Structures*, *49*, 4765–4778. https://doi.org/10.1617/s11527-016-0823-7

Krafcik, M. J., Macke, N. D., & Erk, K. A. (2017). Improved concrete materials with hydrogel-based internal curing agents. *Gels*, *3*(4), 46. https://doi.org/10.3390/gels3040046

Lange, D. A., Khayat, K., D'Ambrosia, M., Farzadnia, N., Gu, Y., Pattaju, K., Clark, J., Shen, C., & Zuo, R. (2021). *Superabsorbent polymers in concrete to improve durability* (Illinois State Toll Highway Authority Report No. ISTHA 18-02R). https://agency.illinoistollway.com/documents/20184/1185382/Superabsorbent+Polymers+in+Concrete+to+Improve+Durability.pdf/e73dae54-794f-46a7-4c34-f98d0a8a6735?version=1.0&t=1638970996969

Lefever, G., Tsangouri, E., Snoeck, D., Aggelis, D. G., De Belie, N., Van Vlierberghe, S., & Van Hemelrijck, D. (2020). Combined use of superabsorbent polymers and nanosilica for reduction of restrained shrinkage and strength compensation in cementitious mortars. *Construction and Building Materials*, *251*, 118966. https://doi.org/10.1016/j.conbuildmat.2020.118966.

Li, Z., Wyrzykowski, M., Dong, H., Granja, J., Azenha, M., Lura, P., & Ye, G. (2020). Internal curing by superabsorbent polymers in alkali-activated slag. *Cement and Concrete Research*, *135*, 106123. https://doi.org/10.1016/j.cemconres.2020.106123.

Liu, F., Wang, J., Qian, X., & Hollingsworth, J. (2017). Internal curing of high-performance concrete using cenospheres. *Cement and Concrete Research*, *95*, 39–46. https://doi.org/10.1016/j.cemconres.2017.02.023

Lura, P., Friedemann, K., Stallmach, F., Mönnig, S., Wyrzykowski, M., & Esteves, L. P. (2011). Kinetics of water migration in cement-based systems containing superabsobent polymers. In V. Mechtcherine & H. W. Reinhardt (Eds.), *Application of superabsorbent polymers (SAP) in concrete construction* (pp. 21–37). Springer Dordrecht. https://doi.org/10.1007/978-94-007-2733-5_4

Ma, X., Liu, J., Wu, Z., & Shi, C. (2017). Effects of SAP on the properties and pore structure of high-performance cement-based materials. *Construction and Building Materials*, *131*, 476–484. https://doi.org/10.1016/j.conbuildmat.2016.11.090

Mechtcherine, V., Schröfl, C., Wyrzykowski, M., Gorges, M., Lura, P., Cusson, D., Margeson, J., De Belie, J., Snoeck, D., Ichimiya, K., Igarashi, S. -I., Falikman, V., Friedrich, S., Bokern, J., Kara, P., Marciniak, A., Reinhardt, H. -W., Sippel, S., Bettencourt Ribeiro, A., . . ., & Weiss, J. (2017). Effect of superabsorbent polymers (SAP) on the freeze–thaw resistance of concrete: Results of a RILEM interlaboratory study. *Materials and Structures*, *50*(1), 1–19. https://doi.org/10.1617/s11527-016-0868-7

Mignon, A., Snoeck, D., Schaubroeck, D., Luickx, N., Dubruel, P., Van Vlierberghe, S., & De Belie, N. (2015). pH-responsive superabsorbent polymers: A pathway to self-healing of mortar. *Reactive and Functional Polymers*, *93*, 68–76. https://doi.org/10.1016/j.reactfunctpolym.2015.06.003

Miller, A. E., Barrett, T. J., Zander, A. R., & Weiss, W. J. (2014). Using a centrifuge to determine moisture properties of lightweight fine aggregate for use in internal curing. *Advances in Civil Engineering Materials*, *3*(1), 20130111. https://doi.org/10.1520/ACEM20130111

Mudiyanselage, T. K., & Neckers, D. C. (2008). Highly absorbing superabsorbent polymer. *Journal of Polymer Science, Part A: Polymer Chemistry*, *46*(4), 1357–1364. https://doi.org/10.1002/pola.22476

Olivier, G., Combrinck, R., Kayondo, M., & Boshoff, W. P. (2018). Combined effect of nano-silica, super absorbent polymers, and synthetic fibres on plastic shrinkage cracking in concrete. *Construction and Building Materials*, *192*, 85–98. https://doi.org/10.1016/j.conbuildmat.2018.10.102

Schröfl, C., Erk, K. A., Siriwatwechakul, W., Wyrzykowski, M., & Snoeck, D. (2022). Recent progress in superabsorbent polymers for concrete. *Cement and Concrete Research*, *151*, 106648. https://doi.org/10.1016/j.cemconres.2021.106648

Schröfl, C., Snoeck, D., & Mechtcherine, V. (2017). A review of characterization methods for superabsorbent polymer (SAP) samples to be used in cement-based construction materials: Report of the RILEM TC 260-RSC. *Materials and Structures*, *50*(197). https://doi.org/10.1617/s11527-017-1060-4

Scott, P. (2024). *The impact of internal curing additives on compressive strength, shrinkage, and internal relative humidity of mortars* (Paper 4409) [Master's thesis, University of Louisville]. https://ir.library.louisville.edu/etd/4409

Seshadri, A. N., Lucas, A. Z., Howarter, J. A., & Erk, K. A. (2025). The impacts of silane functionalized hydrogels on early-age nucleation and growth of cement hydrates. Polymer, 332, 128548. https://doi.org/10.1016/j.polymer.2025.128548

Snoeck, D., Jensen, O. M., & De Belie, N. (2015). The influence of superabsorbent polymers on the autogenous shrinkage properties of cement pastes with supplementary cementitious materials. *Cement and Concrete Research*, *74*, 59–67. https://doi.org/10.1016/J.CEMCONRES.2015.03.020

Snoeck, D., Schaubroeck, D., Dubruel, P., & De Belie, N. (2014). Effect of high amounts of superabsorbent polymers and additional water on the workability, microstructure and strength of mortars with a water-to-cement ratio of 0.50. *Construction and Building Materials*, 72, 148–157. https://doi.org/10.1016/j.conbuildmat.2014.09.012

Snoeck, D., Velasco, L. F., Mignon, A., Van Vlierberghe, S., Dubruel, P., Lodewyckx, P., & De Belie, N. (2015). The effects of superabsorbent polymers on the microstructure of cementitious materials studied by means of sorption experiments. *Cement and Concrete Research*, *77*, 26–35. https://doi.org/10.1016/j.cemconres.2015.06.013

Tenório Filho, J. R., Snoeck, D., & De Belie, N. (2020). Mixing protocols for plant-scale production of concrete with superabsorbent polymers. *Structural Concrete*, *21*(3), 983–991. https://doi.org/10.1002/suco.201900443

Vafaei, B., Farzanian, K., & Ghahremaninezhad, A. (2020). The influence of superabsorbent polymer on the properties of alkali-activated slag pastes. *Construction and Building Materials*, *236*, 117525. https://doi.org/10.1016/j.conbuildmat.2019.117525

Van, V. -T. -A., Rößler, C., Bui, D. -D., & Ludwig, H. -M. (2014). Rice husk ash as both pozzolanic admixture and internal curing agent in ultra-high-performance concrete. *Cement and Concrete Composites*, *53*, 270–278. https://doi.org/10.1016/j.cemconcomp.2014.07.015

Wang, F., Zhou, Y., Peng, B., Liu, Z., & Hu, S. (2009). Autogenous shrinkage of concrete with super-absorbent polymer. *ACI Materials Journal*, *106*(2), 123. https://doi.org/10.14359/56458

Wang, J., Cheng, Y., Yuan, L., Xu, D., Du, P., Hou, P., Zhou, Z., Cheng, X., Liu, S., & Wang, Y. (2020). Effect of nano-silica on chemical and volume shrinkage of cement-based composites. *Construction and Building Materials*, *247*, 118529. https://doi.org/10.1016/j.conbuildmat.2020.118529

Zhang, L., Bian, M., Xiao, Z., Wang, X., & Han, B. (2023). A comprehensive review of cementitious composites modified with nano silica: Fabrication, microstructures, properties and applications. *Construction and Building Materials*, *409*, 133922. https://doi.org/10.1016/j.conbuildmat.2023.133922

Zhu, Q., Barney, C. W., & Erk, K. A. (2015). Effect of ionic crosslinking on the swelling and mechanical response of model superabsorbent polymer hydrogels for internally cured concrete. *Materials and Structures*, *48*, 2261–2276. https://doi.org/10.1617/s11527-014-0308-5

## APPENDICES

**Appendix A. Mill Certificates of Materials**

# Appendix A. Mill Certificates of Materials

# Buzzi Unicem USA

**MILL CERTIFICATION REPORT**
**PORTLAND LIMESTONE CEMENT**
**TYPE 1L (10)**

**Certification Date:** 08/09/23
**Cement Type:** Type IL
**Laboratory:** Greencastle, IN Plant

We hereby certify that this cement complies with current ASTM C595, AASHTO M240 Specifications.
The following data represents the average for the Buzzi Unicem USA cement that was produced in the month of
**July,2023**

| ASTM STANDARD REQUIREMENTS | | | MILL CERTIFICATION VALUES | | | |
|---|---|---|---|---|---|---|
| **CHEMICAL DATA ASTM C-595** | | | **CHEMICAL DATA** | | | |
| $SO_3$ - % | max 3.0%*** | | $SO_3$ - % | 3.35 | | |
| Loss on Ignition - % | max 10% | | Loss on Ignition - % | 5.32 | | |
| Insoluble Residue - % | | | Insoluble Residue - % | 0.63 | | |
| $CO_2$ in Cement - % | A | | $CO_2$ in Cement - % | 4.74 | | |
| Limestone - % | max 15.0 | | Limestone - % | 11.15 | | |
| $CaCO_3$ in Limestone - % | min 70.0 | | $CaCO_3$ in Limestone - % | 92.78 | | |
| Na2O Equivalent - % | | | $Na_2O$ Equivalent - % | 0.62 | | |
| $SiO_2$ -% | A | | $SiO_2$ -% | 18.36 | | |
| $Al_2O_3$ - % | A | | $Al_2O_3$ - % | 4.61 | | |
| $Fe_2O_3$ - % | A | | $Fe_2O_3$ - % | 2.74 | | |
| CaO - % | A | | CaO - % | 62.64 | | |
| MgO - % | max 6.0% | | MgO - % | 3.0 | | |
| | | **PHYSICAL DATA** | | | | |
| Mortar Bar Expansion C-1038 | max 0.020 | | Mortar Bar Expansion C-1038 | 0.001 | | |
| Fineness- Blaine -$cm^2/g$ | min 2600 | ASTM C-204 | Blaine - $cm^2/g$ | 4142 | | |
| Fineness- #325 Sieve Passing (%) | A | ASTM C-430 | #325 Sieve Passing (%) | 92.3 | | |
| Autoclave Expansion % (C151) | max 0.80 | ASTM C-151 | Autoclave Expansion % (C151) | 0.053 | | |
| Time of Set | | | Time of Set | | | |
| Vicat (minutes) | min 45 | ASTM C-191 | Vicat (minutes) Initial | 101 | | |
| | max 375 | | Final | 222 | | |
| Air Content % | max 12 | ASTM C-185 | Air Content % | 8.7 | | |
| Compressive Strength: | | ASTM C-109 | Compressive Strength: | | | |
| 1 day - psi (Mpa) | A | | 1 day - psi (Mpa) | 2256 | (15.56) | |
| 3 day - psi (Mpa) | 1740 (12.0) | | 3 day - psi (Mpa) | 3739 | (25.78) | |
| 7 day - psi (Mpa) | 2760 (19.0) | | 7 day - psi (Mpa) | 4559 | (31.43) | |
| 28 day - psi (Mpa) | A | | 28 day - psi (Mpa) | 5691 | (39.24) | Previous Months Ave |

^A^ *Not Applicable*
*~Adjusted per ASTM C595 Annex 7.1.5*

Additional Information

| Limestone data from XRF | |
|---|---|
| Amount (%) | 11.15 |
| SiO2 (%) | 2.26 |
| Al2O3 (%) | 0.64 |
| Fe2O3 (%) | 0.31 |
| CaO (%) | 51.98 |
| SO3 (%) | 0.36 |

T-1L

| | | |
|---|---|---|
| C3A | | 7.59 |
| Specific Gravity | ASTM C-188 | 3.09 |

** Not applicable.*
*** Adjusted per ASTM C150 Annex A1.6*
**** It is permissible to exceed the values for SO3 content, provided that the Mortar Bar Expansion C1038 does not exceed 0.020 % at 14 days*

ATTN:

| Silo | Bill of Lading | Tons | Date |
|---|---|---|---|
| | | | |

**BUZZI UNICEM USA, Greencastle Plant**
3301 S CR 150W,Greencastle, IN 46135, Phone 765.653.9766

By _____
**Mark Fajt**
**Quality Manager/OIC**

STATE OF INDIANA}
COUNTY OF PUTNAM}

Before me the undersigned, a Notary Public for Putnam County, State of Indiana personally appeared Mark Fajt and acknowledged the the execution of the foregoing instrument this day 2021.

Kyle D. Messmer, Notary Public
My commission expires November 24, 2028.

ECOMATERIAL TECHNOLOGIES

**Materials Testing & Research Facility**
2650 Old State Hwy 113
Taylorsville, GA 30178
770-684-0102

# ASTM C618 / AASHTO M295 Testing of Prairie State Fly Ash

**Sample Date:** 8/1 - 8/31/22 **Report Date:** 10/14/2022
**Sample Type:** Monthly **MTRF ID:** 1736PS
**Sample ID:** MnDOT Split

| Chemical Analysis | Results | | ASTM Limit Class F / C | AASHTO Limit Class F / C |
|---|---|---|---|---|
| Silicon Dioxide (SiO2) | 55.00 | % | | |
| Aluminum Oxide (Al2O3) | 18.37 | % | | |
| Iron Oxide (Fe2O3) | 10.77 | % | | |
| Sum (SiO2+Al2O3+Fe2O3) | 84.14 | % | 50.0 min | 50.0 min |
| Sulfur Trioxide (SO3) | 1.32 | % | 5.0 max | 5.0 max |
| Calcium Oxide (CaO) | 6.15 | % | 18.0 max / >18.0 | 18.0 max / >18.0 |
| Magnesium Oxide (MgO) | 1.45 | % | | |
| Sodium Oxide (Na2O) | 1.20 | % | | |
| Potassium Oxide (K2O) | 2.73 | % | | |
| Total Alkali (Sodium Oxide Equivalent) | 3.0 | % | | |
| Moisture | 0.06 | % | 3.0 max | 3.0 max |
| Loss on Ignition | 0.59 | % | 6.0 max | 5.0 max |
| Available Alkalies, as Na2Oe | 0.91 | % | Not Required | 1.5 max* *when required by purchaser |
| **Physical Analysis** | | | | |
| Fineness, % retained on 45-µm sieve | 19.27 | % | 34 max | 34 max |
| Fineness Uniformity | 0.4 | % | ±5 max | ±5 max |
| Strength Activity Index - 7 or 28 day requirement | | | | |
| 7 day, % of control | 88 | % | 75 min | 75 min |
| 28 day, % of control | 94 | % | 75 min | 75 min |
| Water Requirement, % control | 94 | % | 105 max | 105 max |
| Autoclave Soundness | -0.05 | % | 0.8 max | 0.8 max |
| Density, ASTM C604 | 2.37 | g/cm3 | | |
| Density Uniformity | 0.4 | % | ±5 max | ±5 max |

**The test data listed herein was generated by applicable ASTM methods. The reported results pertain only to the sample(s) or lot(s) tested. This report cannot be reproduced without permission from EM Resources LLC. This material meets the requirements of Florida DOT 929 specification.**

Christy Sieg
Lab Manager

AASHTO ACCREDITED

SKYWAY CEMENT COMPANY

# Material Certification Report

| | |
|---|---|
| Brand: | Skyway Cement |
| Material: | Slag Cement |
| Grade: | 100 |
| Date Range: | April 1-30, 2023 |
| Lot Number: | Multiple Lots |

## Certification

**This cement meets the requirements of ASTM C989 and AASHTO M302 specifications for Grade 100 slag cement.**

## General Information

| | | | |
|---|---|---|---|
| Supplier: | Skyway Cement Company LLC. | Source Location: | Skyway Cement Company LLC. |
| Address: | 3020 East 103rd Street | | 3020 East 103rd Street |
| | Chicago, IL 60617 | | Chicago, IL 60617 |
| Telephone: | (872)302-5910 | Contact: | Roberto Carrillo |
| Date Issued: | 15-May-2023 | | |

The following information is based on average test data during the test period.
The data is typical of slag cement shipped by Skyway Cement Company LLC.; individual shipments may vary.

## Test Data on ASTM Standard Requirements

| Chemical | | | Physical | | |
|---|---|---|---|---|---|
| Item | Limit[A] | Result | Item | Limit[A] | Result |
| | | | +45 µm (No. 325) Sieve (%) | 20 max | 0.61 |
| | | | Blaine Fineness (m2/kg) | - | 563 |
| Sulfide S (%) | 2.5 max | 0.84 | Air Content (%) | 12 max | 3.97 |
| Sulfate Ion - $SO_3$ (%) | - | 0.31 | Slag Activity Index (%) | | |
| | | | Avg 7 Day Index | - | 80 |
| Aluminum Oxide (%) | - | 9.85 | Avg 28 Day Index | 95 min | 108 |
| Chloride - CL (%) | - | 0.12 | Compressive Strength - MPa (psi): | | |
| | | | Slag + Reference Cement | | |
| Total Alkalies as Na2O (%) | - | 0.60 | 7 Day | - | 23 (3380) |
| | | | 28 Day | - | 39 (5688) |
| | | | Reference Cement[B] | | |
| | | | 7 Day | - | 28 (4186) |
| | | | 28 Day | - | 36 (5356) |

## Reference Cement Qualification Data

| Chemical | | | Physical | | |
|---|---|---|---|---|---|
| Item | Limit[A] | Result | Item | Limit[A] | Result |
| Total Alkalies as $Na_2O$ (%) | 0.60 - 0.90 | 0.83 | Blaine Fineness (m^2/kg) | - | 372 |
| $C_3S$ | - | 40.8 | | | |
| $C_2S$ | - | 30.7 | Compressive Strength - MPa (psi): | | |
| $C_3A$ | - | 10.5 | 7 Day | - | 27 (4006) |
| $C_4AF$ | - | 7.8 | 28 Day | 34.5 (5000) min | 35 (5018) |

## Notes

[A]Dashes in the limits columns means Not Applicable

[B]Reference cement results from procedure "Preparation of Specimens". Information on Reference Cement qualification available upon request.

Specific Gravity: 2.89

This data may have been reported on previous mill certificates. It is typical of the cement being currently shipped which was produced in April of 2023.

Quality Manager

Noblesville Stone
P. O. Box 457
Noblesville, Indiana 46061
317-776-4460

# Statistical Analysis Report

**Plant** Noblesville Stone-25109
**Product** #8 AP Stone-0038
**Specification** INDOT #8 AP
**Period** 04/29/94 - 08/01/23

| Sample Id | Date | 1" (25mm) (%) | 3/4" (19mm) (%) | 1/2" (12.5mm) (%) | 3/8" (9.5mm) (%) | #4 (4.75mm) (%) | #8 (2.36mm) (%) | Pan (%) |
|---|---|---|---|---|---|---|---|---|
| 1569840956 | 12/14/22 10:00 | 100.0 | 90.9 | 49.2 | 30.2 | 10.1 | 5.3 | 0.00 |
| 1555441036 | 01/05/23 10:00 | 100.0 | 91.5 | 49.2 | 32.3 | 9.4 | 5.1 | 0.00 |
| 1617606962 | 01/24/23 13:00 | 100.0 | 89.6 | 46.8 | 26.2 | 6.3 | 3.5 | 0.00 |
| 1580376156 | 02/07/23 09:30 | 100.0 | 89.5 | 42.7 | 22.4 | 4.1 | 3.0 | 0.00 |
| 1617602829 | 03/21/23 08:45 | 100.0 | 91.3 | 51.2 | 32.1 | 6.9 | 3.9 | 0.00 |
| 1558047209 | 04/12/23 08:30 | 100.0 | 89.9 | 47.5 | 28.6 | 5.4 | 2.3 | 0.00 |
| 1558043911 | 05/05/23 10:00 | 100.0 | 89.4 | 47.4 | 28.8 | 7.7 | 3.1 | 0.00 |
| 1806078217 | 05/16/23 10:30 | 100.0 | 91.5 | 46.1 | 25.7 | 6.3 | 2.7 | 0.00 |
| 1669933428 | 06/06/23 08:00 | 100.0 | 91.5 | 51.0 | 33.7 | 9.9 | 3.7 | 0.00 |
| 1703355981 | 07/07/23 11:00 | 100.0 | 91.8 | 47.9 | 29.4 | 7.5 | 2.8 | 0.00 |

| | 1" (25mm) (%) | 3/4" (19mm) (%) | 1/2" (12.5mm) (%) | 3/8" (9.5mm) (%) | #4 (4.75mm) (%) | #8 (2.36mm) (%) | Pan (%) |
|---|---|---|---|---|---|---|---|
| Count | 10 | 10 | 10 | 10 | 10 | 10 | 10 |
| Mean | 100.0 | 90.7 | 47.9 | 28.9 | 7.4 | 3.5 | 0.00 |
| St Dev | 0.00 | 0.97 | 2.49 | 3.44 | 1.98 | 1.00 | 0.000 |
| Lower Spec (LSL) | 100 | 75 | 39 | 20 | 0 | 0 | |
| Upper Spec (USL) | 100 | 95 | 59 | 50 | 15 | 10 | |
| PWS | 100.0 | 100.0 | 100.0 | 99.5 | 100.0 | 100.0 | |

Noblesville Sand and Gravel
15215 N. River Avenue
Noblesville, Indiana 46061
317-776-4460

# Statistical Analysis Report

**Plant** Noblesville Sand and Gravel-25108
**Product** #23/#24 Natural Sand/#4 SB/S&I Abr-0955
**Specification** INDOT #23/#24/#4 SB/S&I Abr
**Period** 04/29/94 - 08/01/23

| Sample Id | Date | 3/8" (9.5mm) (%) | #4 (4.75mm) (%) | #8 (2.36mm) (%) | #16 (1.18mm) (%) | #30 (.6mm) (%) | #50 (.3mm) (%) | #100 (.15mm) (%) | #200 (75µm) (%) | Pan (%) |
|---|---|---|---|---|---|---|---|---|---|---|
| 1575999999 | 06/20/23 11:00 | 100.0 | 99.8 | 85.5 | 62.2 | 36.6 | 13.4 | 3.4 | 1.7 | 0.0 |
| 1808136743 | 06/22/23 09:00 | 100.0 | 99.7 | 86.9 | 61.1 | 33.9 | 13.1 | 3.2 | 1.4 | 0.0 |
| 1866777887 | 06/26/23 10:00 | 100.0 | 100.0 | 86.2 | 61.4 | 36.7 | 14.5 | 4.1 | 1.9 | 0.0 |
| 1675737662 | 06/29/23 08:00 | 100.0 | 99.6 | 83.3 | 58.4 | 33.6 | 12.4 | 3.4 | 1.5 | 0.0 |
| 1669930337 | 07/10/23 08:30 | 100.0 | 100.0 | 87.6 | 63.9 | 38.0 | 13.7 | 3.5 | 1.4 | 0.0 |
| 1898635214 | 07/11/23 09:00 | 100.0 | 99.7 | 86.0 | 58.2 | 31.8 | 11.0 | 3.1 | 1.6 | 0.0 |
| 1521899678 | 07/13/23 10:00 | 100.0 | 99.9 | 84.7 | 61.8 | 36.7 | 14.1 | 4.1 | 1.7 | 0.0 |
| 1703359621 | 07/18/23 09:30 | 100.0 | 99.7 | 87.5 | 69.8 | 51.5 | 26.3 | 6.0 | 1.6 | 0.0 |
| 1981583887 | 07/21/23 09:00 | 100.0 | 99.8 | 84.3 | 61.0 | 37.3 | 13.4 | 2.7 | 1.3 | 0.0 |
| 1862786829 | 07/26/23 10:30 | 100.0 | 99.6 | 89.5 | 72.8 | 49.9 | 21.3 | 4.3 | 1.7 | 0.0 |

| | 3/8" (9.5mm) (%) | #4 (4.75mm) (%) | #8 (2.36mm) (%) | #16 (1.18mm) (%) | #30 (.6mm) (%) | #50 (.3mm) (%) | #100 (.15mm) (%) | #200 (75µm) (%) | Pan (%) |
|---|---|---|---|---|---|---|---|---|---|
| Count | 10 | 10 | 10 | 10 | 10 | 10 | 10 | 10 | 10 |
| Mean | 100.0 | 99.8 | 86.2 | 63.1 | 38.6 | 15.3 | 3.8 | 1.6 | 0.0 |
| St Dev | 0.00 | 0.15 | 1.82 | 4.71 | 6.67 | 4.72 | 0.93 | 0.18 | 0.00 |
| Lower Spec (LSL) | 100 | 95 | 80 | 50 | 25 | 7 | 1 | 0 | |
| Upper Spec (USL) | 100 | 100 | 100 | 80 | 60 | 30 | 10 | 3 | |
| PWS | 100.0 | 100.0 | 100.0 | 99.7 | 97.9 | 96.0 | 99.9 | 100.0 | |

## About the Joint Transportation Research Program (JTRP)

On March 11, 1937, the Indiana Legislature passed an act which authorized the Indiana State Highway Commission to cooperate with and assist Purdue University in developing the best methods of improving and maintaining the highways of the state and the respective counties thereof. That collaborative effort was called the Joint Highway Research Project (JHRP). In 1997 the collaborative venture was renamed as the Joint Transportation Research Program (JTRP) to reflect the state and national efforts to integrate the management and operation of various transportation modes.

The first studies of JHRP were concerned with Test Road No. 1—evaluation of the weathering characteristics of stabilized materials. After World War II, the JHRP program grew substantially and was regularly producing technical reports. Over 1,600 technical reports are now available, published as part of the JHRP and subsequently JTRP collaborative venture between Purdue University and what is now the Indiana Department of Transportation.

Free online access to all reports is provided through a unique collaboration between JTRP and Purdue Libraries. These are available at https://docs.lib.purdue.edu/jtrp/.

Further information about JTRP and its current research program is available at https://engineering.purdue.edu/JTRP.

## About This Report

An open access version of this publication is available online. See the URL in the citation below.

Ajuonuma, C. S., Tokpatayeva, R., Seshadri, A. N., Castillo, A., Olek, J., & Erk, K. A. (2025). *Practical implementation of superabsorbent polymers (SAP) for internally cured concrete* (Joint Transportation Research Program Publication No. FHWA/IN/JTRP-2025/19). West Lafayette, IN: Purdue University. https://doi.org/10.5703/1288284317899